

# Supercurrents in Restricted Geometries and Driven by Time-Dependent Electric Fields

Von der Universität Bayreuth  
zur Erlangung des Grades eines  
Doktors der Naturwissenschaften (Dr. rer. nat.)  
genehmigte Abhandlung

von

Martin Endres

geboren am 10.09.1971 in Hermeskeil

1. Gutachter: Prof. Dr. Dierk Rainer
2. Gutachter: Prof. Dr. Werner Pesch

Tag der Einreichung: 23.04.2004  
Tag des Kolloquiums: 26.07.2004



# Contents

<b>List of figures</b>	<b>iii</b>
<b>Zusammenfassung</b>	<b>v</b>
<b>1 Introduction</b>	<b>1</b>
<b>2 Quasiclassical theory</b>	<b>5</b>
2.1 Keldysh structure . . . . .	5
2.2 Nambu-Gor'kov structure . . . . .	6
2.3 Self-consistency equations . . . . .	7
2.4 Physical quantities . . . . .	8
2.5 Matsubara representation . . . . .	9
2.6 Riccati parameterization . . . . .	9
<b>3 Optical conductivity of NS contacts</b>	<b>11</b>
3.1 Introduction . . . . .	11
3.2 Model . . . . .	12
3.3 NS contacts in equilibrium . . . . .	13
3.3.1 Order-parameter profile . . . . .	13
3.3.2 Impurity-induced proximity effect and minigap . . . . .	14

---

3.4	Linear response . . . . .	16
3.4.1	Linearised quasiclassical equations . . . . .	16
3.4.2	Local charge neutrality . . . . .	19
3.4.3	Analytic solution for homogeneous equilibrium . . . . .	19
3.5	Numerical results . . . . .	23
3.5.1	Electrochemical potential and electric field . . . . .	24
3.5.2	Minicharges . . . . .	27
3.5.3	Dissipation . . . . .	30
<b>4</b>	<b>Weak links in superfluid <math>^3\text{He}</math></b>	<b>35</b>
4.1	Introduction . . . . .	35
4.2	Geometry and model . . . . .	37
4.3	Depairing current . . . . .	38
4.4	Pinhole . . . . .	41
4.5	Pinhole in pair-breaking wall . . . . .	42
4.6	Hydrodynamic limit . . . . .	44
4.7	Free-energy functionals . . . . .	45
4.8	Self-consistent solution for finite apertures . . . . .	49
<b>5</b>	<b>Summary</b>	<b>57</b>
<b>A</b>	<b>Notation</b>	<b>59</b>
<b>B</b>	<b>High-energy expansion</b>	<b>61</b>
<b>C</b>	<b>Charge conservation</b>	<b>63</b>
	<b>References</b>	<b>66</b>

# List of Figures

3.1	Profile of the order parameter at a NS contact . . . . .	14
3.2	Density of states for a NS contact . . . . .	15
3.3	Density of states for a SNS structure . . . . .	16
3.4	Conductivity of a homogeneous superconductor . . . . .	23
3.5	Electrochemical potential, $\delta\Phi(\omega, z)$ , in a NSN structure . . . . .	24
3.6	Electrochemical potential drop in a NSN structure . . . . .	25
3.7	Total electric field in a NS contact with a smooth coupling constant, $2 l_N = l_S = 2 \xi_0$ . . . . .	26
3.8	Total electric field versus frequency in a NS contact, $2 l_N = l_S = 2 \xi_0$ . . . .	26
3.9	Total electric field in a NS contact with a smooth coupling constant, $l_N = l_S = \xi_0$ . . . . .	27
3.10	Total electric field in a NSN structure with discontinuous coupling constant, $l_N = l_S = \xi_0$ . . . . .	28
3.11	Total electric field in a NSN structure with discontinuous coupling constant, $2 l_N = l_S = 2 \xi_0$ . . . . .	28
3.12	Discontinuity of the total electric field at the interface of a NS contact . . . .	29
3.13	Induced charge density in a NS contact . . . . .	29
3.14	Local dissipation in a NSN structure, $l_N = l_S = \xi_0$ . . . . .	31
3.15	Local dissipation in a SNS structure . . . . .	31

---

3.16	Local dissipation in a NSN structure, $2 l_N = l_S = 2 \xi_0$ . . . . .	32
3.17	Local dissipation for a NS contact, $l_N = l_S = \xi_0$ . . . . .	32
3.18	Local dissipation for a NS contact, $2 l_N = l_S = 2 \xi_0$ . . . . .	33
4.1	Schematic geometry of the weak link in $^3\text{He-B}$ . . . . .	37
4.2	Depairing current density in bulk superfluids . . . . .	40
4.3	Current-phase relation for a pinhole . . . . .	43
4.4	Texture-dependent current-phase relation in $^3\text{He-B}$ weak links . . . . .	43
4.5	Order-parameter field near a pair-breaking wall . . . . .	50
4.6	Order-parameter field $\Delta_\perp$ for $T = 0.3 T_c$ , $a = \pi \xi_0$ , $\phi = \pi$ . . . . .	51
4.7	Order-parameter field $\Delta_\parallel$ for $T = 0.3 T_c$ , $a = \pi \xi_0$ , $\phi = \pi$ . . . . .	51
4.8	Multiple solutions for self-consistent order parameter . . . . .	52
4.9	Free-energy density for multiple solutions and phase-dependent free energy .	53
4.10	Free-energy density for orifices with radii $a = \xi_0$ and $a = 2 \xi_0$ . . . . .	53
4.11	Particle current density for a hole between two $^3\text{He-B}$ reservoirs, $a = \pi \xi_0$ . .	54
4.12	Particle current density for a hole between two $^3\text{He-B}$ reservoirs, $a = \xi_0$ . . .	55
4.13	Particle current density and current-phase relation, $a = 2 \xi_0$ . . . . .	55
4.14	Current-phase relation, $a = \pi \xi_0$ and $a = \xi_0$ . . . . .	56

# Zusammenfassung

In der vorliegenden Arbeit werden mit Hilfe der Fermi-Flüssigkeitstheorie Ströme in zwei auf den ersten Blick sehr verschiedenen Systemen untersucht, nämlich elektrische Ströme in inhomogenen Supraleitern sowie Teilchenströme in superfluidem  $^3\text{He}$ . In beiden Fällen liegt jedoch ein System wechselwirkender Fermionen zu Grunde, welches mit der Landauschen Theorie für Fermiflüssigkeiten beschrieben werden kann. Diese besagt, dass die niederenergetischen Eigenschaften von wechselwirkenden Fermionen durch die fermionischen Anregungen in der Nähe der Fermifläche, die so genannten Quasiteilchen, charakterisiert werden können. Eine skalare Verteilungsfunktion dieser Anregungen, welche durch eine klassische Boltzmann-Transportgleichung gegeben ist, bestimmt physikalische Messgrößen bei tiefen Temperaturen.

In vielen Metallen als auch in  $^3\text{He}$  findet unterhalb einer kritischen Temperatur ein Übergang zu einer makroskopisch geordneten Phase statt. Obwohl die Mechanismen, die zur Supraleitung bzw. Superfluidität führen, sehr verschieden sind, so ist das wesentliche Merkmal dieser Phasen, die Kohärenz von teilchen- und lochartigen Anregungen, doch beiden gemein. Im Rahmen der Landauschen Theorie kann dieser Kohärenz Rechnung getragen werden, indem die skalare Verteilungsfunktion durch eine  $2 \times 2$  Matrix, den quasiklassischen Propagator, ersetzt wird. Die Diagonalelemente dieses Propagators spielen die Rolle der Verteilungsfunktion für Teilchen- und Lochanregungen, während die Nichtdiagonalelemente deren Kohärenz widerspiegeln. Diese Verschmelzung der Landautheorie mit den Ideen von Bardeen, Cooper und Schrieffer ist die Basis der Fermi-Flüssigkeitstheorie für Supraleiter und Superfluide, welche Ausgangspunkt dieser Arbeit ist. Im Folgenden werden wir synonym auch die Bezeichnung quasiklassische Theorie verwenden.

Nach einem historischen Rückblick auf die Entwicklung der Theorie im ersten Kapitel werden im zweiten die quasiklassischen Gleichungen in einer Notation eingeführt, die es erlaubt, sowohl Supraleiter als auch superfluides  $^3\text{He}$  zu beschreiben. Im dritten Kapitel werden mit Hilfe der linearisierten Gleichungen die dynamischen Eigenschaften von Kon-

takten zwischen normalleitenden und supraleitenden Metallen (NS-Kontakte) untersucht. Im vierten Kapitel werden die stationären Gleichungen benutzt, um die Phasenabhängigkeit von Teilchenströmen durch ein kleines Loch zwischen zwei Reservoirien superflüssigen Heliums zu berechnen. In den folgenden beiden Abschnitten werden die Kapitel drei und vier kurz zusammengefasst.

## Optische Leitfähigkeit von NS-Kontakten

In den siebziger Jahren des vergangenen Jahrhunderts wurden zahlreiche Experimente zu den Eigenschaften von NS-Kontakten durchgeführt. Nachdem experimentell gefunden wurde, dass elektrische Felder in einen Supraleiter eindringen können, falls ein statischer, elektrischer Strom von einem normalleitenden Metall injiziert wird, wurde dies sehr bald mit der Störung der Gleichgewichtsverteilung für Quasiteilchen erklärt. Da das Nichtgleichgewicht über inelastische Streuung relaxiert, hängt die Eindringtiefe des elektrischen Feldes von der mittleren freien Weglänge für inelastische Streuung ab. Dieser Effekt ist am stärksten nahe der Sprungtemperatur, wenn die meisten Quasiteilchen oberhalb der Energielücke injiziert werden. Bei tieferen Temperaturen liegen die Energien der Quasiteilchen größtenteils in dieser Lücke. Andreev-Reflexion führt dann dazu, dass die Anregungen und damit auch das elektrische Feld nur wenige Kohärenzlängen in den Supraleiter eindringen können.

Statt der statischen werden in Kapitel drei dieser Arbeit die dynamischen Eigenschaften von NS-Kontakten untersucht. Dabei interessiert insbesondere die lineare Antwort auf ein zeitabhängiges elektrisches Feld, dessen Frequenz der Energielücke im Anregungsspektrum des Supraleiters entspricht, d.h.  $\hbar\omega = 2 \Delta$ .

Da die Gleichungen der linearen Antworttheorie vom Gleichgewicht abhängen, wird zunächst dieses berechnet. Dazu wird der selbstkonsistente Ordnungsparameter mittels der Matsu-baratechnik bestimmt, danach die Verunreinigungsselbstenergien und der quasiklassische Propagator für reelle Energien. Dabei zeigt sich, dass die Schmutzselbstenergien einen erheblichen Einfluss auf die Zustandsdichte im Normalmetall haben. Im sauberen Grenzfall wird die Zustandsdichte durch die Nähe zum Supraleiter nicht beeinflusst. Erst die Verunreinigungen führen zu einer energieabhängigen Zustandsdichte. Für eine dünne Metallschicht zwischen zwei Supraleitern sorgt dieser Effekt der Verunreinigungen zur Ausbildung einer ortsunabhängigen Energielücke im Normalmetall. Andererseits merkt der Supraleiter unabhängig von den Verunreinigungen stets die Nähe zum normalleitenden Metall.



Die Antwort eines NS-Kontaktes auf ein zeitabhängiges elektrisches Feld wird dominiert von der Kontinuitätsgleichung für die elektrische Ladung und der lokalen Ladungsneutralität, die eine Folge der guten Abschirmung von Ladungsschwankungen in Metallen ist. In effektiv eindimensionalen Geometrien, wie sie hier vorliegen, führt dies zu einem konstanten Strom, der allein durch die Leitfähigkeiten am linken und rechten Rand gegeben ist. Unklar ist jedoch, wie dieser konstante Strom trotz der Inhomogenität des NS-Kontaktes entsteht. Um diese Frage zu beantworten, ist die selbstkonsistente Lösung der quasiklassischen Gleichungen notwendig. Die Rechnungen zeigen, dass im Kontakt ein zusätzliches elektrisches Feld induziert wird, das von der gleichen Größenordnung wie das äußere Feld ist. Dieses induzierte Feld wird von Ladungen im Bereich des Kontaktes erzeugt. Dabei findet man sowohl Ladungen, die an der Grenzfläche lokalisiert sind, als auch solche, die sich über mehrere Kohärenzlängen zu beiden Seiten des Kontaktes verteilen. Erstere treten auf, falls sich die mittlere freie Weglänge für elastische Verunreinigungsstreuung am Kontakt sprunghaft ändert. Unstetigkeiten des Ordnungsparameters können solche Ladungen nicht hervorrufen. Die Supraleitung ist vielmehr für die verschmierten Ladungen verantwortlich. Das Auftreten dieser Ladungen ist kein Widerspruch zur erwähnten Ladungsneutralität, welche nur approximativ gilt. Die berechneten Ladungen sind von höherer Ordnung in den Entwicklungsparametern der Fermi-Flüssigkeitstheorie. Jedoch ist ihr Effekt, ein zusätzliches inneres Feld bzw. elektrochemisches Potential, zu berücksichtigen, um zu einer konsistenten Beschreibung der Kontakte in führender Ordnung zu gelangen.

## Josephson-Kontakte in superfluidem $^3\text{He}$

Nachdem Josephson kohärentes Tunneln zwischen schwach gekoppelten Supraleitern vorhergesagt hatte, dauerte es nicht lange, bis dies experimentell nachgewiesen werden konnte. Obwohl die Analogie zu Supraleitern schon lange bekannt war, gelang der experimentelle Nachweis der verschiedenen Josephson-Effekte in superfluidem Helium auf Grund der kurzen Kohärenzlängen aber erst in den vergangenen Jahren. Die Beobachtung texturabhängiger Superströme führte kürzlich zu einer Reihe neuer theoretischen Arbeiten.

Im vierten Kapitel werden verschiedene Modelle zur Berechnung des Teilchenstromes durch ein kleines, kreisrundes Loch zwischen zwei Behältern mit superfluidem  $^3\text{He}$  gegenübergestellt. Dabei werden wir uns auf tiefe Temperaturen beschränken und die Ginzburg-Landau-Gleichungen nicht diskutieren, da dazu schon umfangreiche Arbeiten existieren.

Öffnungen, die klein gegen die Kohärenzlänge sind, beeinflussen den Ordnungsparameter in den Reservoiren nicht. Da auch die Ströme in diesem Grenzfall punktförmiger Löcher

## ZUSAMMENFASSUNG

---

sehr klein sind, ist deren Einfluss auf den Ordnungsparameter ebenfalls vernachlässigbar. Als Konsequenz dieser fehlenden Kopplung zwischen den Reservoirien führen punktförmige Löcher zwangsläufig zu periodischen Stromphasenbeziehungen. Unabhängig von der Öffnung muss jedoch der Effekt der Trennwand berücksichtigt werden, denn diese wirkt wegen der Symmetrie des Ordnungsparameters paarbrechend. Numerische Rechnungen zeigen, dass die Wand hauptsächlich die Größe des Stromes reduziert, dessen Phasenabhängigkeit aber nur wenig beeinflusst.

Für größere Öffnungen nimmt die Kopplung zwischen den Behältern zu. Dies reduziert einerseits die paarbrechende Wirkung der Wand und hat andererseits eine sich stetig ändernde Phase zur Folge. Letzteres zerstört die Periodizität der Stromphasenbeziehung und kann bei großen Löchern zu mehrdeutigen Lösungen führen. Die selbstkonsistenten Lösungen der quasiklassischen Gleichungen zeigen, dass der Strom schon für relativ kleine Öffnungen über weite Strecken linear von der Phasendifferenz abhängt. Zwar sagt auch eine hydrodynamische Behandlung des Problems diese Linearität voraus, allerdings ist dann der Strom infolge divergierender Stromdichten am Rand des Loches stets viel zu groß. Erstaunlicherweise liefert eine Kombination der hydrodynamisch bestimmten Phase mit der Transportgleichung der quasiklassischen Theorie eine gute Näherung für den Strom. Diese Übereinstimmung bricht zusammen, wenn mit steigender Phasendifferenz die Stromdichte im Loch so groß wird, dass sie selbst paarbrechend wirkt. Es zeigt sich, dass der maximale Strom, falls auf die Lochfläche normiert, kaum von der Größe der Öffnung abhängt. Ferner liegt dieses Maximum zwischen dem Wert für punktförmige Löcher und dem maximalen Superstrom im homogenen Superfluid, welche sich bei tiefen Temperaturen nur um etwa den Faktor zwei unterscheiden.

# Chapter 1

## Introduction

In 1911 Kamerlingh Onnes [1] discovered that the electric resistance of mercury abruptly disappears if the metal is cooled below 4.2 K. The first phenomenological description of superconductivity was given in 1935 by F. and H. London [2] who proposed two equations to reflect the main features of superconductors: perfect conductivity and the exclusion of magnetic fields. The latter property, which distinguishes the true thermodynamic state of superconductivity from perfect conductivity, was first observed in 1933 by Meissner and Ochsenfeld [3]. The next significant step forward towards qualitative as well as quantitative understanding of superconductivity was done by Ginzburg and Landau [4] who introduced the fundamental concept of a complex order parameter. The Ginzburg-Landau equations were the first method of describing inhomogeneous superconductors which lead to the prediction of type-II superconductors by Abrikosov [5]. Though phenomenological at the time proposed, the equations were proven to be the correct limit of the microscopic equations near the transition temperature [6].

It needed more than four decades until a microscopic theory was developed by Bardeen, Cooper, and Schrieffer in 1957 [7]. This theory was then formulated by Gor'kov [6, 8] in the language of Green's functions which allows to study not only inhomogeneous superconductors but also the effect of impurities. The two-particle Gor'kov Green's function still depends on the full space and time coordinates (eight in total) and therefore contains information on microscopic length and time scales. As a consequence, this formalism is very expensive to apply and delivers redundant information as the properties of conventional superconductors vary on the coherence length,  $\xi$ , which is much larger than, e.g., the Fermi wavelength.

## CHAPTER 1. INTRODUCTION

---

In 1968 Eilenberger [9] and, independently, Larkin and Ovchinnikov [10, 11] managed to find equations for the over the microscopic degree of freedom averaged Gor'kov Green's function. These quasiclassical equations are significantly easier than those introduced by Gor'kov without loosing any information on measurable quantities. They provide a powerful method of describing superconductors in equilibrium as well as nonequilibrium [11–13], from the clean to the dirty limit. The theory is valid at all temperatures and may also include strong electron-phonon and electron-electron interaction.

In the clean limit the quasiclassical equations are equivalent to those derived by Andreev [14] by eliminating the microscopic dynamics from the Bogolubov equation [15]. The latter is a Schrödinger equation for a two-component wave function describing electron- and hole-like particles. For dirty superconductors the quasiclassical equations can be simplified further by a Fermi-surface average leading to a diffusion equation as found by Usadel [16].

In the decade after the BCS theory was established many authors extended the basic ideas to other pairing mechanisms which then lead to the prediction of superfluid phases in the Fermi liquid  $^3\text{He}$ , eventually discovered by Osheroff *et al.* [17] in 1972. References on this development are given in a review article by Anderson and Brinkman [18].

With the extension to unconventional pairing mechanisms, reviewed e.g. by Eckern [19] or Serene and Rainer [20], the quasiclassical theory can be seen as the generalisation of Landau's Fermi-liquid theory [21–23] to the superconducting and superfluid state. Landau suggested that at low temperature a system of interacting fermions can be described by a classical distribution function for quasiparticles which are composite states of elementary fermions with the same spin and charge as the noninteracting fermions. The dynamics of these quasiparticles is determined by a Boltzmann transport equation. Particle-hole coherence in superfluids requires that the scalar distribution function is replaced by a  $2 \times 2$  matrix in Nambu-Gor'kov space. The elements of the Nambu-Gor'kov matrices are spin matrices if spin-dependent effects are to be investigated. For nonequilibrium situations it is convenient to use the Keldysh formalism [24] which combines different types of Green's functions to, again, a  $2 \times 2$  matrix. Hence, in the most general case the scalar distribution function is replaced by a  $8 \times 8$  quasiclassical propagator. But, as for normal Fermi liquids, the dynamics is governed by a Boltzmann transport equation. The classical part of the dynamics is given by the motion with Fermi velocity along straight trajectories, the quantum mechanical part is treated by the matrix structure for particle-hole coherence and the spin degree of freedom.

The Fermi-liquid theory for superconductors and superfluids is derived by an expansion in small parameters and is exact in leading order of these parameters. This expansion results from a separation of low-energy, low-frequency, long-wavelength processes from microscopic energy, time, and length scales. Examples for such small parameters are  $k_B T_c / E_f$ ,  $1 / k_f \xi_0$ ,

$1/k_f l$ ,  $\hbar\omega/E_f$ ,  $q/k_f$ , and  $\hbar\omega_D/E_f$ . Here,  $\omega$  and  $q$  stand for frequency and wave number of external perturbations, respectively. The low-energy scale near the Fermi surface is treated in a consistent way and suffices, due to Pauli's exclusion principle, to describe the low-temperature properties. High-energy processes lead to temperature-independent material parameters which cannot be calculated within this theory but have to be taken from experiment or ab initio calculations.

Although the quasiclassical approximation simplifies the microscopic equations significantly, analytic solutions can only be found for homogeneous systems. While the transport equation can straightforwardly be solved, the main difficulties always stem from the self-consistency equations for the order parameter, the impurity self-energies, or the electrochemical potential. As these equations ensure the theory to be conserving, they are especially important if currents flow in the problem under study. In the work at hand the consequences of self-consistency for particle currents are examined for two distinct problems. In chapter 3 we study the properties of a metallic contact between a s-wave superconductor and a normal metal in equilibrium as well as in time-dependent electric fields. In chapter 4 we focus on a comparison of several simplified models with the self-consistent theory for the case of a weak link connecting two reservoirs of the p-wave superfluid  $^3\text{He}$ . In the succeeding chapter the equations of the quasiclassical theory are introduced, not in the most general form, but in such a way that they can be applied to both problems mentioned above.



# Chapter 2

## Quasiclassical theory of superconductors and superfluids

### 2.1 Keldysh structure

In the following sections the notation used in this work is defined. A more general formulation, including e.g. Landau parameters, is given by Eschrig [25]. The fundamental object for describing nonequilibrium within the quasiclassical theory of superconductivity and superfluidity is the Green's function  $\check{g}(\mathbf{R}, \mathbf{p}_f, \epsilon, t)$ . It is a  $2 \times 2$  matrix combining retarded ( $R$ ), advanced ( $A$ ), and Keldysh ( $K$ ) propagators,

$$\check{g} = \begin{pmatrix} \hat{g}^R & \hat{g}^K \\ \hat{0} & \hat{g}^A \end{pmatrix}. \quad (2.1)$$

The quasiclassical propagator  $\check{g}$  depends on spatial position,  $\mathbf{R}$ , Fermi momentum,  $\mathbf{p}_f$ , the distance from the Fermi surface described by the energy variable  $\epsilon$ , and the time  $t$ . Below, the arguments of the Green's functions and the potentials are dropped for convenience. The quantum mechanical degrees of freedom, i.e. particle-hole coherence and spin, are described by the  $4 \times 4$  Nambu-Gor'kov matrices  $\hat{g}^{R,A,K}$ . The classical part of the dynamics of quasiparticles is given by the motion with the Fermi velocity  $\mathbf{v}_f(\mathbf{p}_f)$  along straight trajectories.

The central equation determining  $\check{g}$  is a Boltzmann transport equation for matrices,

$$\left[ \epsilon \hat{\tau}_3 \check{1} - \check{h}, \check{g} \right]_{\otimes} + i\hbar \mathbf{v}_f \cdot \nabla \hat{g} = \check{0}, \quad (2.2)$$

supplemented by the normalization condition

$$\check{g} \otimes \check{g} = -\pi^2 \check{1}. \quad (2.3)$$

In eq. (2.2)  $\check{h}$  is equivalent with the order parameter,  $\check{\Delta}_{mf}$ , when we consider superfluid  $^3\text{He}$ , but additionally includes impurity self-energies,  $\check{\sigma}_{imp}$ , and external potentials,  $\check{v}_{ext}$ , when we study charged Fermi liquids:

$$\check{h} = \check{\Delta}_{mf} + \check{\sigma}_{imp} + \check{v}_{ext} = \begin{pmatrix} \hat{h}^R & \hat{h}^K \\ \hat{0} & \hat{h}^A \end{pmatrix}, \quad \check{\Delta}_{mf} = \begin{pmatrix} \hat{\Delta}_{mf} & \hat{0} \\ \hat{0} & \hat{\Delta}_{mf} \end{pmatrix}, \quad (2.4)$$

$$\check{\sigma}_{imp} = \begin{pmatrix} \hat{\sigma}_{imp}^R & \hat{\sigma}_{imp}^K \\ \hat{0} & \hat{\sigma}_{imp}^A \end{pmatrix}, \quad \check{v}_{ext} = \begin{pmatrix} e\Phi\hat{1} - \frac{e}{c} \mathbf{v}_f \cdot \mathbf{A}\hat{\tau}_3 & \hat{0} \\ \hat{0} & e\Phi\hat{1} - \frac{e}{c} \mathbf{v}_f \cdot \mathbf{A}\hat{\tau}_3 \end{pmatrix}. \quad (2.5)$$

Here,  $\check{1}$  and  $\hat{1}$  are unity matrices in Keldysh and Nambu-Gor'kov space, respectively. The non-commutative folding product  $\otimes$  is defined in appendix A, and  $\hat{\tau}_i$ , with  $i = 1, 2, 3$ , stands for the Pauli matrices which act on particle-hole space. The self-energy for impurities with concentration  $c_i$  is given through the t-matrix  $\check{t}_i$ :

$$\check{\sigma}_{imp}(\mathbf{p}_f) = \sum_{i=1}^N c_i \check{t}_i(\mathbf{p}_f, \mathbf{p}_f),$$

$$\check{t}_i(\mathbf{p}_f, \mathbf{p}'_f) = \hat{u}_i(\mathbf{p}_f, \mathbf{p}'_f)\check{1} + N_f \left\langle \hat{u}_i(\mathbf{p}_f, \mathbf{p}''_f)\check{1} \otimes \check{g}(\mathbf{p}''_f) \otimes \check{t}_i(\mathbf{p}''_f, \mathbf{p}'_f) \right\rangle_{\mathbf{p}''_f}. \quad (2.6)$$

The impurity potentials  $\check{u}_i$  are diagonal in Keldysh space. The external potentials are given by the electrochemical potential,  $\Phi$ , and the vector potential,  $\mathbf{A}$ . The charge of an electron,  $e$ , is chosen negative, and  $c$  denotes the speed of light. The brackets,  $\langle \dots \rangle$ , indicate a Fermi-surface average which is explained in appendix A.

## 2.2 Nambu-Gor'kov structure

The elements of the Nambu-Gor'kov matrices describing the particle-hole nature of quasi-particles are parameterized in the following way:

$$\hat{g}^K = \begin{pmatrix} g^K & f^K \\ -\tilde{f}^K & -\tilde{g}^K \end{pmatrix} = \begin{pmatrix} \sigma_y g_0^K \sigma_y + \mathbf{g}^K \cdot \boldsymbol{\sigma} & [f_s^K + \mathbf{f}_t^K \cdot \boldsymbol{\sigma}] i\sigma_y \\ -i\sigma_y [\tilde{f}_s^K + \tilde{\mathbf{f}}_t^K \cdot \boldsymbol{\sigma}] & \sigma_y [\tilde{g}_0^K - \tilde{\mathbf{g}}^K \cdot \boldsymbol{\sigma}] \sigma_y \end{pmatrix}, \quad (2.7)$$



$$\hat{g}^{R,A} = \begin{pmatrix} g^{R,A} & f^{R,A} \\ \tilde{f}^{R,A} & \tilde{g}^{R,A} \end{pmatrix}, \quad \hat{h}^{R,A} = \begin{pmatrix} \Sigma^{R,A} & \Delta^{R,A} \\ \tilde{\Delta}^{R,A} & \tilde{\Sigma}^{R,A} \end{pmatrix}, \quad \hat{h}^K = \begin{pmatrix} \Sigma^K & \Delta^K \\ -\tilde{\Delta}^K & -\tilde{\Sigma}^K \end{pmatrix}. \quad (2.8)$$

Note that  $\Delta^{R,A,K}$  and  $\tilde{\Delta}^{R,A,K}$  do not stand for the order parameter exclusively, but the off-diagonal part of the sum of self-energies. The matrix which describes the pairing energy has the form

$$\hat{\Delta}_{mf} = \begin{pmatrix} 0 & \Delta_{mf} \\ \tilde{\Delta}_{mf} & 0 \end{pmatrix} = \begin{pmatrix} 0 & [\Delta_s + \mathbf{\Delta}_t \cdot \boldsymbol{\sigma}] i\sigma_y \\ i\sigma_y [\Delta_s^* + \mathbf{\Delta}_t^* \cdot \boldsymbol{\sigma}] & 0 \end{pmatrix}. \quad (2.9)$$

All elements of the Nambu-Gor'kov matrices are in general  $2 \times 2$  spin matrices. The Keldysh propagator and the order-parameter matrix are further split up into scalar and vector components to indicate singlet and triplet pairing in superconductors and helium, respectively. The components of the vector  $\boldsymbol{\sigma}$  are the Pauli matrices  $\sigma_x$ ,  $\sigma_y$ , and  $\sigma_z$  which act on spin space. The above parameterization introduces more matrix elements than needed as symmetries relating them are not used. But for clarifying the structure of, e.g., the Riccati equations, which are introduced below, it is advantageous not to restrict the notation to a minimum number of independent parameters. The relations connecting Nambu-Gor'kov matrix elements result from particle-hole and time-reversal symmetry. They are given by Serene *et al.* [20]. With the sign convention chosen above, the relation  $\tilde{x}(\mathbf{R}, \mathbf{p}_f, \epsilon, t) = x^*(\mathbf{R}, -\mathbf{p}_f, -\epsilon, t)$  holds for any spin matrix  $x$  defined in eqs. (2.7) to (2.9).

## 2.3 Self-consistency equations

The quasiclassical equations have to be supplemented by the self-consistency equations for the order parameter. They are given by

$$\Delta_s(\mathbf{R}, \mathbf{p}_f, t) = N_f \int_{-\epsilon_c}^{\epsilon_c} \frac{d\epsilon}{4\pi i} \left\langle V_s(\mathbf{p}_f, \mathbf{p}'_f) f_s^K(\mathbf{R}, \mathbf{p}'_f, \epsilon, t) \right\rangle_{\mathbf{p}'_f} \quad (2.10)$$

for singlet pairing and by

$$\mathbf{\Delta}_t(\mathbf{R}, \mathbf{p}_f, t) = N_f \int_{-\epsilon_c}^{\epsilon_c} \frac{d\epsilon}{4\pi i} \left\langle V_t(\mathbf{p}_f, \mathbf{p}'_f) \mathbf{f}_t^K(\mathbf{R}, \mathbf{p}'_f, \epsilon, t) \right\rangle_{\mathbf{p}'_f} \quad (2.11)$$

for triplet pairing.

The pairing interaction,  $V_{s(t)}(\mathbf{p}_f, \mathbf{p}'_f)$ , cannot be calculated within the Fermi-liquid theory

but has to be determined by experiments. The energy integrals in eqs. (2.10) and (2.11) have a logarithmic divergence and therefore have to be limited to a finite cutoff energy,  $\epsilon_c$ . The cutoff is a purely technical parameter which has no influence on physical quantities. It can be eliminated in favour of a reference system as, e.g., the zero-temperature limit (see eq. (4.9)) or the transition temperature. In numerical calculations the cutoff was eliminated using the solution of the corresponding homogeneous system. The details of this method are described by Eschrig [26].

## 2.4 Physical quantities

The low-energy contributions to physical quantities, which are responsible for temperature-dependent effects, can be calculated by suitable traces over the Keldysh propagator. Additionally, there are temperature-independent high-energy contributions. Serene and Rainer [20] have shown that the formula for a quantity  $M$  has the general form

$$M(\mathbf{R}, t) = M_0 + M_1(V_{ext})(\mathbf{R}, t) + N_f \int_{-\infty}^{\infty} \frac{d\epsilon}{4\pi i} \frac{1}{2} \text{Tr}_4 \left\langle \hat{m} \hat{g}^K(\mathbf{R}, \mathbf{p}_f, \epsilon, t) \right\rangle_{\mathbf{p}_f} . \quad (2.12)$$

Here,  $M_0$  is the high-energy part of the equilibrium value of  $M$  while  $M_1$  describes the high-energy response which is linear in the external perturbation  $V_{ext}$ . For some quantities the high-energy terms can be calculated using very general properties like gauge or Galilean invariance. The linear operator  $\hat{m}$  just chooses the proper combination of diagonal elements. The main quantity of interest in this work, for both the study of a normal metal-superconductor contact as well as superflow through an orifice connecting two reservoirs of  $^3\text{He}$ , is the particle current density which is solely determined by the low-energy contribution,

$$\mathbf{j}(\mathbf{R}, t) = N_f \int_{-\infty}^{\infty} \frac{d\epsilon}{4\pi i} \frac{1}{2} \text{Tr}_4 \left\langle \hat{\tau}_3 \mathbf{v}_f(\mathbf{R}, \mathbf{p}_f, t) \hat{g}^K(\mathbf{R}, \mathbf{p}_f, \epsilon, t) \right\rangle_{\mathbf{p}_f} . \quad (2.13)$$

Although metals screen charge fluctuations very effectively, the charge density proves to be very important when the response of a superconductor to electromagnetic perturbations is studied. It is calculated via

$$\rho(\mathbf{R}, t) = \rho_0(\mathbf{R}, t) - 2eN_f e\Phi(\mathbf{R}, t) + N_f \int_{-\infty}^{\infty} \frac{d\epsilon}{4\pi i} \frac{1}{2} \text{Tr}_4 \left\langle e \hat{g}^K(\mathbf{R}, \mathbf{p}_f, \epsilon, t) \right\rangle_{\mathbf{p}_f} . \quad (2.14)$$

The high-energy contributions consist here of the equilibrium electronic charge density,  $\rho_0(\mathbf{R}, t)$ , which is cancelled by the positive background in the metal, and the potential

$\Phi(\mathbf{R}, t)$  which includes the external perturbation as well as the response to the former. The density of states,  $N_f$ , does not include the spin degree of freedom requiring an explicit factor 2.

## 2.5 Matsubara representation

In thermal equilibrium retarded, advanced, and Keldysh propagators are connected by the relation

$$\hat{g}^K = \tanh \frac{\epsilon}{2k_B T_c} (\hat{g}^R - \hat{g}^A) . \quad (2.15)$$

The retarded (advanced) propagator is analytic in the upper (lower) complex energy plane. The integrals in eqs. (2.10), (2.11), or (2.12) can then be evaluated by a contour integration and replaced by a sum over the poles of the Fermi distribution function:

$$N_f \int_{-\infty}^{\infty} \frac{d\epsilon}{4\pi i} \frac{1}{2} Tr_4 \langle \hat{m} \hat{g}^K(\mathbf{R}, \mathbf{p}_f, \epsilon) \rangle_{\mathbf{p}_f} = N_f k_B T \sum_{n=-\infty}^{\infty} \frac{1}{2} Tr_4 \langle \hat{m} \hat{g}^M(\mathbf{R}, \mathbf{p}_f, \epsilon_n) \rangle_{\mathbf{p}_f} . \quad (2.16)$$

The energies  $\epsilon_n = (2n+1)\pi k_B T$  are called Matsubara energies. The Matsubara propagator is defined by retarded and advanced functions according to

$$\hat{g}^M(\mathbf{R}, \mathbf{p}_f, \epsilon_n) = \begin{cases} \hat{g}^R(\mathbf{R}, \mathbf{p}_f, i\epsilon_n) & \text{for } \epsilon_n > 0 \\ \hat{g}^A(\mathbf{R}, \mathbf{p}_f, i\epsilon_n) & \text{for } \epsilon_n < 0 \end{cases} . \quad (2.17)$$

The transport equation and the self-energies in Matsubara representation are defined in analogy to the equation above. Instead of awkward integrals over the BCS singularities, which require a dense energy grid, the Matsubara technique needs only few evaluations of the propagator as typical sums converge rapidly. A further advantage for numerical calculations is that imaginary energies guarantee smooth functions, oscillatory solutions typical of real energies beyond the gap edge are avoided.

## 2.6 Riccati parameterization

An inconvenient property of the matrix transport equation (2.2), especially for numerical calculations, is that it possesses fundamental, exponentially decaying and exploding, unphysical solutions. The physical solution is then given by a commutator of these and the

normalization condition [27]. A considerable simplification of the quasiclassical equations can be achieved by parameterizing the Green's functions by a set of spin matrices, named Riccati amplitudes [25, 28–32]. Although this transformation leads to nonlinear instead of linear equations, it is favourable as the equations are easy to handle and stable if solved in the correct direction. Furthermore, normalization is, by construction, automatically satisfied. The parameterization chosen here reads:

$$\hat{g}^{R,A} = \mp i\pi \hat{N}^{R,A} \otimes \begin{pmatrix} (1 + \gamma^{R,A} \otimes \tilde{\gamma}^{R,A}) & 2\gamma^{R,A} \\ -2\tilde{\gamma}^{R,A} & -(1 + \tilde{\gamma}^{R,A} \otimes \gamma^{R,A}) \end{pmatrix}, \quad (2.18)$$

$$\hat{g}^K = -2\pi i \hat{N}^R \otimes \begin{pmatrix} (x^K - \gamma^R \otimes \tilde{x}^K \otimes \tilde{\gamma}^A) & -(\gamma^R \otimes \tilde{x}^K - x^K \otimes \gamma^A) \\ -(\tilde{\gamma}^R \otimes x^K - \tilde{x}^K \otimes \tilde{\gamma}^A) & (\tilde{x}^K - \tilde{\gamma}^R \otimes x^K \otimes \gamma^A) \end{pmatrix} \otimes \hat{N}^A. \quad (2.19)$$

Normalization is guaranteed by the matrices

$$\hat{N}^{R,A} = \begin{pmatrix} (1 - \gamma^{R,A} \otimes \tilde{\gamma}^{R,A})^{-1} & 0 \\ 0 & -(1 - \tilde{\gamma}^{R,A} \otimes \gamma^{R,A})^{-1} \end{pmatrix}. \quad (2.20)$$

With this parameterization the transport equation transforms into six Riccati-type equations:

$$i\hbar \mathbf{v}_f \cdot \nabla \gamma^{R,A} + 2\epsilon \gamma^{R,A} = \gamma^{R,A} \otimes \tilde{\Delta}^{R,A} \otimes \gamma^{R,A} + \Sigma^{R,A} \otimes \gamma^{R,A} - \gamma^{R,A} \otimes \tilde{\Sigma}^{R,A} - \Delta^{R,A}, \quad (2.21)$$

$$i\hbar \mathbf{v}_f \cdot \nabla \tilde{\gamma}^{R,A} - 2\epsilon \tilde{\gamma}^{R,A} = \tilde{\gamma}^{R,A} \otimes \Delta^{R,A} \otimes \tilde{\gamma}^{R,A} + \tilde{\Sigma}^{R,A} \otimes \tilde{\gamma}^{R,A} - \tilde{\gamma}^{R,A} \otimes \Sigma^{R,A} - \tilde{\Delta}^{R,A}, \quad (2.22)$$

$$i\hbar \mathbf{v}_f \cdot \nabla x^K + i\hbar \partial_t x^K + (-\gamma^R \otimes \tilde{\Delta}^R - \Sigma^R) \otimes x^K + x^K \otimes (-\Delta^A \otimes \tilde{\gamma}^A + \Sigma^A) = \\ -\gamma^R \otimes \tilde{\Sigma}^K \otimes \tilde{\gamma}^A + \Delta^K \otimes \tilde{\gamma}^A + \gamma^R \otimes \tilde{\Delta}^K - \Sigma^K, \quad (2.23)$$

$$i\hbar \mathbf{v}_f \cdot \nabla \tilde{x}^K - i\hbar \partial_t \tilde{x}^K + (-\tilde{\gamma}^R \otimes \Delta^R - \tilde{\Sigma}^R) \otimes \tilde{x}^K + \tilde{x}^K \otimes (-\tilde{\Delta}^A \otimes \gamma^A + \tilde{\Sigma}^A) = \\ -\tilde{\gamma}^R \otimes \Sigma^K \otimes \gamma^A + \tilde{\Delta}^K \otimes \gamma^A + \tilde{\gamma}^R \otimes \Delta^K - \tilde{\Sigma}^K. \quad (2.24)$$

While the linear transport equation (2.2) is a boundary value problem, the eqs. (2.21) to (2.24) are initial value problems. If supplemented with the correct initial value, the Riccati equations for  $\gamma^R$ ,  $\tilde{\gamma}^A$ , and  $x^K$  are stable in positive  $\mathbf{v}_f$  direction whereas those for  $\tilde{\gamma}^R$ ,  $\gamma^A$ , and  $\tilde{x}^K$  are stable in opposite direction. Thus, for the first (second) group of functions the value at the “beginning” (“end”) of a given trajectory must be known. Usually, these points are in the bulk where the initial values are well known. Even if this is not the case, it is sufficient to start with an approximate solution a few coherence lengths away from the point where the solution is needed. Any error in the initial value will decay exponentially provided that the initial value is not completely off.

# Chapter 3

## Optical conductivity of NS contacts

### 3.1 Introduction

In the early 70s experiments on the electric resistance of normal metal superconducting metal contacts showed that an electric field penetrates into the superconductor when a current flows through the contact [33–36]. Rieger *et al.* [37] studied the contact resistance near the transition temperature using a time-dependent Ginzburg-Landau equation. Pippard *et al.* [33] argued that the resistance results from quasiparticles injected from the normal layer with energies above the gap. Inelastic scattering reestablishes the equilibrium distribution of quasiparticles and hence determines the penetration depth of the electric field. The effect is strongest near the transition temperature when the energy gap for excitations in the superconductor is small compared to the thermal energy  $k_B T_c$  and the majority of injected quasiparticles penetrates into the superconductor. At low temperature Andreev reflection [14] becomes increasingly important as it reduces the fraction of quasiparticles which can penetrate into the superconductor considerably and, consequently, also the extra resistance. Particle-like excitations with energies below the gap are converted into hole-like excitations with reversed velocity and vice versa. Above the gap the portion of quasiparticles which are Andreev reflected decreases with increasing distance from the Fermi surface. This reflection takes place within a few coherence lengths of the contact which is much shorter than the mean free path for inelastic scattering in the materials studied experimentally. Hence, Andreev reflection reduces the extra resistance of the contact.

A first quantitative analysis of the ideas just described was given by Tinkham and Clarke [38] and in more detail by Tinkham [39] for tunnel junctions. They calculated the relaxation

time for the imbalance between hole-like and particle-like branches in the superconductor produced by quasiparticle injection and related that relaxation time to the potential drop measured in experiments.

A microscopic theory based on Green's functions was developed by Schmid and Schön [40] and applied or extended by many authors [41–45]. In contrast to the two-fluid model used by Pippard *et al.* [33], which distinguishes between a quasiparticle current and a supercurrent, there is no such decomposition in the microscopic theory. This difference leads to various definitions of relaxation times for branch-imbalance responsible for the contact resistance. The conceptional differences of the approaches were discussed by Clarke *et al.* [46].

For small ballistic contacts Blonder *et al.* [47] combined the semiconductor tunnelling model with the Bogolubov equations to describe the branch-imbalance induced by an injected current. Via a barrier of variable strength they were able to cover the whole range from tunnelling to metallic contacts.

All articles cited above have in common that the nonequilibrium in the superconductor is caused by a steady injection of a current. In contrast to this we shall now examine the response of the contact to a time-dependent electric field with frequencies comparable to the energy gap in the density of states. The method for tackling this problem was developed by Eschrig [26] and applied by him and Marquardt [48] to the case of an isolated vortex. Self-consistency being essential for charge conservation, an integro-differential equation for six functions coupled via the order parameter, the electrochemical potential, and the self-energies for elastic impurity scattering has to be solved - a problem too big at the time when NS contacts were studied originally but now accessible by standard personal computers.

## 3.2 Model

The interfaces between different metals are assumed to be infinite planes parallel to the  $xy$ -plane. With the electric field applied perpendicular to the interfaces, the problem is one-dimensional in the space coordinates. The interfaces are fully transparent as we are interested in the case with maximal coupling between the metals. The metals are chosen identical apart from the coupling constant, i.e. the superconducting transition temperature, and the impurity mean free path. These material parameters change either abruptly at the interfaces or smoothly like a hyperbolic tangent over typically a few coherence lengths. The Fermi surface is cylindrical. An extension to a spherical Fermi surface is straightforward. The same trajectories have to be calculated, only the angular averaging has to be changed. This will affect the length scale for spatial variations but does not change results qualita-

tively. The pairing symmetry always corresponds to s-wave pairing. For d-wave symmetry the conductivity is anisotropic requiring the orientation of the Fermi surface with respect to the field as additional parameter.

In this chapter only isotropic impurity scattering is considered which is characterised by a dimensionless scattering cross section,  $\sigma$ , and a lifetime or inverse scattering rate,  $\tau(z)$ . These parameters are defined through

$$\sigma = \frac{(\pi N_f u)^2}{1 + (\pi N_f u)^2} \quad \text{and} \quad \frac{1}{\tau(z)} = 2c(z)u \frac{\pi N_f u}{1 + (\pi N_f u)^2} . \quad (3.1)$$

The scatterers are, for simplicity, limited to a single species with scattering potential  $u$  and spatially varying concentration  $c(z)$ . The impurity self-energy is then given by the solution of the t-matrix equation (2.6). The lifetime corresponds to a mean free path  $l = v_f \tau$  which equals the zero-temperature coherence length,  $\xi_0$ , for  $\tau = \hbar/(2\pi k_B T_c)$ . This intermediate regime between clean and dirty limit, where the full theory is needed, will be examined in the subsequent sections.

### 3.3 NS contacts in equilibrium

Before investigating the dynamics, the equilibrium state of a normal metal superconducting metal contact is studied as the equilibrium quasiclassical propagator determines the coefficients of the linear response equations and, hence, contains already all information for small perturbations from equilibrium. Some (qualitative and quantitative) equilibrium properties for non-homogeneous superconductors are reviewed below.

#### 3.3.1 Order-parameter profile

The linear response properties strongly depend on the coupling between the normal metal and the superconducting metal. A surface with non-ideal transmittance decreases this coupling. The effect of a finite reflectivity on the order parameter in equilibrium is shown in fig. 3.1. With increasing reflectivity the suppression of the order parameter becomes smaller until the superconductor is completely decoupled from the normal metal and reaches its bulk value. In this work the focus lies on the effect which the proximity of normal and superconducting metals has on the electric conductivity. In the following all calculations will be restricted to ideally transparent interfaces. For studying the effect of rough or specularly reflecting interfaces, it is again advantageous to formulate the boundary conditions in terms

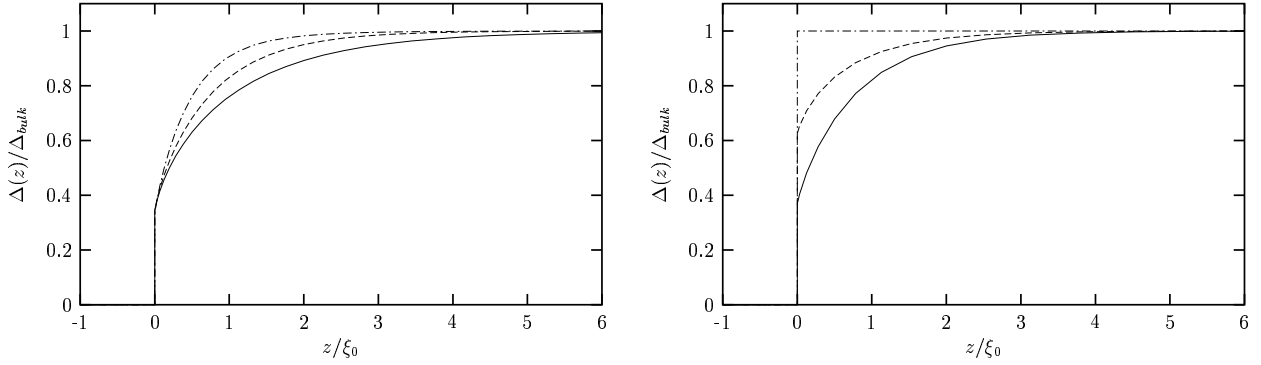


Figure 3.1: Order parameter for a contact between a normal metal and a superconducting metal for  $T = 0.3 T_c$  and  $\sigma = 0$ . The graph on the left shows the dependence on the mean free path for elastic impurity scattering. A short mean free path reduces the coherence length and results in a steeper profile of the order parameter. The curves correspond to the clean limit (solid line),  $l = \xi_0$  (dashed line), and  $l = 0.2 \xi_0$  (dashed-dotted line). On the right, the dependence of the order parameter on the reflectivity,  $R$ , is plotted for  $R = 0, 0.5$ , and  $1$  (solid, dashed, and dashed-dotted line, respectively).

of Riccati amplitudes which naturally separate incoming and outgoing trajectories [25]. In contrast, the full matrix propagators always carry information prior to and after hitting the interface leading to far more complicated, non-linear equations with unphysical, spurious solutions [49]. For further references on boundary models also see section 4.5.

### 3.3.2 Impurity-induced proximity effect and minigap

Impurity scattering does not only influence the order-parameter profile (see fig. 3.1) but is especially important for a change in the density of states in a normal metal in contact with a superconductor. The density of states on the normal side of a NS contact will be unchanged by the proximity to a superconductor if the self-consistency of the impurity self-energy is not taken into account (unless there exists a non-vanishing coupling constant in the normal metal). Consequently, a clean normal metal shows no sign of a proximity effect. This changes when particle-hole coherence is induced in the normal metal by impurity self-energies which cause states to be shifted away from the Fermi level. Figure 3.2 demonstrates the effect of a finite mean free path on the density of states in a NS contact. In contrast to the normal metal, the superconductor is already affected by the contact without self-consistency. At the interface itself the density of states equals the constant normal density



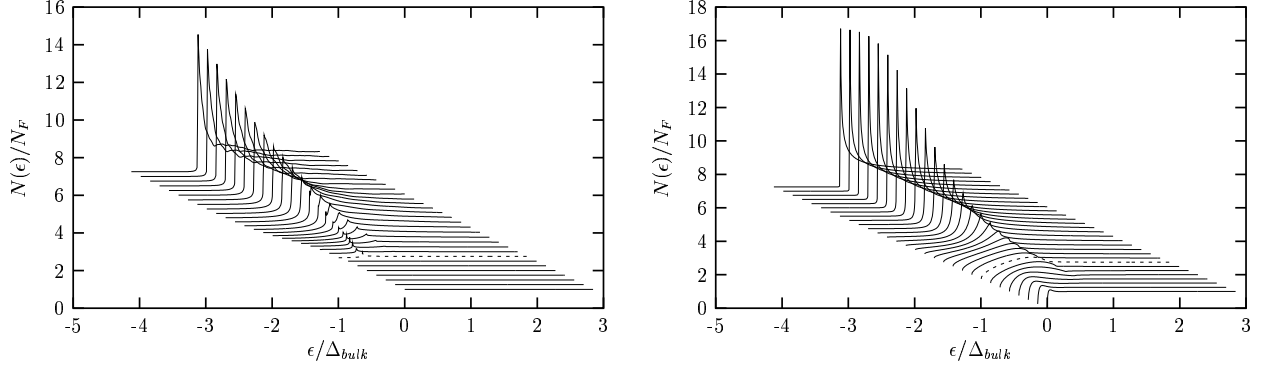


Figure 3.2: Density of states for a NS structure for  $T = 0.3 T_c$ ,  $l = \xi_0$ , and  $\sigma = 10^{-3}$ . The curves correspond to different positions in the structure, from bulk normal metal in the front towards homogeneous superconductor in the back. The dashed line displays the density of states at the interface. The graph on the left shows the result without self-consistency for the impurity self-energies. The density of states in the normal metal is unchanged while in the superconductor it is already altered by the proximity of the interface. The proximity effect in the normal metal only appears if the impurities are treated self-consistently which is shown in the right graph. Each curve starts at zero energy, with an additional vertical and horizontal offset.

of states although the order parameter does not vanish at low temperatures. Obviously, self-consistent impurity self-energies have to be achieved. The modification in the density of state in NS contacts was experimentally shown by Guéron *et al.* [50].

Apart from a mediation by impurities, particle-hole coherence in the normal metal can also be caused by a non-vanishing coupling constant. A self-consistent calculation of the order parameter then results in an order parameter induced in the normal metal which in turn changes the density of states.

A gap in the density of states of a normal metal can be induced by a superconductor not only if there is finite coupling in the metal, but already if impurities are present. Belzig *et al.* [51, 52] showed that a thin layer of normal metal on top of a superconductor develops a minigap in the dirty limit. The minigap decreases with increasing normal metal thickness and with increasing impurity lifetime. The size of the gap is constant throughout the whole layer, but the shape of the density of states changes with the distance from the interface. An equivalent geometry is a SNS structure. Figure 3.3 shows that a minigap already develops for an intermediate impurity lifetime,  $l = \xi_0$ , far from the dirty limit studied by the Usadel equations [16]. As in the dirty limit, the size of the minigap is independent of position, but the shape of the density of states varies in space. Similar results were published by Volkov *et al.* [53, 54], Golubov *et al.* [55, 56], and McMillan [57]. In the

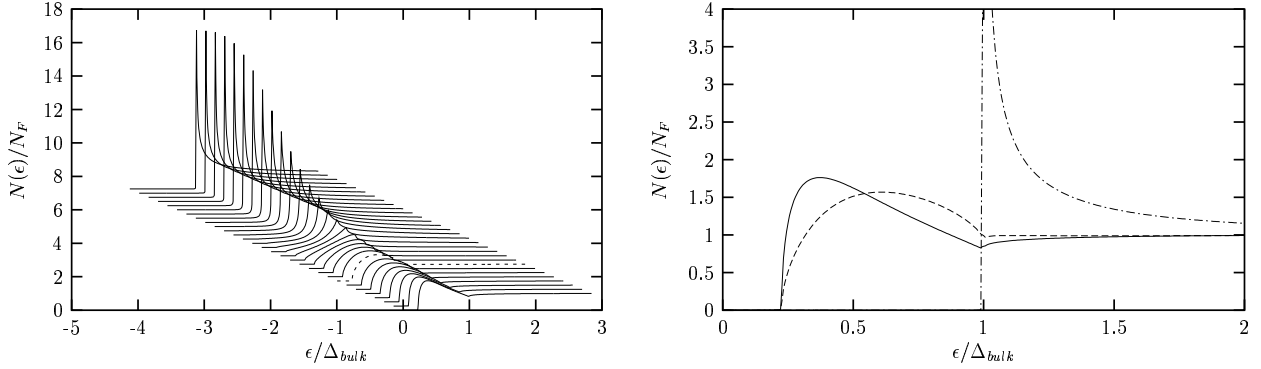


Figure 3.3: Density of states for a SNS structure for  $T = 0.3 T_c$ ,  $l = \xi_0$ , and  $\sigma = 10^{-3}$ . The thickness of the normal metal is  $\xi_0$ . The curves in the left graph correspond to different positions, from the centre of the normal metal for the curve in the front towards the bulk superconductor in the back of the graph. The dashed line shows the density of states at the interface. The impurity-induced proximity effect results in a minigap in the normal metal at the Fermi energy. Each curve starts at zero energy, with an additional vertical and horizontal offset. The graph on the right shows the density of states for three positions within the sandwich: the centre of the structure (solid line), the SN interface (dashed line), and far inside the superconductor (dotted-dashed line). The minigap is constant throughout the normal region.

clean limit, however, no gap in the excitation spectrum appears for arbitrary thickness of the normal layer. The situation is again different for a non-vanishing coupling constant in the normal layer which results in a gap in the density of states for any strength of coupling. These effects were already found by Saint-James [58] using the Bogolubov equations.

## 3.4 Linear response

### 3.4.1 Linearised quasiclassical equations

We are interested in the response of a superconductor to an external electromagnetic field. For sufficiently small perturbations this response can be studied by expanding the Green's functions and the self-energies up to linear order:

$$\check{g} = \check{g}_0 + \delta\check{g} \quad , \quad \check{\Delta} = \check{\Delta}_0 + \delta\check{\Delta} \quad , \quad \check{\sigma} = \check{\sigma}_0 + \delta\check{\sigma}. \quad (3.2)$$

The transport equation (2.2) and the normalization condition (2.3) read in linear order:

$$\left[ \check{\epsilon} - \check{h}_0, \delta \check{g} \right]_{\otimes} + i\hbar \mathbf{v}_f \cdot \nabla \delta \check{g} = \left[ \delta \check{h}, \check{g}_0 \right]_{\otimes} \quad , \quad \delta \check{g} \otimes \check{g}_0 + \check{g}_0 \otimes \delta \check{g} = \check{0} \quad . \quad (3.3)$$

In this form retarded, advanced, and Keldysh Green's functions are coupled even for given self-energies. By introducing the anomalous Green's function and self-energy,

$$\delta \hat{g}^a = \delta \hat{g}^K - \delta \hat{g}^R \otimes F + F \otimes \delta \hat{g}^A \quad , \quad (3.4)$$

$$\delta \hat{h}^a = \delta \hat{h}^K - \delta \hat{h}^R \otimes F + F \otimes \delta \hat{h}^A \quad , \quad \delta \hat{h}^K = \delta \hat{\sigma}_{imp}^K \quad , \quad F = \tanh \frac{\epsilon}{2k_B T} \quad , \quad (3.5)$$

both the transport equation as well as the normalization condition split up in three decoupled equations of the form:

$$\left[ \epsilon \hat{\tau}_3 - \hat{h}_0, \delta \hat{g} \right]_{\otimes} + i\hbar \mathbf{v}_f \cdot \nabla \delta \hat{g} = \left[ \delta \hat{h}, \hat{g}_0 \right]_{\otimes} \quad (3.6)$$

and

$$\delta \hat{g} \otimes \hat{g}_0 + \hat{g}_0 \otimes \delta \hat{g} = \hat{0} \quad , \quad (3.7)$$

respectively. Above, the indices  $R$ ,  $A$ , and  $a$  of the response functions have been dropped. Further, the retarded (advanced) equilibrium quantities must be chosen in the equations for the retarded (advanced) Green's functions and when they are multiplied by an anomalous function from the right (left). The full time-dependent quantities do not appear in the equations below. The index "0" indicating equilibrium can therefore be dropped for brevity.

For numerical calculations it is again advantageous to use the corresponding linearised Riccati equations. The expansion of the retarded and advanced Green's functions (2.18) then reads

$$\begin{aligned} \delta \hat{g}^{R,A} &= \mp 2\pi i \hat{N}_+^{R,A} \\ &\begin{pmatrix} \left( \delta \gamma^{R,A} \tilde{\gamma}_-^{R,A} + \gamma_+^{R,A} \delta \tilde{\gamma}^{R,A} \right) & \left( \delta \gamma^{R,A} + \gamma_+^{R,A} \delta \tilde{\gamma}^{R,A} \gamma_-^{R,A} \right) \\ - \left( \delta \tilde{\gamma}^{R,A} + \tilde{\gamma}_+^{R,A} \delta \gamma^{R,A} \tilde{\gamma}_-^{R,A} \right) & - \left( \delta \tilde{\gamma}^{R,A} \gamma_-^{R,A} + \tilde{\gamma}_+^{R,A} \delta \gamma^{R,A} \right) \end{pmatrix} \hat{N}_-^{R,A} \quad . \end{aligned} \quad (3.8)$$

The anomalous response function is parameterized by

$$\delta \hat{g}^a = -2\pi i \hat{N}_+^R \begin{pmatrix} \left( \delta x^a - \gamma_+^R \delta \tilde{x}^a \tilde{\gamma}_-^A \right) & - \left( \gamma_+^R \delta \tilde{x}^a - \delta x^a \gamma_-^A \right) \\ - \left( \tilde{\gamma}_+^R \delta x^a - \delta \tilde{x}^a \tilde{\gamma}_-^A \right) & \left( \delta \tilde{x}^a - \tilde{\gamma}_+^R \delta x^a \gamma_-^A \right) \end{pmatrix} \hat{N}_-^A \quad . \quad (3.9)$$

The elements of the Nambu-Gor'kov matrices  $\delta \hat{h}$  are defined as follows:

$$\delta \hat{h}^{R,A} = \begin{pmatrix} \delta \Sigma^{R,A} & \delta \Delta^{R,A} \\ \delta \tilde{\Delta}^{R,A} & \delta \tilde{\Sigma}^{R,A} \end{pmatrix} \quad , \quad \delta \hat{h}^a = \begin{pmatrix} \delta \Sigma^a & \delta \Delta^a \\ -\delta \tilde{\Delta}^a & -\delta \tilde{\Sigma}^a \end{pmatrix} \quad . \quad (3.10)$$

As we want to study the linear response for a fixed external frequency, the functions in the equations (3.8) and (3.9) have been Fourier transformed with respect to the time argument. The folding product (see appendix A) then simplifies to a matrix multiplication with an additional shift of the energy variable of the equilibrium quantities by  $\pm \hbar\omega/2$ . This shift is indicated by the indices “+” and “−”. The linear equations determining the Riccati matrices were derived by Eschrig [25, 26]. They are given by:

$$\begin{aligned} i\hbar\mathbf{v}_f \cdot \nabla \delta\gamma^{R,A} + 2\epsilon \delta\gamma^{R,A} - \left(\gamma^{R,A} \tilde{\Delta}^{R,A} + \Sigma^{R,A}\right)_+ \delta\gamma^{R,A} - \delta\gamma^{R,A} \left(\tilde{\Delta}^{R,A} \gamma^{R,A} - \tilde{\Sigma}^{R,A}\right)_- \\ = \gamma_+^{R,A} \delta\tilde{\Delta}^{R,A} \gamma_-^{R,A} + \delta\Sigma^{R,A} \gamma_-^{R,A} - \gamma_+^{R,A} \delta\tilde{\Sigma}^{R,A} - \delta\Delta^{R,A} , \end{aligned} \quad (3.11)$$

$$\begin{aligned} i\hbar\mathbf{v}_f \cdot \nabla \delta\tilde{\gamma}^{R,A} - 2\epsilon \delta\tilde{\gamma}^{R,A} - \left(\tilde{\gamma}^{R,A} \Delta^{R,A} + \tilde{\Sigma}^{R,A}\right)_+ \delta\tilde{\gamma}^{R,A} - \delta\tilde{\gamma}^{R,A} \left(\Delta^{R,A} \tilde{\gamma}^{R,A} - \Sigma^{R,A}\right)_- \\ = \tilde{\gamma}_+^{R,A} \delta\Delta^{R,A} \tilde{\gamma}_-^{R,A} + \delta\tilde{\Sigma}^{R,A} \tilde{\gamma}_-^{R,A} - \tilde{\gamma}_+^{R,A} \delta\Sigma^{R,A} - \delta\tilde{\Delta}^{R,A} , \end{aligned} \quad (3.12)$$

$$\begin{aligned} i\hbar\mathbf{v}_f \cdot \nabla \delta x^a + \hbar\omega \delta x^a - \left(\gamma^R \tilde{\Delta}^R + \Sigma^R\right)_+ \delta x^a - \delta x^a \left(\Delta^A \tilde{\gamma}^A - \Sigma^A\right)_- \\ = -\gamma_+^R \delta\tilde{\Sigma}^a \tilde{\gamma}_-^A + \delta\Delta^a \tilde{\gamma}_-^A + \gamma_+^R \delta\tilde{\Delta}^a - \delta\Sigma^a , \end{aligned} \quad (3.13)$$

$$\begin{aligned} i\hbar\mathbf{v}_f \cdot \nabla \delta\tilde{x}^a - \hbar\omega \delta\tilde{x}^a - \left(\tilde{\gamma}^R \Delta^R + \tilde{\Sigma}^R\right)_+ \delta\tilde{x}^a - \delta\tilde{x}^a \left(\tilde{\Delta}^A \gamma^A - \tilde{\Sigma}^A\right)_- \\ = -\tilde{\gamma}_+^R \delta\Sigma^a \gamma_-^A + \delta\tilde{\Delta}^a \gamma_-^A + \tilde{\gamma}_+^R \delta\Delta^a - \delta\tilde{\Sigma}^a . \end{aligned} \quad (3.14)$$

These linear equations have the same stability properties as the full equations, i.e.  $\delta\gamma^R$ ,  $\delta\tilde{\gamma}^A$ , and  $\delta x^a$  are stable in  $\mathbf{v}_f$  direction, while  $\delta\tilde{\gamma}^R$ ,  $\delta\gamma^A$ , and  $\delta\tilde{x}^a$  have to be solved in opposite direction.

These equations have to be supplemented by the self-energy equations in linear response. The corrections for the  $t$ -matrices are

$$\delta\hat{t}^{R,A}(\mathbf{p}_f, \mathbf{p}'_f) = N_f \left\langle \hat{t}_+^{R,A}(\mathbf{p}_f, \mathbf{p}''_f) \delta\hat{g}^{R,A}(\mathbf{p}''_f) \hat{t}_-^{R,A}(\mathbf{p}''_f, \mathbf{p}'_f) \right\rangle_{\mathbf{p}''_f} \quad (3.15)$$

and

$$\delta\hat{t}^a(\mathbf{p}_f, \mathbf{p}'_f) = N_f \left\langle \hat{t}_+^R(\mathbf{p}_f, \mathbf{p}''_f) \delta\hat{g}^a(\mathbf{p}''_f) \hat{t}_-^A(\mathbf{p}''_f, \mathbf{p}'_f) \right\rangle_{\mathbf{p}''_f} . \quad (3.16)$$

The response of the order parameter is calculated via

$$\delta\hat{\Delta}_{mf}(\mathbf{p}_f) = N_f \int_{-\epsilon_c}^{+\epsilon_c} \frac{d\epsilon}{4\pi i} \left\langle V(\mathbf{p}_f, \mathbf{p}'_f) \delta\hat{f}^K(\mathbf{p}'_f) \right\rangle_{\mathbf{p}'_f} . \quad (3.17)$$

Here,  $\delta\hat{f}^K$  stands for the off-diagonal part of the Keldysh response.

### 3.4.2 Local charge neutrality

The condition of charge neutrality leads to a self-consistency equation for the electrochemical potential which reads

$$e\delta\Phi = \int \frac{d\epsilon}{4\pi i} \frac{1}{4} \text{Tr}_4 \left\langle \delta \hat{g}^K(\mathbf{p}_f) \right\rangle_{\mathbf{p}_f} . \quad (3.18)$$

Eschrig [26] derived eq. (3.18), which is valid in leading order of the expansion parameter of Fermi-liquid theory, by applying an order-of-magnitude analysis to the Maxwell equations.

### 3.4.3 Analytic solution for homogeneous equilibrium

In general, the quasiclassical linear response equations have to be solved numerically. However, for systems with spatially homogeneous equilibrium analytical expressions can be achieved which can serve as a good starting point for iterating the self-consistency equations. An example of such a homogeneous system is a s-wave superconductor with a piecewise constant impurity lifetime characterising isotropic impurity scattering. As a consequence of the normalization condition (2.3), the quasiclassical propagator is independent of the space coordinate. The procedure described below then results in an expression which guarantees charge conservation and even charge neutrality. For systems with non-homogeneous equilibrium, e.g. a SNS contact, the analytical expression is a good starting point far away from the inhomogeneity. In one-dimensional systems charge conservation causes corrections to the self-energies in linear response even in regions with homogeneous equilibrium. This is the main reason why the partly analytical treatment is useful.

Let us consider a homogeneous s-wave superconductor with an isotropic impurity scattering, characterised by the lifetime  $\tau$ . The equilibrium Green's functions and self-energies then read

$$\hat{g}^{R,A}(\epsilon) = -\pi \frac{\epsilon \hat{\tau}_3 - \hat{\Delta}}{\sqrt{|\Delta|^2 - (\epsilon \pm i\eta)^2}} , \quad \hat{\sigma}^{R,A}(\epsilon) = \frac{1}{2\pi\tau} \left( \frac{\sqrt{1-\sigma}}{\sigma} \hat{1} + \hat{g}^{R,A}(\epsilon) \right) . \quad (3.19)$$

In the following, the self-energy term proportional to the unity matrix will be dropped as it commutes with the propagators for an energy-independent, dimensionless scattering cross section,  $\sigma$ , which we will assume here. In this case the commutator on the left hand side of eq. (3.6) can easily be calculated using the normalization condition (3.7):

$$\left[ \epsilon \hat{\tau}_3 - \hat{h}, \delta \hat{g} \right]_{\otimes} = C \hat{g} \otimes \delta \hat{g} = \begin{cases} C^{R,A} \hat{g}_+^{R,A} \delta \hat{g}^{R,A} \\ C^a \hat{g}_+^R \delta \hat{g}^a = -C^a \delta \hat{g}^a \hat{g}_-^A \end{cases} , \quad (3.20)$$

with

$$C^{R,A} = \frac{-1}{\pi} \left( \sqrt{|\Delta|^2 - (\epsilon + \hbar\omega/2 \pm i\eta)^2} + \sqrt{|\Delta|^2 - (\epsilon - \hbar\omega/2 \pm i\eta)^2} + \frac{\hbar}{\tau} \right) \quad (3.21)$$

and

$$C^a = \frac{-1}{\pi} \left( \sqrt{|\Delta|^2 - (\epsilon + \hbar\omega/2 + i\eta)^2} + \sqrt{|\Delta|^2 - (\epsilon - \hbar\omega/2 - i\eta)^2} + \frac{\hbar}{\tau} \right). \quad (3.22)$$

For evaluating the folding product a harmonic time dependence of the external perturbation with frequency  $\omega$  is assumed. The effect of the product is then a shift in the energy argument of the equilibrium quantity by  $\pm \hbar\omega/2$ , i.e. for any equilibrium quantity  $\hat{A}$  and response  $\delta\hat{X}$  the folding product can be simplified as follows:

$$\begin{aligned} \hat{A}(\epsilon) \otimes \delta\hat{X} &= \hat{A}(\epsilon + \hbar\omega/2) \delta\hat{X} =: \hat{A}_+ \delta\hat{X}, \\ \delta\hat{X} \otimes \hat{A}(\epsilon) &= \delta\hat{X} \hat{A}(\epsilon - \hbar\omega/2) =: \delta\hat{X} \hat{A}_-. \end{aligned} \quad (3.23)$$

Below, we intensively use the abbreviations

$$\{\delta\hat{X}\}_{\hat{g}} = \frac{1}{\pi^2} \hat{g}_+ \delta\hat{X} \hat{g}_- + \delta\hat{X} \quad \text{and} \quad [\delta\hat{X}]_{\hat{g}} = \delta\hat{X} \hat{g}_- - \hat{g}_+ \delta\hat{X}. \quad (3.24)$$

The symbols just introduced obey the relations

$$\hat{g}_+ [\delta\hat{X}]_{\hat{g}} = \pi^2 \{\delta\hat{X}\}_{\hat{g}} = -[\delta\hat{X}]_{\hat{g}} \hat{g}_- \quad \text{and} \quad \hat{g}_+ \{\delta\hat{X}\}_{\hat{g}} = -[\delta\hat{X}]_{\hat{g}} = -\{\delta\hat{X}\}_{\hat{g}} \hat{g}_-. \quad (3.25)$$

When a spatially constant electric field is now applied, we expect a constant linear response. For a contact of two metals with different bulk conductivities a constant current, which is required by charge conservation and charge neutrality, can only be achieved if the response is such that an additional electric field is induced. This corresponds to an electrochemical potential with a constant slope. Thus, we search for a solution of the form:

$$\delta\hat{g} = \delta\hat{g}_0 + \delta\hat{g}_1 z, \quad \delta\hat{h} = \delta\hat{h}_0 + \delta\hat{h}_1 z. \quad (3.26)$$

The transport equations then transform into

$$C \hat{g}_+ \delta\hat{g}_0 + i\hbar v_f \cos \vartheta \delta\hat{g}_1 = \delta\hat{h}_0 \hat{g}_- - \hat{g}_+ \delta\hat{h}_0 = [\delta\hat{h}_0]_{\hat{g}} \quad (3.27)$$

and

$$C \hat{g}_+ \delta\hat{g}_1 = \delta\hat{h}_1 \hat{g}_- - \hat{g}_+ \delta\hat{h}_1 = [\delta\hat{h}_1]_{\hat{g}}. \quad (3.28)$$

Multiplying by  $\hat{g}_+$  leads to

$$\delta\hat{g}_1 = \frac{-1}{C} \left\{ \delta\hat{h}_1 \right\}_{\hat{g}} \quad (3.29)$$

and

$$\delta\hat{g}_0 = \frac{-1}{C} \left\{ \delta\hat{h}_0 \right\}_{\hat{g}} + \frac{i\hbar v_f \cos \vartheta}{C^2 \pi^2} \left[ \delta\hat{h}_1 \right]_{\hat{g}} . \quad (3.30)$$

As the functions  $\delta\hat{h}_i$  themselves depend on  $\delta\hat{g}$ , we have not yet achieved a closed solution. In the subsequent steps, the self-consistency conditions have to be implemented in eqs. (3.29) and (3.30). The simplest self-consistency is that for the impurity self-energies as they do not couple different energies. Additionally, they do not couple retarded, advanced, and anomalous functions. The right hand side of eq. (3.29) does not depend on the angle  $\vartheta$  between the external field and a given trajectory because  $\delta\hat{h}_1$  contains only terms which are averaged over the Fermi surface. Hence, the spatially linear part of  $\delta\hat{g}$  is independent of the trajectory. As a consequence, the corresponding impurity self-energy is proportional to  $\delta\hat{g}_1$ . Equation (3.29) then simplifies using the normalization condition (3.7):

$$\delta\hat{\sigma}_1 = \frac{1}{2\pi\tau} \delta\hat{g}_1 \quad , \quad \delta\hat{g}_1 = \frac{1}{D} \left\{ \delta\hat{v}_1 \right\}_{\hat{g}} , \quad (3.31)$$

with

$$D = -C - \frac{\hbar}{\pi\tau} \quad , \quad \delta\hat{v}_1 = \delta\hat{h}_1 - \delta\hat{\sigma}_1 . \quad (3.32)$$

Equation (3.30) is now averaged over the Fermi surface to eliminate the spatially constant part of the impurity self-energy. The second term and the contribution of the external perturbation then vanish and the impurity self-energies are expressed through the electrochemical potential and the order parameter. Equation (3.30) can then be simplified to

$$\delta\hat{g}_0 = \frac{-1}{C} \left\{ \delta\hat{v}_{ext} \right\}_{\hat{g}} + \frac{1}{D} \left\{ \delta\hat{v}_0 \right\}_{\hat{g}} + \frac{i\hbar v_f \cos \vartheta}{CD\pi^2} \left[ \delta\hat{v}_1 \right]_{\hat{g}} , \quad (3.33)$$

$$\delta\hat{v}_{ext}^{R,A} = \frac{-e}{c} v_f \delta A \cos \vartheta \hat{\tau}_3 \quad , \quad \delta\hat{v}_{ext}^a = (F_+ - F_-) \delta\hat{v}_{ext}^{R,A} . \quad (3.34)$$

The expressions  $\delta\hat{v}_{0,1}$  contain the order-parameter response as well as the electrochemical potential. The calculation of these involves an energy integral of suitable traces of the Keldysh response function. Thus,  $\delta\hat{v}_{0,1}$  not only couple the three types of functions but also all energies. The Keldysh response is given by the following formulae:

$$\delta\hat{g}^K = F_- \delta\hat{g}^R - F_+ \delta\hat{g}^A + \delta\hat{g}^a = \delta\hat{g}_0^K + \delta\hat{g}_1^K z , \quad (3.35)$$

$$\begin{aligned}
 \delta \hat{g}_0^K &= F_- \left\{ \frac{-1}{C^R} \left\{ \delta \hat{v}_{ext}^R \right\}_{\hat{g}} + \frac{1}{D^R} \left\{ \delta \hat{v}_0^R \right\}_{\hat{g}} + \frac{i\hbar v_f \cos \vartheta}{\pi^2 C^R D^R} \left[ \hat{v}_1^R \right]_{\hat{g}} \right\} \\
 &- F_+ \left\{ \frac{-1}{C^A} \left\{ \delta \hat{v}_{ext}^A \right\}_{\hat{g}} + \frac{1}{D^A} \left\{ \delta \hat{v}_0^A \right\}_{\hat{g}} + \frac{i\hbar v_f \cos \vartheta}{\pi^2 C^A D^A} \left[ \hat{v}_1^A \right]_{\hat{g}} \right\} \\
 &+ \left\{ \frac{-1}{C^a} \left\{ \delta \hat{v}_{ext}^a \right\}_{\hat{g}} + \frac{-1}{D^a} \left\{ \delta \hat{v}_0^a \right\}_{\hat{g}} + \frac{i\hbar v_f \cos \vartheta}{\pi^2 C^a D^a} \left[ \hat{v}_1^a \right]_{\hat{g}} \right\} ,
 \end{aligned} \tag{3.36}$$

$$\begin{aligned}
 \delta \hat{g}_1^K &= F_- \frac{1}{D^R} \left\{ \delta \hat{v}_1^R \right\}_{\hat{g}} - F_+ \frac{1}{D^A} \left\{ \delta \hat{v}_1^A \right\}_{\hat{g}} + \frac{1}{D^a} \left\{ \delta \hat{v}_1^a \right\}_{\hat{g}} , \\
 \delta \hat{v}_i^{R,A} &= \delta \hat{\Delta}_i + e \delta \hat{\Phi}_i , \quad \delta \hat{v}_i^a = (F_+ - F_-) \delta \hat{v}_i^{R,A} , \quad i = 0, 1 .
 \end{aligned} \tag{3.37}$$

These equations have to be supplemented by the self-consistency equations

$$\delta \hat{\Delta} = N_f \int_{\epsilon_c}^{\epsilon_c} \frac{d\epsilon}{4\pi i} \langle V \delta f^K \rangle_{\mathbf{p}_f} \quad \text{and} \quad e \delta \hat{\Phi} = e \delta \Phi \hat{1} = \hat{1} \int \frac{d\epsilon}{4\pi i} \frac{1}{2} Tr \langle \delta \hat{g}^K \rangle_{\mathbf{p}_f} . \tag{3.38}$$

Equations (3.35) to (3.38) correspond to an eigenvalue problem of the form

$$\begin{pmatrix} e \delta \hat{\Phi} \\ \delta \hat{\Delta} \end{pmatrix} = M \begin{pmatrix} e \delta \hat{\Phi} \\ \delta \hat{\Delta} \end{pmatrix} . \tag{3.39}$$

The elements of the matrix  $M$  are given by the integrals in eq. (3.38) and were evaluated numerically. The solution of this linear equation fixes  $\delta \hat{\Delta}$  when  $e \delta \hat{\Phi}$  is chosen. The electrochemical potential itself is then determined by requiring continuity and charge conservation. For a metal with constant coupling constant and piecewise constant impurity lifetime this leads to the exact result for the electrochemical potential. The propagator itself, however, has additional, exponentially decaying contributions which ensure continuity of the propagator at the inhomogeneities and a smooth change in the spectral current density. These have to be calculated numerically. If the coupling constant also varies, e.g. in a NSN contact, then the equilibrium Green's functions are not homogeneous near the contacts and a full numerical calculation is already needed for the electrochemical potential. However, by ignoring the changes near the contacts the procedure described above provides a good guess as starting point for the iteration of the self-energies which already guarantees charge conservation and charge neutrality at distances of a few coherence lengths from the contacts.

In the case of a vanishing coupling constant, i.e. a normal metal, the equations simplify drastically. The eigenvalue problem (3.39) reduces to an identity, i.e. holds automatically for any value of the electrochemical potential. Matching the currents for a system consisting of two wires with different resistivities then leads to the simple result already given by Ohm's law and the continuity equation, i.e. a jump of the electric field at the contact. This



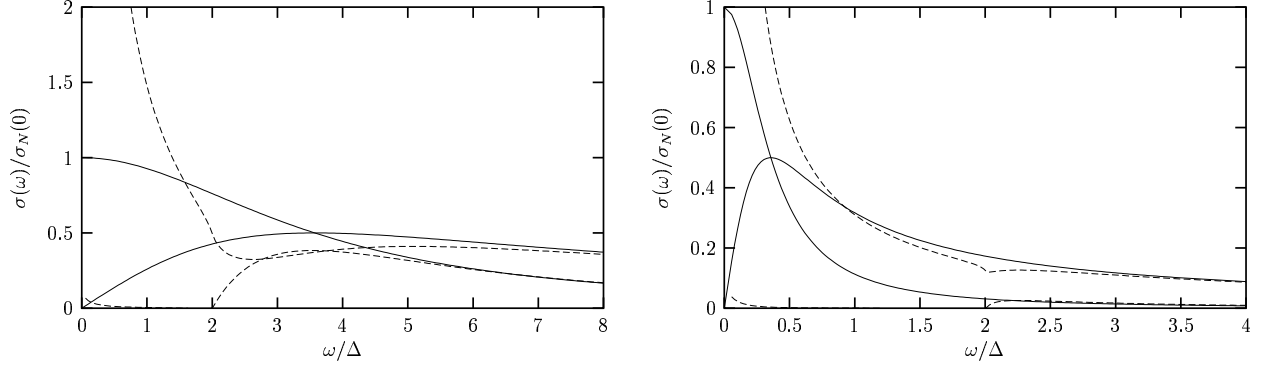


Figure 3.4: Frequency-dependent conductivity for a homogeneous superconductor (dashed lines) and a normal metal (solid lines) at  $T = 0.3 T_c$ . The curves are normalised by the static Drude conductivity. In the superconductor, the reactive part of the conductivity diverges for low frequency and significant dissipation only starts for  $\omega = 2 \Delta$ . On the left graph the impurity mean free path equals the coherence length while on the right  $l = 10 \xi_0$ .

discontinuity corresponds to charges bound to an atomic neighbourhood of the contacts. Although these length scales are not accessible for the quasiclassical theory, the surface charges are correctly taken into account as the theory is a conserving approximation up to first order in the expansion parameters.

In addition to the surface charges there are charges spread over the contact region with the coherence length and the impurity mean free path as the characteristic length scales for any system with non-homogeneous equilibrium Green's functions. To study these problems the full theory is needed and will be applied in the succeeding section. Remarkably, Ohm's law, charge conservation, and charge neutrality already suffices for calculating the current for any one-dimensional series like SNS, NSN, etc..

### 3.5 Numerical results

The externally applied field has the form  $\delta \mathbf{E}^{ext}(t) = \delta E^{ext} e^{-i\omega t} \mathbf{e}_z$ . With  $\mathbf{E} = -\frac{1}{c} \frac{\partial \mathbf{A}}{\partial t}$  the perturbation in eq. (2.5) reads

$$\delta \hat{v}_{ext}(t) = \frac{e \mathbf{v}_f \cdot \delta \mathbf{E}^{ext}(t)}{-i\omega} \hat{\tau}_3. \quad (3.40)$$

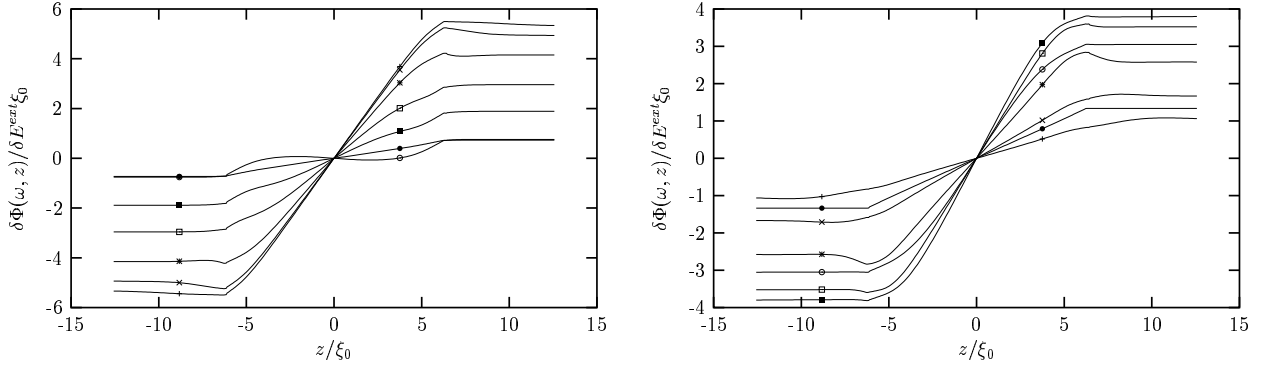


Figure 3.5: Electrochemical potential,  $\delta\Phi(\omega, z)$ , in a NSN structure. The thickness of the superconducting film is  $4\pi \xi_0$ ,  $l_N = \xi_0 = 0.5 l_S$ , and  $T = 0.3 T_c$ . The discontinuous impurity lifetime leads to a kink in the electrochemical potential at the interfaces (at  $z = \pm 2\pi \xi_0$ ). On the left the in-phase component is plotted for frequencies  $\omega/\Delta = 0.28, 0.57, 1.1, 1.7, 2.0, 2.3$ , and  $5.7$  (bottom to top at  $z = -10 \xi_0$ ). The right plot shows the out-of-phase component for frequencies as indicated by the symbols defined in the first plot.

The calculations are performed for the Fourier transformed quantities which favours the complex external field in eq. (3.40). For the discussion below we take the real part of this field,  $\delta E^{ext} \cos \omega t$ . The real part of the response functions  $\delta X(\omega)$  then gives the component which is in phase with the external perturbation while the imaginary part describes the component which is delayed by  $\pi/2$  having the time dependence  $\sin \omega t$ . Note that in the rest of this chapter and the corresponding figures  $\hbar = 1$ .

### 3.5.1 Electrochemical potential and electric field

As a consequence of charge neutrality an electrochemical potential is built up in the systems under study which in turn induces an internal electric field. The external and internal fields are of same order of magnitude and sum up to the total electric field

$$\mathbf{E}^{tot}(t) = \mathbf{E}^{ext}(t) - \nabla \delta\Phi(t) . \quad (3.41)$$

Figure 3.5 shows the electrochemical potential for a superconductor sandwiched between two identical metals for various frequencies. The superconducting film has a width  $d_S = 4\pi \xi_0$  which is thick enough to have little interference between the two NS interfaces. This is the reason why the global shape looks very much like the one the analytical treatment described above predicts, i.e. a constant gradient connecting the two plateaus in the normal

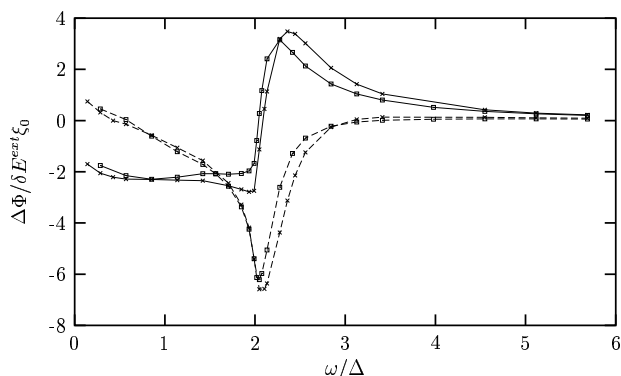


Figure 3.6: Electrochemical potential drop,  $\Delta\Phi$ , in a NSN structure. The thickness of the superconducting film is  $4\pi \xi_0$ ,  $l_N = \xi_0$ , and  $T = 0.3 T_c$ . The potential drop which would appear without any proximity effect is subtracted. Thus,  $\Delta\Phi$  represents the drop at the interfaces only. Solid lines belong to the component which is in phase with the external field, dashed lines to a time dependence  $\sin \omega t$ . Crosses indicate an impurity mean free path  $l_S = \xi_0$ , squares correspond to  $l_S = 2 \xi_0$ . The step in the impurity lifetime has little effect on  $\Delta\Phi$ .

electrodes. Near the interfaces, however, the detailed shape clearly differs from a ramp. The kink directly at the interfaces is less pronounced. Instead of surface charges only, the self-consistent solution needs both, charges localised atomically close to the interfaces and charges spread over the whole contact. The charge bound to the interface is a consequence of the discontinuity of the impurity mean free path and disappears if the change takes place on a length scale accessible by the quasiclassical theory. The total charge is zero as the structure, when seen from large distances, is equivalent to an uncharged capacitor. As a measure for the effect the proximity of superconductor and normal metal has on the dynamical behaviour one may take the height of the ramp reduced by the potential drop calculated by neglecting the proximity effects:

$$\Delta\Phi(\omega) = \delta\Phi(\omega, z = \infty) - \delta\Phi(\omega, z = -\infty) - \frac{-\sigma_N}{\sigma_S} \delta E^{ext} d_S. \quad (3.42)$$

Here,  $\sigma_N$  and  $\sigma_S$  are the bulk conductivities of the normal metal and the superconductor, respectively (see fig. 3.4). The frequency dependence of  $\Delta\Phi$  is shown in fig. 3.6.

In contrast to this global measure of the proximity effect, the local electric field gives information on spatial dependencies. Figure 3.9 shows the total electric field for a single NS contact. The field varies slowly between the bulk values which are already given by Ohm's law and charge conservation. The fact that the field does not vanish deep inside the superconductor for frequencies  $\omega < 2 \Delta$  is due to the time-dependent current. Field and current are  $90^\circ$  out of phase. The field only accelerates the current, no damping occurs (see fig. 3.17). The spatial structures disappear for larger frequencies as the two electrodes are then practically identical metals.

The situation is different if the impurity lifetime changes abruptly at an interface. This

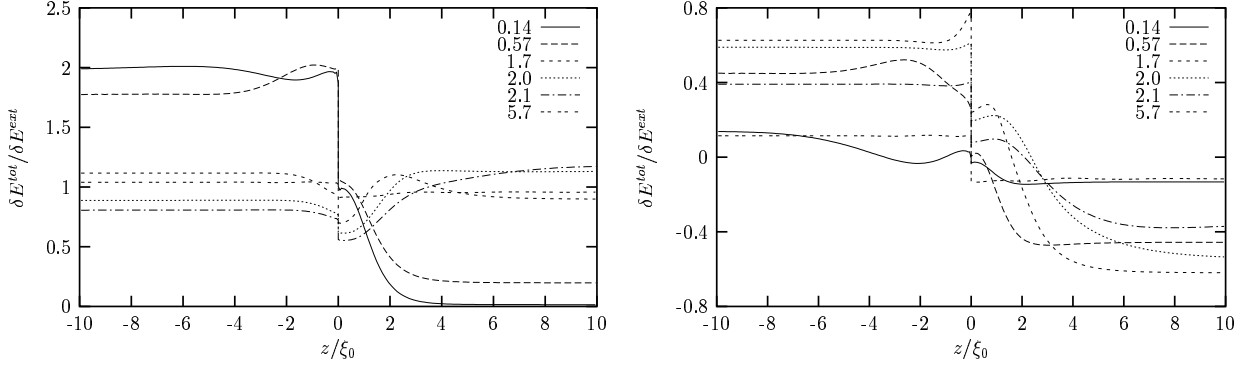


Figure 3.7: Total electric field,  $E^{tot}(\omega, z)$ , in a NS contact. The change of the coupling constant is smeared over one coherence length. The interface is positioned at  $z = 0$ . The impurity mean free path is discontinuous at the interface,  $l_N = \xi_0$  and  $l_S = 2 \xi_0$  (Born limit),  $T = 0.3 T_c$ . The legends indicate the value of  $\omega/\Delta$ . The step in the impurity lifetime results in a discontinuity in the total electric field which is due to surface charges localised at the interface. The left (right) graph belongs to the component in phase (out of phase) with the external field.

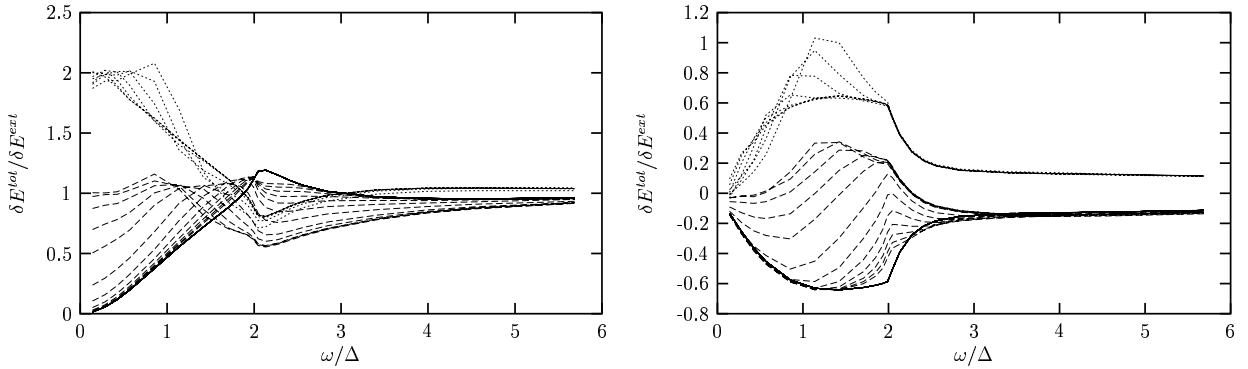


Figure 3.8: Total electric field,  $E^{tot}(\omega, z)$ , in a NS contact. The change in the coupling constant is smeared over one coherence length. The interface is positioned at  $z = 0$ . The impurity mean free path is discontinuous at the interface,  $l_N = \xi_0$  and  $l_S = 2 \xi_0$  (Born limit),  $T = 0.3 T_c$ . Dashed lines correspond to increasing distance from the interface on the superconducting side (top to bottom at low frequencies), dotted lines stand for different positions inside the normal metal, and solid lines belong to the fields far away from the interface. The left (right) graph belongs to the component in phase (out of phase) with the external field.

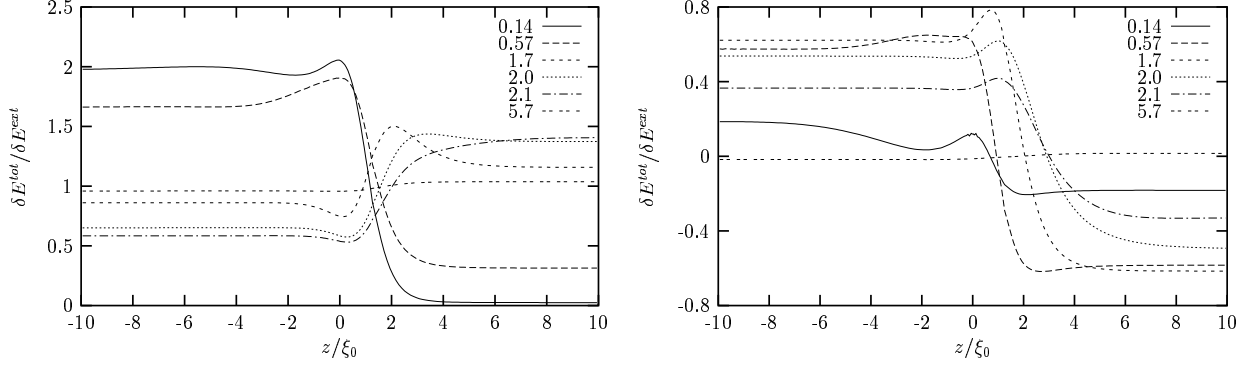


Figure 3.9: Total electric field,  $E^{tot}(\omega, z)$ , in a NS contact. The change of the coupling constant is smeared over one coherence length. The interface is positioned at  $z = 0$ . The impurity mean free path,  $l$  (Born limit), equals the coherence length,  $\xi_0$ , and  $T = 0.3 T_c$ . The legends indicate the value of  $\omega/\Delta$ . The left (right) graph belongs to the component in phase (out of phase) with the external field.

results in a discontinuous total electric field which can be seen in fig. 3.7. The step is solely caused by the impurities, the discontinuity of the order parameter does not produce such an effect. This is demonstrated in figs. 3.10 and 3.11 where the field has sharp features at the interfaces but is continuous everywhere if the impurity lifetime is smooth. The frequency dependence of the field step is plotted in fig. 3.12. The self-consistent calculation results in a smaller step when compared with the non-self-consistent one. Also, the sharp feature at the gap edge  $\omega = 2 \Delta_0$  is smoothened. The figs. 3.7, 3.10, and 3.11 show a peak of the electric field inside the superconductor which moves with frequency. The peak position roughly follows the local gap edge  $\omega = 2 \Delta(z)$ .

From figs. 3.7 to 3.11 it is apparent that on the side of the normal metal the characteristic length scale for the electric field to relax to the bulk value substantially increases for low frequencies. This is due to the fact that the energy shift  $\pm \omega/2$  then connects equilibrium states which can both lie near the Fermi level where the proximity effect of the superconductor is strongest.

### 3.5.2 Minicharges

The extremely good screening in metals for frequencies well below the plasma frequency leads to a very effective suppression of charge fluctuations, i.e. to local charge neutrality, which in turn allows us to calculate the electrochemical potential via eq. (3.18). The laws

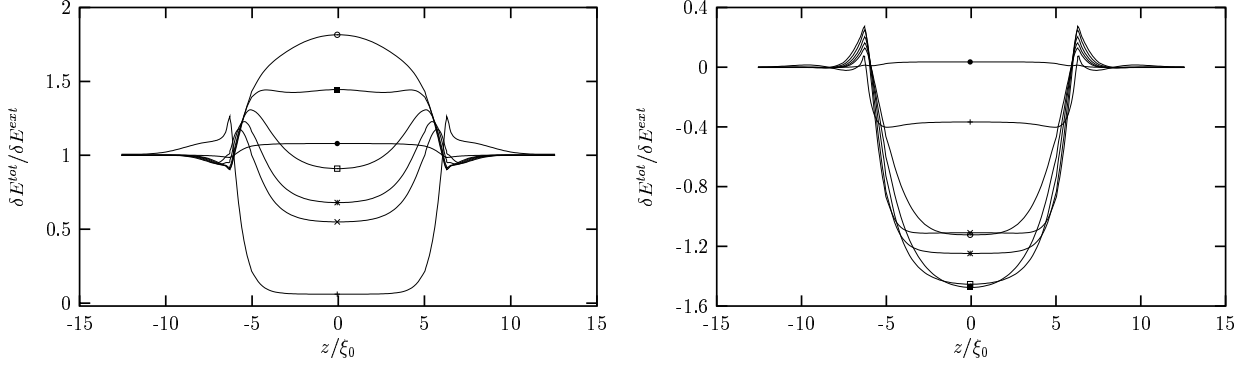


Figure 3.10: Total electric field,  $E^{tot}(\omega, z)$ , in a NSN structure with discontinuous coupling constant. The impurity mean free path,  $l$  (Born limit), equals the coherence length,  $\xi_0$ , the thickness of the superconducting film is  $4\pi \xi_0$ , and  $T = 0.3 T_c$ . Plotted on the left is the component which is in phase with the externally applied field, i.e.  $\sim \cos \omega t$ . The curves correspond to  $\omega/\Delta = 0.6, 1.7, 1.8, 2.0, 2.1, 2.3$ , and  $5.7$  (from bottom to top at  $z = 0$ ). The right graph shows the field component  $\sim \sin \omega t$ . The symbols indicate frequencies as defined on the left.

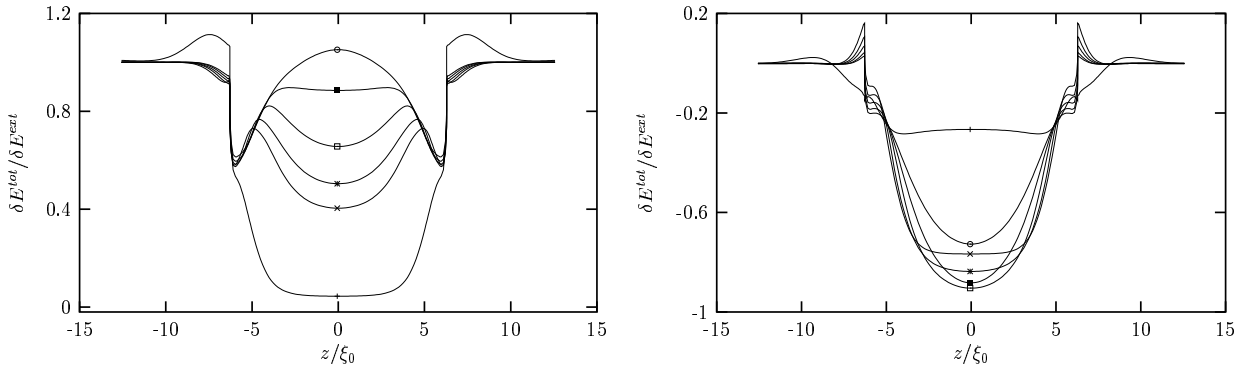


Figure 3.11: Total electric field,  $E^{tot}(\omega, z)$ , in a NSN structure with discontinuous coupling constant and impurity mean free paths  $l_N = \xi_0$  and  $l_S = 2 \xi_0$ . The thickness of the superconducting film is  $4\pi \xi_0$ ,  $T = 0.3 T_c$ . The discontinuity in the impurity lifetime results in a step of the electric field which is caused by surface charges. The component which is in phase with the externally applied field, i.e.  $\sim \cos \omega t$ , is displayed in the left graph. The curves correspond to  $\omega/\Delta = 0.6, 1.7, 1.8, 2.0, 2.1$ , and  $2.3$  (from bottom to top at  $z = 0$ ). The other graph shows the field component  $\sim \sin \omega t$ . The symbols indicate the frequencies as defined on the left.

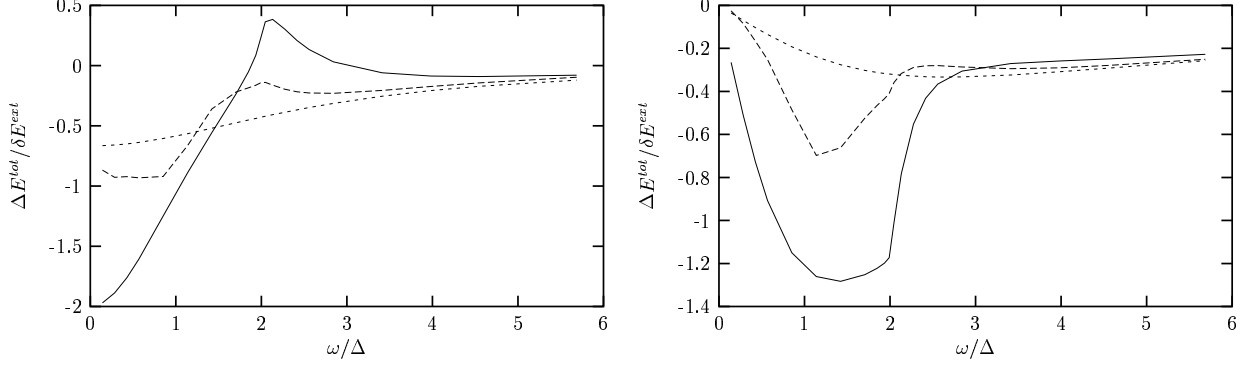


Figure 3.12: Discontinuity of the total electric field,  $\Delta E^{tot}(\omega)$ , at the interface of a NS contact. The change in the coupling constant is smeared over one coherence length. The impurity mean free path is discontinuous at the interface,  $l_N = \xi_0$  and  $l_S = 2 \xi_0$  (Born limit),  $T = 0.3 T_c$ . The long-dashed line is the fully self-consistent solution, the solid line shows the solution without any proximity effect, and the dashed curve corresponds to a NN contact with the same impurity lifetimes. The left (right) graph belongs to the component in phase (out of phase) with the external field.

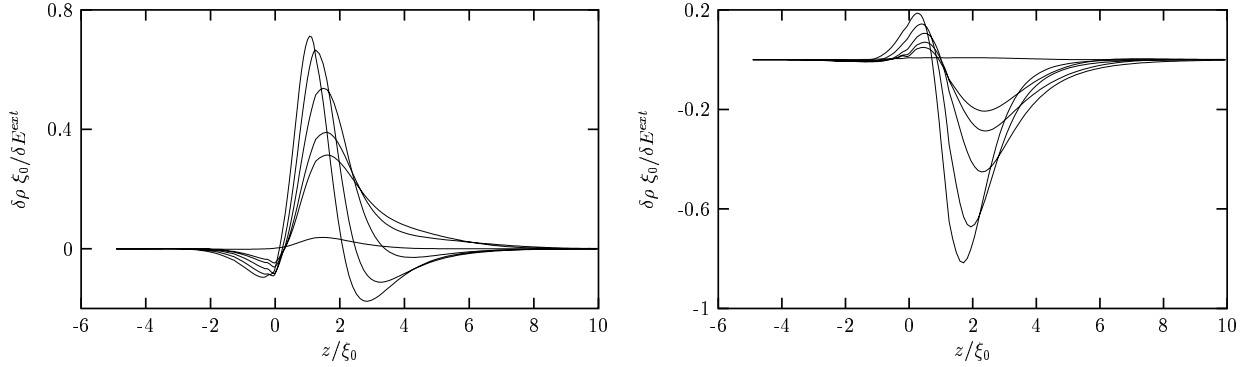


Figure 3.13: Induced charge density in a NS contact. The change in the coupling constant is smeared over one coherence length. The interface is positioned at  $z = 0$ . The impurity mean free path,  $l_S = l_N$  (Born limit), equals the coherence length,  $\xi_0$ , and  $T = 0.3 T_c$ . The curves correspond to  $\omega/\Delta = 1.7, 1.8, 2.0, 2.1, 2.3$ , and  $5.7$ . For the component in phase with the external field (left graph) the maxima decrease with increasing frequency. On the right: the component  $\sim \sin \omega t$  shows minima which increase with frequency.

of electrodynamics then require a charge density

$$\delta\rho = -\nabla^2\delta\Phi(\mathbf{r}, t) . \quad (3.43)$$

This is not in contradiction to charge neutrality just stated above. The electrochemical potential is of first order in the expansion parameter of the Fermi-liquid theory. Quasiclassical propagators vary on a scale given by the coherence length which is large when compared with atomic length scales which means that derivatives are of order  $1/\xi$ . Hence, the charge densities defined in eq. (3.43) are of third order in the expansion parameters while the quasiclassical theory takes only the leading order into account. However, the minicharges spread over many coherence lengths and their contribution to the electric field can therefore not be neglected, i.e. a self-consistent calculation of the electrochemical potential is necessary.

In fig. 3.13 the charge density for a NS contact with constant impurity lifetime is plotted. The charge densities have strong peaks inside the superconductor while only little charge is induced in the normal metal. The total charge localised near the contact is non-zero. It is simply given by the difference of the bulk electric field on both sides of the contact. The charging of the contact cannot be described in leading order Fermi-liquid theory which predicts a spatially constant current which is of first order in the expansion parameter. But this does not lead to an inconsistency as an inhomogeneity of the current in next to leading order acting for a short time given by the plasma frequency already suffices to charge the contact. Thus, the time dependence of this minicharge is clearly a higher order process, but its effect is already correctly dealt with in leading order.

### 3.5.3 Dissipation

We define a local dissipation in the contact by the time averaged quantity

$$P(z, \omega) = \int_0^{2\pi/\omega} \delta\mathbf{j}(t) \cdot \delta\mathbf{E}^{tot}(z, t) dt . \quad (3.44)$$

The proximity to a superconductor causes an increased dissipation in the normal metal close to the interfaces for  $\omega$  smaller than  $2\Delta$ . Above the gap edge there is hardly any space dependence in the normal metal (see figs. 3.14 to 3.18). At frequencies comparable with the gap edge the peak in the local dissipation moves inside the superconductor for NS or NSN structures until it finally disappears for  $\omega$  much larger than  $2\Delta$ .



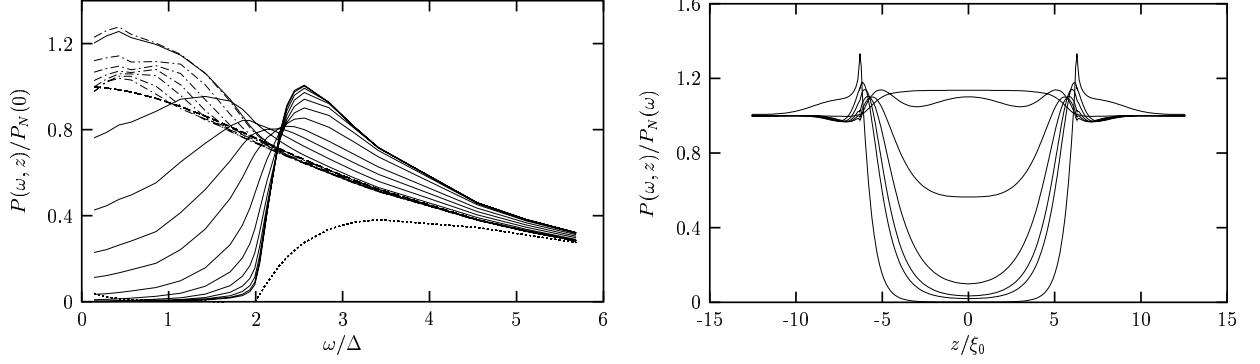


Figure 3.14: Local dissipation,  $P(\omega, z)$ , in a NSN structure with discontinuous coupling constant. The thickness of the superconducting film is  $4\pi \xi_0$ ,  $l = \xi_0$  (Born limit), and  $T = 0.3 T_c$ . The frequency dependence of the local dissipation is plotted in the graph on the left. The solid lines show the local dissipation inside the superconducting film for increasing distances from the interface (top to bottom at small frequencies). For the largest distances from the interfaces, i.e. at the centre of the structure, the dissipation is close to that of a homogeneous superconductor for  $\omega < 2 \Delta_0$  but substantially increased for larger frequencies. The dotted-dashed lines belong to different positions inside the normal metal. The dashed (dotted) line corresponds to the dissipation in a homogeneous normal metal (superconductor). The curves are normalised by the dissipation of a normal metal at vanishing frequency,  $P_N(0)$ . On the right, the space dependence of the local dissipation is shown. The contacts are at  $z = \pm 2\pi \xi_0$ , the curves correspond to  $\omega/\Delta = 0.6, 1.7, 1.8, 2.0, 2.1, 2.3$ , and  $5.7$  (from bottom to top at  $z = 0$ ). The curves are normalised by the dissipation of a homogeneous normal metal,  $P_N(\omega)$ .

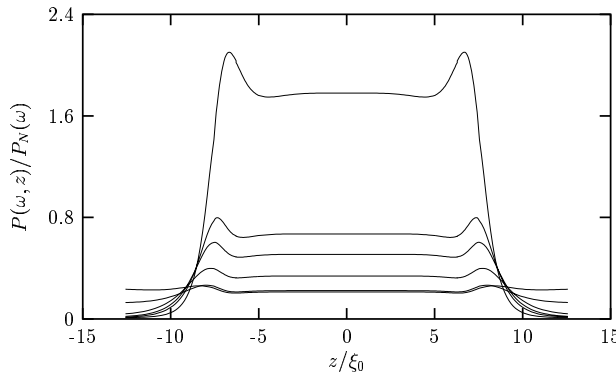


Figure 3.15: Local dissipation,  $P(\omega, z)$ , in a SNS structure. The change in the coupling constant is smeared over one coherence length. The impurity mean free path,  $l$  (Born limit), equals the coherence length,  $\xi_0$ , the thickness of the normal metal film is  $4\pi \xi_0$ , and  $T = 0.3 T_c$ . The contacts are at  $z = \pm 2\pi \xi_0$ , the curves correspond to  $\omega/\Delta = 1.1, 1.7, 1.8, 2.0, 2.1$ , and  $2.3$  (from top to bottom at  $z = 0$ ).

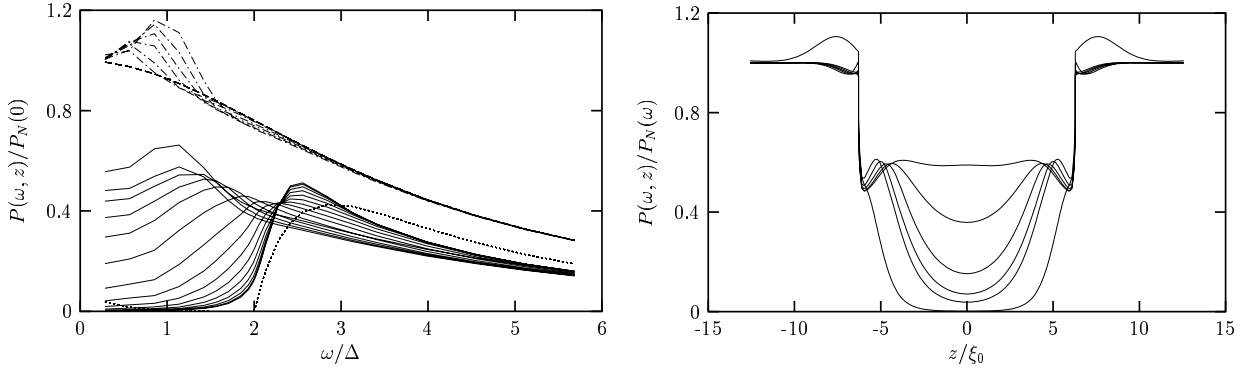


Figure 3.16: Local dissipation,  $P(\omega, z)$ , in a NSN structure with discontinuous coupling constant and impurity mean free path,  $l_N = \xi_0$  and  $l_S = 2 \xi_0$ . The thickness of the superconducting film is  $4\pi \xi_0$ ,  $T = 0.3 T_c$ . The left plot displays the frequency dependence of the local dissipation for various positions in the superconductor (solid lines) and the normal metal (dashed-dotted line). The dashed (dotted) line corresponds to the dissipation in a homogeneous normal metal (superconductor). The second plot shows the space dependence of the local dissipation. The contacts are at  $z = \pm 2\pi \xi_0$ , the curves correspond to  $\omega/\Delta = 0.6, 1.7, 1.8, 2.0, 2.1, 2.3$ , and  $5.7$  (from bottom to top at  $z = 0$ ).

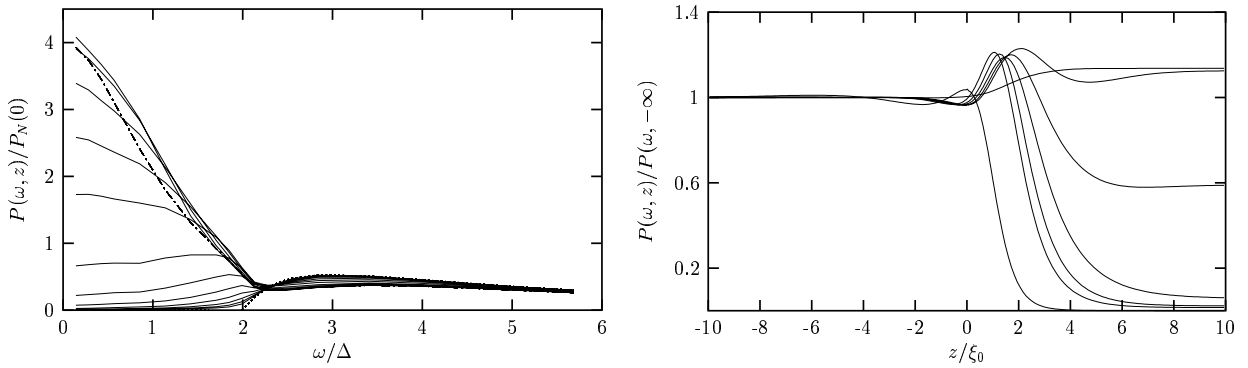


Figure 3.17: Local dissipation,  $P(\omega, z)$ , for a NS contact at  $z = 0$ . The change in the coupling constant is smeared over one coherence length,  $l = \xi_0$  (Born limit), and  $T = 0.3 T_c$ . The frequency dependence of the local dissipation is illustrated on the left. The solid lines display the local dissipation inside the superconductor for increasing (from top to bottom at low frequencies) distance from the interface. The dotted-dashed (dotted) line corresponds to the dissipation in the normal metal (superconductor) without any proximity effect. The right graph shows the space dependence of the local dissipation. The curves correspond to  $\omega/\Delta = 0.14, 1.7, 1.8, 2.0, 2.1, 2.3$ , and  $5.7$  (from bottom to top at  $z = 5 \xi_0$ ).

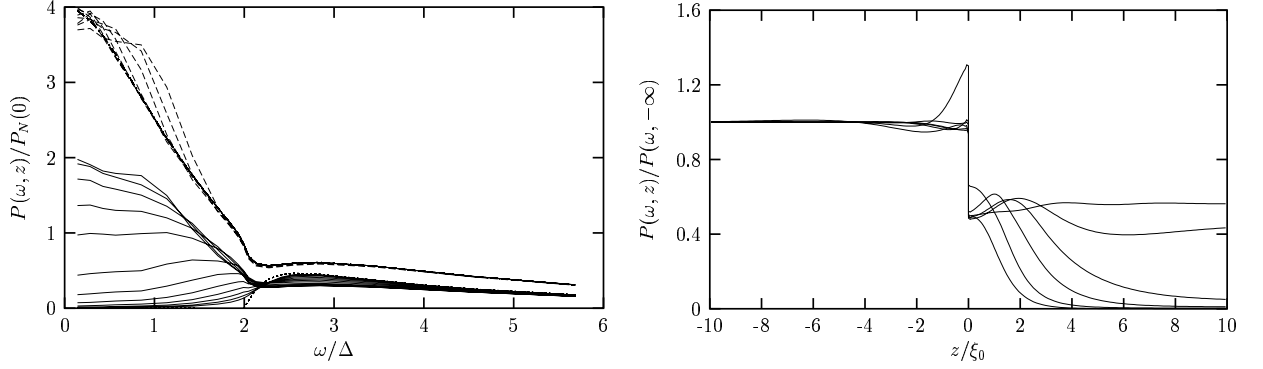


Figure 3.18: Local dissipation,  $P(\omega, z)$ , for a NS contact for the same parameters as in fig. 3.17, but a discontinuous impurity mean free path at the interface,  $l_N = \xi_0$  and  $l_S = 2 \xi_0$ . The graph on the left illustrates the frequency dependence of the local dissipation. The solid lines display the local dissipation inside the superconductor for increasing (from top to bottom at low frequencies) distance from the interface, the dashed lines correspond to different positions inside the normal metal. The dotted-dashed (dotted) line corresponds to the dissipation in the normal metal (superconductor) without any proximity effect. The space dependence of the local dissipation is shown on the right. The curves correspond to  $\omega/\Delta = 0.14, 1.1, 1.7, 2.0, 2.1$ , and  $5.7$  (from bottom to top at  $z = 5 \xi_0$ ). For  $\omega = 1.1 \Delta$  there is a strong peak in the local dissipation of the normal metal.



# Chapter 4

## Weak links in superfluid $^3\text{He}$

### 4.1 Introduction

Since the prediction of coherent coupling between superconductors connected by a weak link by Josephson [59] in 1962 there has been intensive work by both theoreticians and experimentalists on its fundamental principles and the applications in, e.g., superconducting quantum interference devices (SQUIDs). A review on weak links in superconductors was, e.g., written by Likharev [60]. The discovery of high- $T_c$  superconductors has reinforced activity on phase-sensitive phenomena like the Josephson effect to determine the unconventional pairing symmetry in these new materials. To the most spectacular belong the tri-crystal experiments by Kirtley *et al.* [61, 62] which strongly support the  $d_{x^2-y^2}$  pairing symmetry in cuprate superconductors. In analogy to superconductors, the quantum liquids  $^4\text{He}$  and  $^3\text{He}$  were also expected to show dissipationless, phase-dependent current flow between two reservoirs connected via small pores. Close to the transition temperature Josephson predicted a sinusoidal current phase relation,

$$I(\phi) = I_c \sin \phi, \quad (4.1)$$

where  $\phi$  is the difference of the macroscopic phases on both sides of the weak link. As a requirement for observing this oscillatory current, the weak link (orifice in helium or e.g. insulating layer in superconductors) must have characteristic dimensions comparable to the coherence length. Eventually, this requirement is always met as the coherence length diverges at  $T_c$ . However, close to the phase transition fluctuations may become too large to observe the effect. Due to the small coherence lengths ( $\xi_0 = 70 \text{ nm}$  in  $^3\text{He}$  [63] and

$\xi_0 = 0.15 \text{ nm}$  in  $^4\text{He}$  [64], both at zero pressure) it needed considerable effort to confirm this effect experimentally whereas in conventional superconductors this can be achieved by standard methods of semiconductor technology. In 2001 the Josephson effect was observed in the Bose condensate of  $^4\text{He}$  by Sukhatme *et al.* [65]. In the Fermi liquid  $^3\text{He}$  experimental evidence was achieved by Avenel and Varoquaux [64, 66] more than ten years earlier.

Pereverzev *et al.* [67] showed that a whole array of weak links can be described by a single one. Their weak link consisted of a  $50 \text{ nm}$  thick silicon nitride membrane with a square array of  $65 \times 65$  apertures separating two reservoirs of superfluid  $^3\text{He}$ . The spacing of the pores was  $3 \mu\text{m}$ , their diameter  $100 \text{ nm}$  each. Driving a second membrane by an applied voltage a pressure difference,  $p(t)$ , was created between the reservoirs. The analogue of the ac Josephson effect describes the time evolution of the phase difference for a given pressure difference through the equation [68]

$$\hbar \frac{\partial \phi(t)}{\partial t} = -\mu(t) = -\frac{2m p(t)}{\rho} . \quad (4.2)$$

In eq. (4.2)  $\mu$  stands for the difference in chemical potential,  $m$  for the atomic mass, and  $\rho$  for the mass density. The factor two reflects the paired nature of the superfluid, similar to the charge  $2e$  for a Cooper pair in superconductors. By recording the movement of the driving membrane both  $p(t)$  and  $I(t)$  were known leading to a current-phase relation  $I(\phi)$  which was indeed sinusoidal.

Other effects known from superconducting weak links have recently also been discovered. Examples for those are Shapiro steps seen by Simmonds *et al.* [69] or quantum interference in a SQUID-like geometry [70]. In the latter experiment the analogue to the magnetic flux which causes an interference pattern in SQUIDS is the rotation flux through a loop of two weak links originating in the rotation of the earth.

The order parameter in a Fermi liquid with triplet pairing is a complex vector quantity which leads to a larger variety of phenomena compared to conventional Josephson junctions. The direction dependence of the order parameter causes pair-breaking near walls and an extreme sensitivity to surface roughness. For a more detailed description of expected effects in weak links of Fermi liquids with unconventional pairing symmetry see Rainer and Sauls [71] and references therein. In recent years experiments in Berkley [72, 73] revealed an unconventional Josephson effect which stimulated new theoretical studies of weak links in  $^3\text{He}$ . In contrast to the unique current-phase relation in s-wave superconductors two distinct functions  $I(\phi)$  were found. In the so called  $\pi$ -state dissipationless, pendulum-like current oscillations were observed around local minima of free energy at  $\phi = 0$  and  $\phi = \pi$ . The additional minimum at  $\phi = \pi$  is believed to be due to orientational effects of the order parameter [74–77].

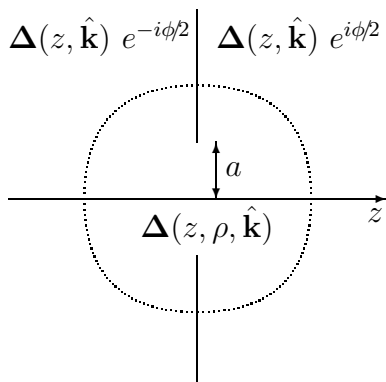


Figure 4.1: Schematic geometry of a circular orifice between two helium reservoirs. The order parameter is calculated self-consistently inside the dotted line, outside of it, the phase is fixed and the order-parameter profile is that of two half-spaces separated by a specularly reflecting wall.

Previous theoretical studies of supercurrents in restricted geometries can be divided into two major approaches. Firstly, in the case of infinitely small holes, the pinhole limit, the coupling between two reservoirs causes a current but it does not influence the order parameter on both sides of the weak link. Secondly, near the critical temperature calculations also simplify significantly as the quasiclassical equations then merge into the Ginzburg-Landau equations [78]. In the following we focus on the low-temperature properties of two half-spaces of superfluid  $^3\text{He}$  connected by an orifice of finite size. The aim is to study the importance of self-consistent calculations in the transition from a pinhole to a large hole which can finally be described using hydrodynamic equations.

## 4.2 Geometry and model

We assume two superfluid reservoirs of  $^3\text{He}$  separated by a thin, infinite wall in the  $xy$ -plane. The wall shall be specularly reflecting with a circular orifice of radius  $a$ . The origin of the coordinates is at the centre of the hole (see fig. 4.2). The reservoirs are in the B-phase which is described by an order parameter with a uniform energy gap of the form

$$\Delta(\hat{\mathbf{k}}) = R\hat{\mathbf{k}} \Delta(T) e^{i\varphi} \quad , \quad \Delta(\hat{\mathbf{k}}) \cdot \Delta^*(\hat{\mathbf{k}}) = \Delta^2(T) \quad . \quad (4.3)$$

The rotation matrix,  $R(\hat{\mathbf{n}}, \theta)$ , describes the relative orientation of orbital angular momentum and spin and can be parameterized by an axis,  $\hat{\mathbf{n}}$ , and an angle,  $\theta$ . There are a number of small interactions which determine the rotation matrix. The most important of those is the dipole interaction between the nuclear moments of  $^3\text{He}$ . In the B-phase the dipole energy is minimised by a relative spin-orbit rotation given by the Leggett angle,  $\theta_L = \arccos(-1/4)$ , and an arbitrary axis  $\hat{\mathbf{n}}$  [79, 80]. The degeneracy with respect to the axis is lifted by a magnetic field which then prefers  $\hat{\mathbf{n}}$  to be parallel to the applied field [81].

The presence of a wall destroys the uniformity of the energy gap. The dipole interaction then pins the rotation axis to the normal of the wall. In high fields a magnetic surface energy may compete with the latter effect. The competition of different effects in general leads to a space dependent relative orientation in nontrivial geometries. However, the length scale over which this so called texture changes is much larger than the coherence length which is characteristic of the pair-breaking effect of the wall and the size of the orifices studied here. Hence, we neglect the effect of the texture assuming a spatially constant rotation matrix. As the wall shall further not be spin active the system is degenerate with respect to  $R$ . For all numerical calculations  $R$  is chosen to be the identity.

The presence of the wall causes the order parameter to split up into a component parallel and perpendicular to the wall. As a consequence the gap then depends on the position on the Fermi surface and on the distance from the wall. The orifice additionally breaks translational symmetry parallel to the wall resulting in a dependence on the distance from the  $z$ -axis,  $\rho$ . In summary, the order parameter has the form

$$\Delta(\mathbf{R}, \hat{\mathbf{k}}) = \Delta_{\parallel}(z, \rho) k_x \hat{\mathbf{e}}_x + \Delta_{\parallel}(z, \rho) k_y \hat{\mathbf{e}}_y + \Delta_{\perp}(z, \rho) k_z \hat{\mathbf{e}}_z . \quad (4.4)$$

The phase far from the hole is chosen as  $\text{sign}(z)\phi/2$  which leads to the relation  $\Delta_{\parallel,\perp}(z, \rho) = \Delta_{\parallel,\perp}^*(-z, \rho)$ .

In the next sections supercurrent densities are calculated for the limiting cases of a homogeneous superfluid, a pinhole between two reservoirs of  $^3\text{He-B}$ , and potential flow for a fluid with vanishing viscosity. These are followed by a section on the free-energy expression which is applied to the multivalued solutions of the quasiclassical equations. The results of self-consistent calculations are discussed at the end of this chapter.

### 4.3 Depairing current

In the following section we want to calculate the order parameter if a homogeneous current is applied in the absence of any geometric constriction. For simplicity, Fermi-liquid corrections, which result in a renormalization of the quasiparticle mass and the superfluid velocity [80], are neglected. The effect of those was studied by Vollhardt *et al.* [82] and Kleinert [83]. The current is introduced by a constant phase gradient, i.e. the order parameter is assumed to have the form

$$\Delta(\mathbf{R}, \hat{\mathbf{k}}) = \left\{ \Delta_{\perp} k_x \hat{\mathbf{e}}_x + \Delta_{\perp} k_y \hat{\mathbf{e}}_y + \Delta_{\parallel} k_z \hat{\mathbf{e}}_z \right\} e^{iqz} . \quad (4.5)$$

The order parameter is split up into a component perpendicular and parallel to the current as it will no longer be isotropic as soon as the current becomes pair-breaking. The com-



ponents  $\Delta_{\parallel}$  and  $\Delta_{\perp}$  are chosen to be real. Note that in this section the indices  $\perp$  and  $\parallel$  refer to the orientation relative to the phase gradient or current. The effect of the phase gradient is a shift of the Matsubara energies by  $i\frac{1}{2}v_f\hbar q\hat{\mathbf{k}}\cdot\mathbf{e}_z =: iu\cos\theta$ . Including this shift in energy, the quasiclassical equations are solved by the homogeneous solution

$$\hat{g}^M(\hat{\mathbf{k}}, \epsilon_n) = -i\pi \frac{(\epsilon_n + iu\cos\theta)\hat{\tau}_3 - \hat{\Delta}(\hat{\mathbf{k}})}{\sqrt{|\Delta|^2 + (\epsilon_n + iu\cos\theta)^2}}. \quad (4.6)$$

The gap equations (2.11) for the two components of the order parameter and the particle current density (2.13) then read:

$$\begin{pmatrix} \Delta_{\parallel} \\ \Delta_{\perp} \end{pmatrix} = \frac{3}{4}N_f V \pi T \sum_{\epsilon_n} \int_0^{\pi} \begin{pmatrix} 2\Delta_{\parallel} \cos^2 \theta \\ \Delta_{\perp} \sin^2 \theta \end{pmatrix} \frac{\sin \theta \, d\theta}{\sqrt{|\Delta|^2 + (\epsilon_n + iu\cos\theta)^2}}, \quad (4.7)$$

$$j = -iN_f v_f \pi T \sum_{\epsilon_n} \int_0^{\pi} \cos \theta \frac{\epsilon_n + iu\cos\theta}{\sqrt{|\Delta|^2 + (\epsilon_n + iu\cos\theta)^2}} \sin \theta \, d\theta. \quad (4.8)$$

The coupled gap equations have in general to be solved numerically. In the Ginzburg-Landau regime, however, analytical results can be achieved [84]. In the limit  $T \rightarrow 0$  the sum over Matsubara energies can be replaced by an integral, i.e.  $2\pi T \sum_{\epsilon_n} \rightarrow \int d\epsilon$ . Eliminating the energy cutoff,  $\epsilon_c$ , by the zero-temperature BCS energy gap,  $\Delta_0$ , via

$$\frac{1}{N_f V} = \ln \frac{\epsilon_c}{\Delta_0}, \quad (4.9)$$

the energy integration then simplifies eq. (4.7) to

$$\begin{pmatrix} \Delta_{\parallel} \\ \Delta_{\perp} \end{pmatrix} \ln \Delta_0 = \frac{3}{2} Re \int_0^1 \begin{pmatrix} 2\Delta_{\parallel} z^2 \\ \Delta_{\perp} (1 - z^2) \end{pmatrix} \left\{ \ln \Delta(z) + \operatorname{arccosh} \frac{uz}{\Delta(z)} \right\} dz, \quad (4.10)$$

with

$$\Delta(z) = \sqrt{\Delta_{\perp}^2 + (\Delta_{\parallel}^2 - \Delta_{\perp}^2)z^2}. \quad (4.11)$$

Kupriyanov *et al.* [85] studied this problem for a clean s-wave superconductor with  $\Delta_{\perp} = \Delta_{\parallel}$ . The two gap equations above are then equivalent leading to the result [86]

$$\Delta = \Delta_0 \begin{cases} 1 & \text{for } r > 1 \\ \frac{r}{1+r^2} e^{\sqrt{1-r^2}} & \text{for } r < 1 \end{cases}, \quad (4.12)$$

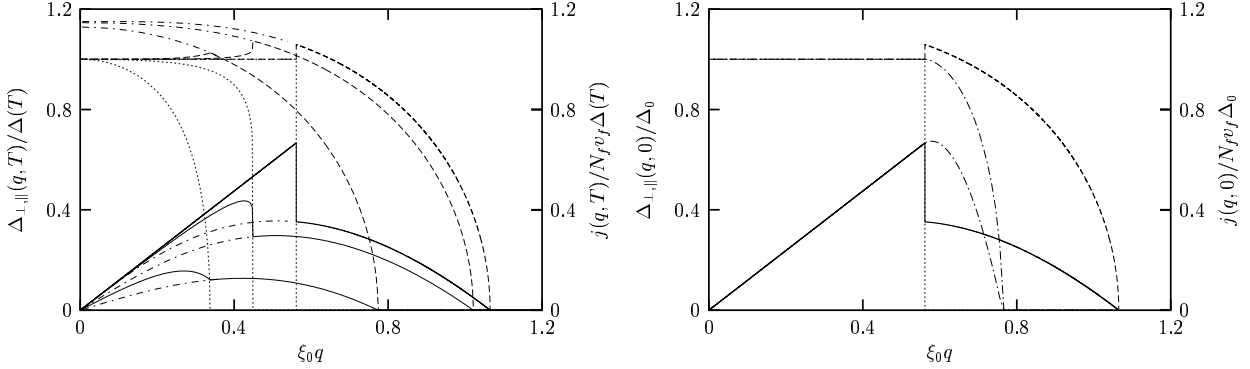


Figure 4.2: Particle current density and order parameter for bulk  $^3\text{He-B}$  with constant phase gradient,  $q$ . The graph on the left shows the particle current density (solid lines) and the order-parameter component parallel (dotted lines) and perpendicular (dashed lines) to the gradient at temperatures  $T/T_c = 0, 0.3$ , and  $0.7$ . At a critical  $q$  there is a phase transition to a planar state for which the current density and the order parameter is plotted in dashed-dotted lines. On the right, the particle current density and the order parameter are compared with those of a s-wave superconductor (dashed-dotted line) at  $T = 0$ . The isotropic p-wave state is for vanishing temperature and below the phase transition to the planar state equivalent to the s-wave state.

$$j = \frac{1}{3} N_f \hbar v_f^2 q \begin{cases} 1 & \text{for } r > 1 \\ 1 - \sqrt{(1 - r^2)^3} & \text{for } r < 1 \end{cases} \quad (4.13)$$

No pair-breaking occurs as long as the parameter  $r = \Delta/u$  is larger than one, the current is then strictly linear to the phase gradient.

The two gap equations (4.10) can also be simplified further for the planar state when  $\Delta_{\parallel} = 0$ . Order parameter and current density are in this case determined via

$$\Delta_{\perp} = \Delta_0 \frac{1}{2} e^{\frac{8+5r^2}{6+6r^2}} \frac{r}{\sqrt{1+r^2}} \quad , \quad j = \frac{1}{3} N_f \hbar v_f^2 q \frac{r^2}{1+r^2} \quad , \quad r = \frac{\Delta_{\perp}}{u} \quad (4.14)$$

In contrast to the isotropic s-wave order parameter, pair-breaking starts immediately when a current is applied even at vanishing temperature. The isotropic B-phase behaves like a s-wave as long as pair-breaking is absent. When it starts, the order parameter parallel to the current is suppressed to zero leading to a phase transition into the planar state. Hence, at zero temperature the B-phase is described by the s-wave formulae if  $\Delta_0 > u$  and by those of the A-phase (eq. (4.14)) if  $\Delta_0 < u$  (see fig. 4.2). For higher temperatures the gap equations are solved numerically. The results are plotted in fig. 4.2. For low currents the B-phase is similar to the s-wave. When pair-breaking starts, the isotropy of the order parameter is distorted, i.e. the perpendicular component is increased at the expense of the

order parameter parallel to the current. Finally, the B-phase undergoes a transition into the planar state.

## 4.4 Pinhole

In the opposite limit to free space in the preceding section we now calculate the current density in a hole between two reservoirs of  $^3\text{He-B}$ . For holes small compared to the coherence length the current through the hole has no effect on the order parameter. If the pair-breaking effect of the walls is neglected, the quasiclassical equations have to be solved for a piecewise constant order parameter which can easily be done. For calculating the current the propagator is only needed in the hole which simplifies the problem even further as the Riccati amplitudes are then given by the homogeneous solutions

$$\gamma^M = \text{sign}(\epsilon_n) \frac{i \Delta_{mf}}{|\epsilon_n| + \sqrt{\epsilon_n^2 + |\Delta|^2}} \quad , \quad \tilde{\gamma}^M = \text{sign}(\epsilon_n) \frac{-i \tilde{\Delta}_{mf}}{|\epsilon_n| + \sqrt{\epsilon_n^2 + |\Delta|^2}} \quad . \quad (4.15)$$

Here, the matrices  $\Delta_{mf}$  and  $\tilde{\Delta}_{mf}$  have to be taken “before” the step, which is defined by the direction of stability of the functions  $\gamma^M$  and  $\tilde{\gamma}^M$ , respectively (see section 2.6). In the Matsubara representation the current density (2.13) is given by

$$\begin{aligned} \mathbf{j} &= N_f k_B T \sum_n \int \frac{d\Omega}{4\pi} \frac{1}{2} \text{Tr}_4 \left\{ \mathbf{v}_f \hat{\tau}_3 \hat{g}^M(\mathbf{R}, \mathbf{p}_f, \epsilon_n) \right\} \\ &= 2N_f v_f k_B T \sum_n \int \frac{d\Omega}{4\pi} \hat{\mathbf{k}} g_0^M(\hat{\mathbf{k}}, \epsilon_n) \quad . \end{aligned} \quad (4.16)$$

The scalar component of  $g^M$ ,  $g_0^M$ , is defined analogously to eq. (2.7). If the order parameter “before” the step is  $\Delta_1$  for  $\gamma$  and  $\Delta_2$  for  $\tilde{\gamma}$ , respectively, some basic algebraic manipulations lead to the expression

$$g_0^M(\hat{\mathbf{k}}, \epsilon_n) = -i\pi \text{sign}(\epsilon_n) \frac{c^2 - a^2 - \mathbf{b} \cdot \mathbf{b}}{(c - a)^2 + \mathbf{b} \cdot \mathbf{b}} \quad , \quad (4.17)$$

with

$$c = - \left( \epsilon_n + \sqrt{\epsilon_n^2 + |\Delta_1|^2} \right) \left( \epsilon_n + \sqrt{\epsilon_n^2 + |\Delta_2|^2} \right) \quad , \quad a = \Delta_1 \cdot \Delta_2^* \quad , \quad \mathbf{b} = \Delta_1 \times \Delta_2^* \quad . \quad (4.18)$$

At first sight, the terms for positive and negative energies seem to cancel each other. This is, in general, not the case as the indices 1 and 2 have to be interchanged if the sign of the

energy changes which is equivalent to a complex conjugation of eq. (4.17). In the case of a constant order parameter on both sides of the hole with the same magnitude,  $|\Delta|$ , and orientation,  $R$ , but a phase difference  $\phi$  eqs. (4.16) to (4.18) lead to the current density

$$j = \frac{1}{2} \pi N_F v_F |\Delta| \sin \frac{\phi}{2} k_B T \sum_{\epsilon_n} \frac{2|\Delta| \cos \frac{\phi}{2}}{\epsilon_n^2 + |\Delta|^2 \cos^2 \frac{\phi}{2}} . \quad (4.19)$$

The sum above can be evaluated by a contour integration [87]. The final result is [88]

$$j = \frac{1}{2} \pi N_F v_F |\Delta| \sin \frac{\phi}{2} \tanh \frac{|\Delta| \cos \frac{\phi}{2}}{2k_B T} . \quad (4.20)$$

This is the same result as for a s-wave superconductor [89] due to the quasi isotropic energy gap in bulk  $^3\text{He-B}$ . The expression in eq. (4.20) represents the usual Josephson current-phase relation in the limit of vanishing order parameter near  $T_c$ :

$$j = \frac{1}{8} \pi N_F v_F |\Delta| \frac{|\Delta|}{k_B T} \sin \phi . \quad (4.21)$$

For low temperature the current-phase relation is no longer sinusoidal, but is skewed to higher phases. Phase and temperature dependence of the pinhole current density is shown in fig. 4.3.

Yip [76] extended this calculation for the case of different rotation matrices on both sides of the pinhole and found a state with a different current-phase relation, named  $\pi$ -state, whose significant features are a much lower current density and an additional minimum of the free energy at a phase difference  $\pi$ . The consequence of the latter property is a sign change in the current for  $0 < \phi < \pi$ . The  $\pi$ -state exist for a wide range of textures, examples are shown in fig. 4.4.

## 4.5 Pinhole in pair-breaking wall

In the previous paragraph a constant order parameter was assumed. However, due to the direction dependence the order parameter is altered near walls. For a specularly reflecting wall the component perpendicular to the wall,  $\Delta_\perp$ , changes sign upon reflection. This causes pair-breaking which suppresses this component to zero while the parallel components,  $\Delta_\parallel$ , are slightly increased compared to the bulk value. This effect was shown by Buchholtz *et al.* [90] and can be seen in fig. 4.5. The effect of the wall is less dramatic if some kind of roughness is introduced because the mixing of trajectories by a rough wall smoothens the

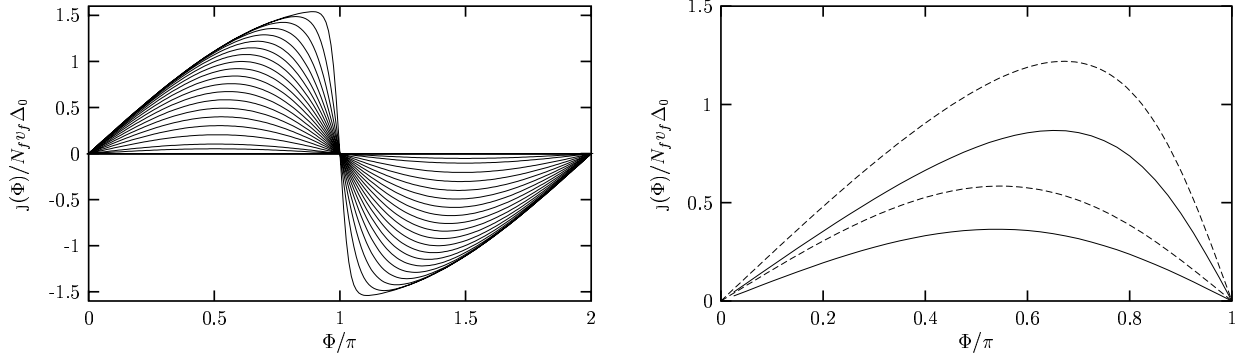


Figure 4.3: Current-phase relation for a pinhole between two  $^3\text{He-B}$  reservoirs. On the left, the order parameter is assumed to be undistorted by the presence of the wall. This assumption then leads to the same phase dependence as for a s-wave superconductor. The temperatures are chosen equidistant between  $T = 0.05 T_c$  and  $T = 0.95 T_c$  (top to bottom). The lowest current corresponds to  $T = 0.975 T_c$ . In the right graph the pair-breaking effect of a specularly reflecting wall is included for the dashed curves but neglected for the solid ones. The temperatures are  $T = 0.3 T_c$  and  $T = 0.7 T_c$ .

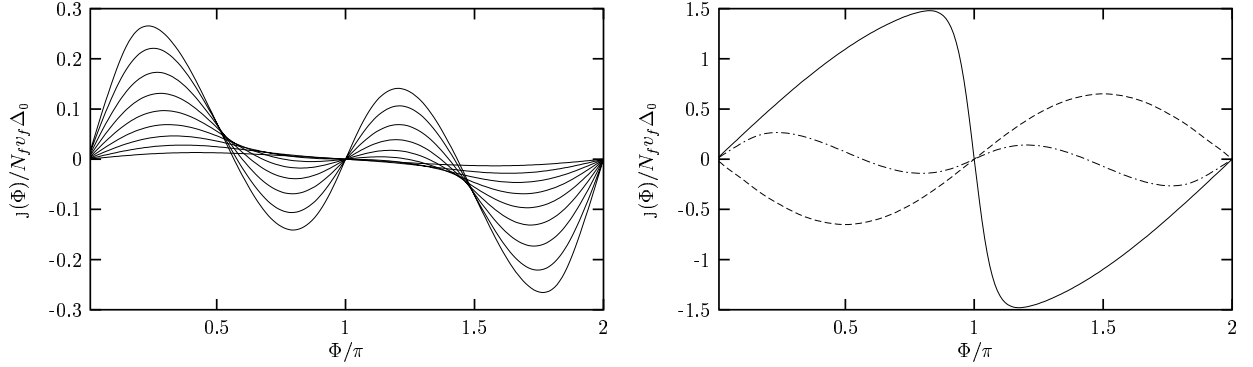


Figure 4.4: Current-phase relation for a pinhole between two  $^3\text{He-B}$  reservoirs. The order parameter is a step function of the form  $\Delta(z, \hat{\mathbf{k}}) = \Delta(T) e^{i \text{sign}(z)\phi/2} R(\hat{\mathbf{n}}, \theta(\text{sign}(z)))\hat{\mathbf{k}}$ . In the left plot the rotation matrices are given through  $\hat{\mathbf{n}} = \hat{\mathbf{e}}_z$  and  $\theta = \text{sign}(z)\theta_L$ . The lines correspond to temperatures  $T/T_c = 0.1, 0.2, \dots, 0.9$  (from top to bottom at the maximum). The different relative orientation of spin and angular momentum leads to a reduced current density in the  $\pi$ -state. The graph on the right shows the textural dependence of the current at  $T = 0.1 T_c$ . The solid line describes the case of equal texture on both sides of the hole, i.e. the case equivalent to s-wave superconductors. The dotted-dashed line is taken from the left plot and the dashed line belongs to the pair  $R(\hat{\mathbf{e}}_x, \theta + \pi), R(\hat{\mathbf{e}}_x, \theta)$ . The last case may occur if a magnetic field is applied in a direction deviating from the  $z$ -axis by the angle  $\theta_L$ .

sudden change of  $\Delta_\perp$ . That component is then not completely suppressed. The detailed profile of the order parameter near a rough wall depends on the model used to describe reflection. The most prominent models describing the effect of rough surfaces in  $^3\text{He-B}$  are the “randomly rippled wall” [91, 92], the “randomly oriented mirror” [93], the “thin dirty layer” [94–96], and the model by Ovchinnikov [97, 98]. The latter is an ingenious formulation of the thin layer model for the limit of a diffusively reflecting wall and needs the lowest effort to be implemented in numerical calculations.

The main impact a wall has on the pinhole current density is a reduction of its magnitude but less a change in the phase dependence as the phase is still discontinuous at the orifice. The pinhole current densities for a constant order parameter and a self-consistent calculation are compared in fig. 4.3 for two different temperatures. The effect of diffusive walls is similar, the reduction of the current being slightly stronger and the phase dependence qualitatively the same [99]. As above, the shape of the current-phase relation is drastically changed if textural effects are included which again leads to the  $\pi$ –state. Details on textural effects on pinhole current densities including pair-braking walls are given by Viljas *et al.* [74].

## 4.6 Hydrodynamic limit

If the orifice between the helium reservoirs is sufficiently large, the effect of the pair-breaking walls becomes less important, and the order parameter has almost everywhere its bulk value. Additionally, the phase  $\phi$  will vary slowly and will not influence the order parameter. We can then assume that the current density is proportional to the local phase gradient. The proportionality follows from an expansion of eq. (4.8) for a small gradient of the phase. Together with the continuity equation this leads to

$$\mathbf{j} = \frac{1}{3} \hbar N_f v_f^2 \sum_{n=-\infty}^{\infty} \frac{\pi k_B T |\Delta|^2}{\sqrt{(|\Delta|^2 + \epsilon_n^2)^3}} \nabla \phi =: \frac{1}{3} \alpha(T) \hbar N_f v_f^2 \nabla \phi, \quad (4.22)$$

$$\nabla \mathbf{j} = \frac{1}{3} \alpha(T) \hbar N_f v_f^2 \nabla^2 \phi = 0. \quad (4.23)$$

In the limit of vanishing temperature the sum, which is abbreviated by  $\alpha(T)$ , equals one and we recover the result given by eq. (4.13). The problem is now described by the potential flow of an incompressible, frictionless liquid. This problem was studied by Anderson [68]. The boundary conditions are a mixture of von Neumann and Dirichlet type boundary conditions, given by constants in the orifice and at infinity and an impenetrable wall. This

is equivalent to the electrostatic problem of a charged metal disc. The solution for a hole of radius  $a$  is [100]

$$\phi(z, \rho) = \phi(\infty) \operatorname{sign}(z) \left\{ 1 - \frac{2}{\pi} \arcsin \frac{2a}{\sqrt{(\rho - a)^2 + z^2} + \sqrt{(\rho + a)^2 + z^2}} \right\}. \quad (4.24)$$

The total current through the orifice is then given by  $I = \frac{4}{3}\alpha(T)\hbar N_f v_f^2 a \phi(\infty)$ . However, the solution must not be taken too seriously as it shows a diverging current density at the edge of the orifice,

$$j(z = 0, \rho < a) = \frac{2}{3\pi}\alpha(T) \hbar N_f v_f^2 \phi(\infty) \frac{1}{\sqrt{a^2 - \rho^2}}, \quad (4.25)$$

and, hence, is in contradiction to the assumption of a slowly varying phase. The exercise here is, nevertheless, useful as eq. (4.24) serves as a good starting point for self-consistent calculations. The current calculated assuming potential flow is far too high. The reason is that close to the edges of the orifice the phase gradient is neither small nor constant. However, if the current is calculated via the quasiclassical equations using the hydrodynamic order parameter, the result is then a good approximation if the radius is large enough to neglect the pair-breaking effect of the walls and if the phase difference is small enough to avoid pair-breaking current densities. For an orifice of radius  $\pi \xi_0$  there is hardly any difference to the self-consistent solution for phase differences up to  $3\pi/2$  (see fig. 4.14).

## 4.7 Free-energy functionals

Several approaches exist to derive a quasiclassical expression for the free-energy density leading to different results, i.e. there is no unique functional for the free-energy density. However, the spatial integral over these densities results in the same total free energy.

Eilenberger [9] ingeniously guessed an expression whose stationarity conditions with respect to the order parameter, the propagator, and the vector potential delivers the gap equation, the quasiclassical transport equation, and Ampère's law, respectively. The major advantage of Eilenberger's free-energy functional is its efficiency in numerical calculations, but it lacks a systematic derivation.

A whole class of systematic derivations of a quasiclassical free energy is based on the free-energy functional of Luttinger and Ward [101] supplemented by the magnetic field energy:

$$\Omega(\hat{G}, \hat{\Sigma}, \hat{V}) = -TR \left\{ \hat{\Sigma} \hat{G} + \ln \left[ -\hat{G}_0^{-1} + \hat{\Sigma} + \hat{V} \right] \right\} + \Phi(\hat{G}) + \int d^3R \frac{(\mathbf{B} - \mathbf{B}_a)^2}{8\pi}. \quad (4.26)$$

Here,  $TR$  is an abbreviation for a summation over Matsubara frequencies, an integral over phase space, and the trace over  $4 \times 4$  matrices,

$$TR\{\dots\} = k_B T \sum_{n=-\infty}^{\infty} \int \frac{d^3 k}{(2\pi)^3} \int d^3 R \frac{1}{2} \text{Tr}_4 \{\dots\} . \quad (4.27)$$

The self-energy,  $\hat{\Sigma}$ , is given by the functional derivative of the  $\Phi$ -functional,  $\Phi(\hat{G})$ , with respect to the Green's function,  $\hat{G}$ ,

$$\delta\Phi(\hat{G}) = TR\{\hat{\Sigma}\delta\hat{G}\} . \quad (4.28)$$

The equation above guarantees stationarity of  $\Omega$  in  $\hat{G}$ . Additionally, the free-energy functional is stationary in  $\hat{\Sigma}$  as a consequence of Dyson's equation,

$$\hat{G} = \left(\hat{G}_0^{-1} - \hat{\Sigma} - \hat{V}\right)^{-1} , \quad (4.29)$$

where  $\hat{V}$  stands for the external potential. Equation (4.29) is often used as a starting point for the derivation of the quasiclassical transport equation via the so called "left-right" trick [102].

For achieving a quasiclassical free energy,  $\hat{G}$  and  $\hat{\Sigma}$  have to be replaced by low-energy quantities like  $\hat{g}$  and  $\hat{\Delta}$ . This can straightforwardly be done for all but the logarithmic term of eq. (4.26). The latter can be transformed by first differentiating it with respect to some suitable parameter, then performing the  $\xi$ -integration and finally re-integrating over the artificially introduced parameter. There are several possibilities to implement this trick which in general lead to different free-energy densities. We follow here an approach by Thuneberg *et al.* [27] applied for the case of superfluid  $^3\text{He}$  [103]. The parameter  $\lambda$  is introduced as follows:

$$\begin{aligned} \Delta\Omega(\hat{G}, \hat{\Sigma}, \hat{V}, \lambda) &= \Omega(\hat{G}, \hat{\Sigma}, \hat{V}, \lambda) - \Omega(\hat{G}_N, \hat{\Sigma}_N, \hat{V}, \lambda) \\ &= -TR\left\{\lambda\hat{\Sigma}\hat{G} + \ln\left[-\hat{G}_0^{-1} + \hat{\Sigma}_N + \hat{V} + \lambda\left(\hat{\Sigma} - \hat{\Sigma}_N\right)\right]\right\} + \lambda\Phi(\hat{G}) \\ &\quad + TR\left\{\lambda\hat{\Sigma}_N\hat{G}_N + \ln\left[-\hat{G}_0^{-1} + \hat{\Sigma}_N + \hat{V} + \lambda\left(\hat{\Sigma}_N - \hat{\Sigma}_N\right)\right]\right\} - \lambda\Phi(\hat{G}_N) \\ &\quad + \lambda \int d^3 R \frac{(\mathbf{B}-\mathbf{B}_a)^2}{8\pi} \\ &= -TR\left\{\lambda\Delta\hat{\Sigma}\hat{G} + \ln\left[-\hat{G}_N^{-1} + \lambda\Delta\hat{\Sigma}\right]\right\} + TR\left\{-\hat{G}_N^{-1}\right\} + \lambda \int d^3 R \frac{(\mathbf{B}-\mathbf{B}_a)^2}{8\pi} \\ &\quad + \lambda \left[\Phi(\hat{G}) - \Phi(\hat{G}_N) - TR\left\{\hat{\Sigma}_N(\hat{G} - \hat{G}_N)\right\}\right] . \end{aligned}$$



Here,  $\hat{G}_N$  and  $\hat{\Sigma}_N$  are Green's function and self-energy in the normal state,  $\Delta\hat{\Sigma} = \hat{\Sigma} - \hat{\Sigma}_N$ . The expression above gives the difference in free energy between the superfluid and the normal state for  $\lambda = 1$  and vanishes for  $\lambda = 0$  as this corresponds to the normal state. Applying the trick of differentiation with respect to  $\lambda$ ,  $\xi$ -integration, and re-integration then leads to a quasiclassical expression for the free energy

$$\Delta\Omega = -Tr\{\hat{\Delta}\hat{g}\} + \int_0^1 d\lambda Tr\{\hat{g}_\lambda\hat{\Delta}\} + \Phi(\hat{g}) + \int d^3R \frac{(\mathbf{B} - \mathbf{B}_a)^2}{8\pi}. \quad (4.30)$$

The auxiliary function  $\hat{g}_\lambda$  is defined as the solution of the quasiclassical equation in which  $\hat{\Delta}$  has been replaced by  $\lambda\hat{\Delta}$ . The generalised trace is now defined as

$$Tr\{\dots\} = k_B T N_f \int d^3R \sum_{n=-\infty}^{\infty} \frac{1}{2} Tr_4 \langle \dots \rangle_{\mathbf{p}_f}. \quad (4.31)$$

Using  $\delta\Phi(\hat{g}) = Tr\{\hat{\Delta}\delta\hat{g}\}$ , we can eliminate  $\Phi(\hat{g})$  in eq. (4.30) which leads to the final result for the free energy

$$\Delta\Omega = \int_0^1 d\lambda Tr\left\{\left(\hat{g}_\lambda - \frac{1}{2}\hat{g}\right)\hat{\Delta}\right\} + \int d^3R \frac{(\mathbf{B} - \mathbf{B}_a)^2}{8\pi}. \quad (4.32)$$

Note that for intermediate values of the parameter  $\lambda$  there is no physical interpretation of the auxiliary function  $\hat{g}_\lambda$ , only the limiting values of  $\lambda$  correspond to physical systems. This may be disappointing, but it pays off as the order parameter has to be calculated only once.

A physically more satisfying derivation of the quasiclassical free energy can be achieved if only the coupling constant is multiplied by  $\lambda$ , thus if the parameter is used to switch on the coupling smoothly [104–106]. Requiring stationarity in  $\hat{g}_\lambda$  and  $\hat{\Delta}_\lambda$ , the auxiliary systems are then physically well defined. However, the price is immense because the order parameter has to be calculated self-consistently for all intermediate values of  $\lambda$ .

In yet another derivation  $\lambda$  replaces the discrete Matsubara energies [107, 108]. Again, the physical interpretation is not clear, the numerical effort needed is comparable with the approach used here.

For the geometry studied here we are not interested in the free energy compared to the normal state which must diverge for an infinite volume. The reference system is chosen to be the reservoirs separated by the wall. Hence we calculate the change in free energy due to the orifice and the phase difference between the reservoirs,

$$\Omega_o = \Delta\Omega(\text{orifice}, \phi) - \Delta\Omega(\text{wall}) = \int_{-\infty}^{\infty} \Omega_z(z) dz. \quad (4.33)$$

The free-energy density  $\Omega_z(z)$  is introduced to illustrate the qualitative dependence of the free energy on the distance from the wall (fig. 4.10). As mentioned above, this definition is not unique, but depends on the free-energy functional used.

Prior to calculating the free energy the order parameter field has to be calculated self-consistently which also delivers with practically no additional costs the current-phase relation,  $I(\phi)$ . Instead of applying eq. (4.32), requiring similar effort as the calculation of the order parameter, the free energy can be calculated via

$$I(\phi) = \frac{2}{\hbar} \frac{\partial \Omega}{\partial \phi} . \quad (4.34)$$

This very fundamental formula which reflects that particle number and phase are conjugate variables was derived by Anderson [68] and can be seen as a generalisation of the relation known for Josephson junctions

$$E_J(\phi) = \frac{1}{2} \hbar I_c (1 - \cos \phi) \quad , \quad I(\phi) = \frac{2}{\hbar} \frac{\partial E_J}{\partial \phi} = I_c \sin \phi , \quad (4.35)$$

where  $E_J$  and  $I_c$  are the Josephson coupling energy and the critical particle current, respectively.

As a test for consistency, eq. (4.34) is derived for the geometry given here starting from the quasiclassical free-energy expression (4.32) derived earlier by applying an infinitesimal local gauge transformation  $\phi(\mathbf{R}) \rightarrow \phi(\mathbf{R}) + \delta\phi(\mathbf{R})$ . The change in free energy then reads

$$\delta\Omega_o(\phi) = \int_V \frac{\partial \Omega(\hat{g})}{\partial \hat{g}} \delta\hat{g} \, d^3\mathbf{R} + \int_{\partial V} \left\{ \frac{\partial \Omega(\nabla f, \nabla \tilde{f})}{\partial \nabla f} \delta f + \frac{\partial \Omega(\nabla f, \nabla \tilde{f})}{\partial \nabla \tilde{f}} \delta \tilde{f} \right\} d\mathbf{S} . \quad (4.36)$$

The self-consistent calculation of  $\hat{g}$  guarantees the stationarity of the free energy with respect to the propagator. Hence, the volume integral above vanishes. Far from the aperture the free-energy density,  $\Omega$ , reduces to a functional quadratic in the gradients of the off-diagonal parts of  $\hat{g}$ . For convenience the gauge transformation at the boundary,  $\partial V$ , is now specified to

$$\delta\phi(\partial V) = \begin{cases} 0 & \text{for } z < 0 \\ \delta\phi = \text{constant} & \text{for } z > 0 \end{cases} . \quad (4.37)$$

Under this gauge transformation the off-diagonal transforms at the boundary according to

$$f(\partial V) \rightarrow e^{i\delta\phi(\partial V)} f(\partial V) = f(\partial V) + i\delta\phi(\partial V) f(\partial V) , \quad (4.38)$$

$$\tilde{f}(\partial V) \rightarrow e^{-i\delta\phi(\partial V)} \tilde{f}(\partial V) = \tilde{f}(\partial V) - i\delta\phi(\partial V) \tilde{f}(\partial V) . \quad (4.39)$$

The variation of the free energy has then the form

$$\delta\Omega_o(\phi) = \int_{\partial V_+} \left\{ i \frac{\partial\Omega(\nabla f, \nabla \tilde{f})}{\partial \nabla f} f - i \frac{\partial\Omega(\nabla f, \nabla \tilde{f})}{\partial \nabla \tilde{f}} \tilde{f} \right\} \delta\phi \, d\mathbf{S} = \frac{\hbar}{2} I(\phi) \delta\phi. \quad (4.40)$$

Evaluation of the term in brackets for large distances from the orifice leads exactly to the expression on the right hand side of eq. (4.22) if multiplied by the factor  $2/\hbar$ . Thus, the integration over the boundary for positive  $z$ ,  $\partial V_+$ , gives the current leaving  $V$  and by particle conservation the current through the aperture.

Viljas and Thuneberg [74] derived a quasiclassical free energy for pinholes which is also based on the functional defined in eq. (4.26). In their approach the wall is described as an impurity scatterer and the  $\lambda$ -integration is performed over the scattering strength. In contrast to eq. (4.32) where an explicit volume integration is needed, their derivation leads to an Josephson coupling energy localised at the pinhole, again in accordance with eq. (4.34). This extreme example of a free-energy density emphasises that there is a wide range of qualitatively very different functionals which lead to the same observable physical effects.

The simple method of calculating a free energy via eq. (4.34) only works as long as only the dependence on the soft variable  $\phi$  is wanted. For the change in free energy due to the wall or for the comparison of different branches of  $I(\phi)$  the quasiclassical free-energy functional (4.32) was computed numerically (see figs. 4.9 and 4.10).

## 4.8 Self-consistent solution for finite apertures

The previous sections describe various limiting cases in which the calculation of the current through the orifice for given phases at infinity simplifies drastically. In the following, these limits are compared with the fully self-consistent quasiclassical solution.

To calculate the latter, the order parameter is iteratively determined on a two-dimensional grid reflecting the dependence on  $z$  and  $\rho$ . The grid is chosen densest near the edge of the orifice and near the wall. As no time-dependence is considered, the Matsubara representation can be used. As a consequence, no singularities occur in the Fermi-surface average which is performed over a two-dimensional grid of trajectories. However, some care has to be taken at the discontinuity at angles which separate trajectories reflected at the wall from those passing through the orifice. The coupling strength and the energy cutoff are eliminated using the homogeneous solution. Details for this procedure were given by

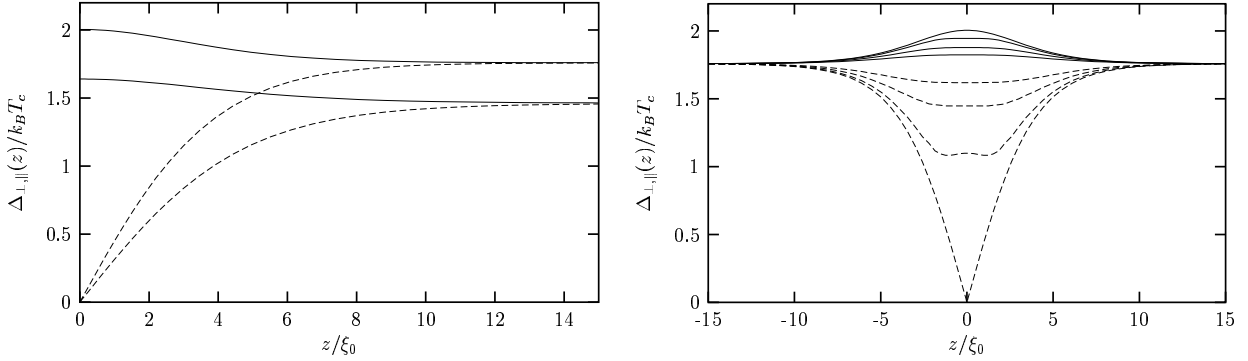


Figure 4.5: The self-consistent order parameter near a specularly reflecting wall is plotted in the left graph. The components parallel (solid line) to the surface are increased above the bulk value while the component which changes sign in a reflection (dashed line) is suppressed and vanishes at the wall. The temperatures are  $T = 0.3 T_c$  and  $T = 0.7 T_c$ . On the right: Order parameter along the symmetry axis of a circular hole in a wall between two reservoirs at  $T = 0.3 T_c$ . The pair-breaking effect of the wall diminishes with increasing hole radius. The radii  $r/\xi_0 = 0, 1, 2$ , and  $\pi$ .

Eschrig [26]. The phase difference is defined by fixing the phases at the boundary of the numerical grid which is at  $\sim 20 \xi$ . The differential equations for the matrices  $\gamma$  and  $\tilde{\gamma}$  are calculated using a fifth-order Runge-Kutta method with adaptive step-size control. The order parameter along a given trajectory is interpolated by a cubic spline.

If there is no phase difference between the two reservoirs, the order-parameter field is determined by a competition between the pair-breaking effect of the walls and the orifice which supports a bulk-like order parameter. In fig. 4.5 the order parameter along the symmetry axis is plotted for different radii of the aperture. At the centre of the hole the component parallel to the  $z$ -axis recovers rather quickly showing only a small suppression for a radius of about three coherence lengths. This, of course, happens at the expense of the components perpendicular to the  $z$ -axis.

The situation is more complicated if a phase difference is considered. For  $\phi = \pi$ , e.g., the imaginary part of the order parameter as defined in section (4.2) changes sign at  $z = 0$ , similar to a reflection at the wall. Consequently, hardly any dependence on  $\rho$  can be seen for the  $z$ -component in the second plot of fig. 4.6. For the corresponding real part, however, the wall still causes a suppression to zero while it has its maximum in the hole where the imaginary part vanishes (see fig. 4.6). For the radial component of the order parameter both, real and imaginary part, strongly depend on  $\rho$ . The sign change in the imaginary part

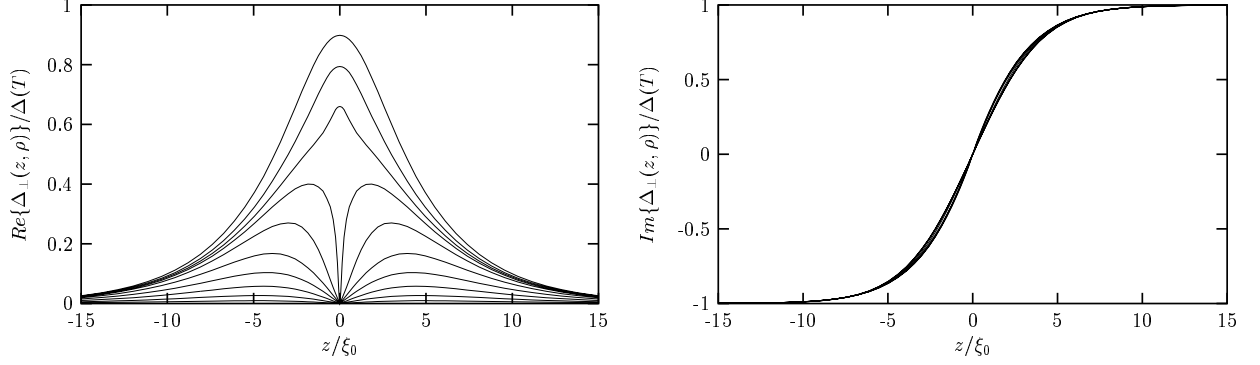


Figure 4.6: Self-consistent order parameter for an orifice of radius  $a = \pi \xi_0$  at  $T = 0.3 T_c$  and the phase difference  $\phi = \pi$ . For each line the distance to the symmetry axis,  $\rho$ , is constant. The left graph displays the real part of the component parallel to the symmetry axis. The maxima decrease with increasing  $\rho$ . On the right, the imaginary part of the parallel component hardly shows any dependence on  $\rho$ .

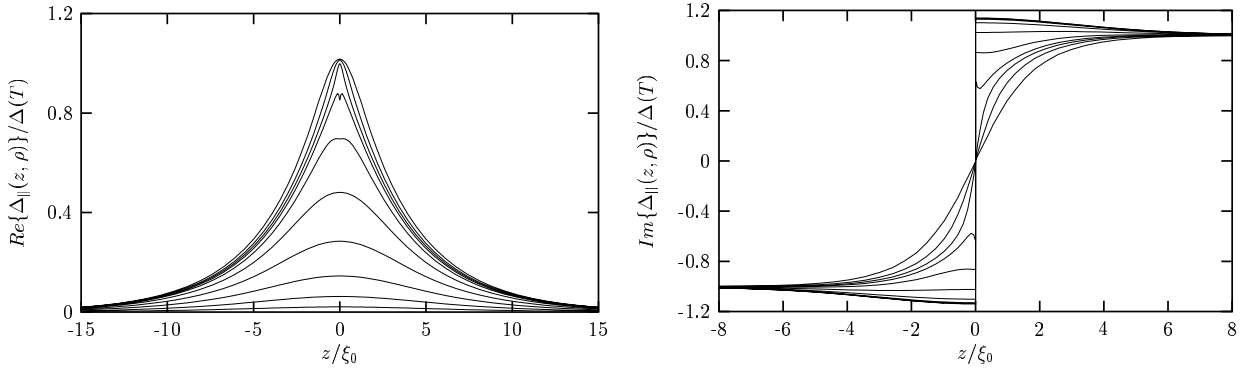


Figure 4.7: Self-consistent order parameter for an orifice of radius  $a = \pi \xi_0$  at  $T = 0.3 T_c$  and the phase difference  $\phi = \pi$ . For each line the distance to the symmetry axis,  $\rho$ , is constant. In the left graph the maxima of the real part of the component perpendicular to the symmetry axis decrease with increasing  $\rho$ . On the right, the imaginary part is discontinuous for  $\rho > a$ .

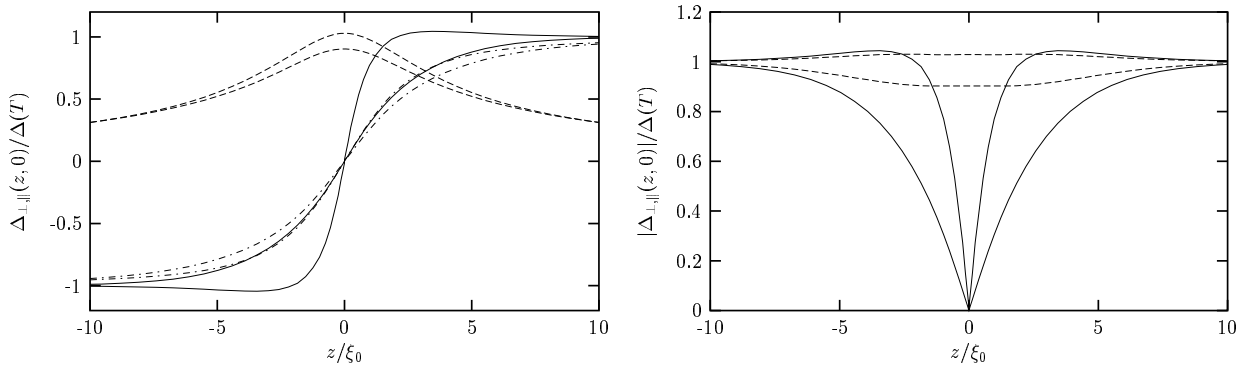


Figure 4.8: Multiple solutions for self-consistent order parameter. The phase difference  $\phi = \pi$ , the temperature  $T = 0.3 T_c$ , and the radius of the orifice  $a = \pi \xi_0$ . On the left: The solid lines show the order parameter which is effectively real and hence cannot carry any current. The dashed and dotted-dashed lines correspond to real and imaginary part of the current carrying configuration. The curves with a larger (smaller) modulus belong to the component parallel (perpendicular) to the wall. On the right: The absolute values of the order parameter for the same configurations. The real order parameter (solid lines) must go through zero to change sign while the complex fields have nearly constant moduli.

is discontinuous for  $\rho > a$ . Again, the real part is maximal where the imaginary one goes to zero (fig. 4.7). The moduli of the order parameter are the same as in the case without any phase difference. Thus, the phase gradient does not act pair-breaking for radii larger than  $\sim 2 \xi_0$ , only the phase of the order parameter varies. This is in contrast to a vortex in a superconductor or superfluid where the order parameter goes to zero at the centre while the phase is constant (apart from a single discontinuous change by  $\pi$ ) on straight lines through the centre of the vortex. A similar solution is found if the phase difference is not increased by small steps starting from zero but set to  $\pi$  immediately. A self-consistent solution can then be achieved which is solely imaginary (or equivalently solely real). The sign change in this solution takes place at  $z = 0$  where all components of the order parameter vanish for  $\rho < a$ . As there is no true phase change, this solution carries no current. In fig. 4.8 this order parameter is compared with the solution described earlier. In numerical calculations the currentless solution was not stable, even small perturbations of the phase (not the modulus) lead to the current carrying state. No new branch of solutions was found around this singular point. For radii larger than the coherence length the strong suppression of the order parameter costs more energy than the varying phase, the free energy of the currentless state is larger than that of the state carrying current (see fig. 4.9).

In pinhole calculations the small current through the orifice has no influence on the order

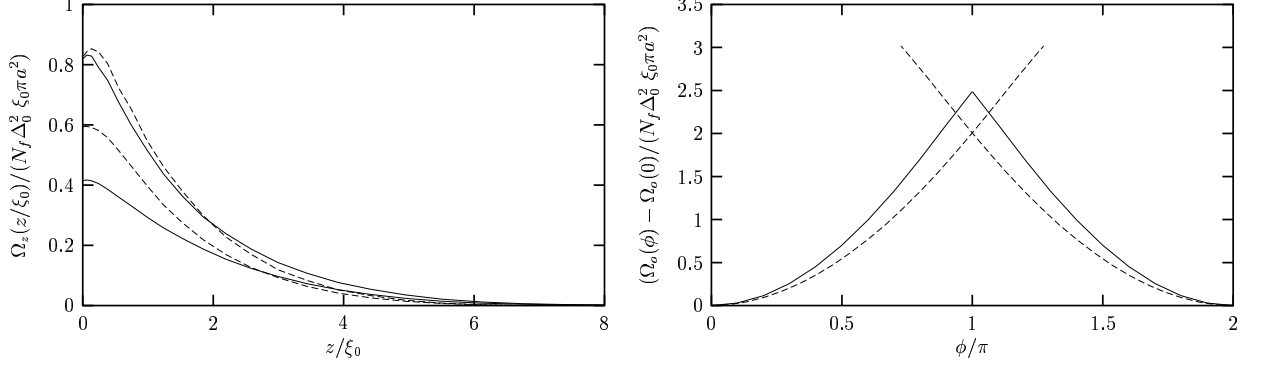


Figure 4.9: On the left: Free-energy density integrated over the radial variable,  $\rho$ , for the temperature  $T = 0.3 T_c$  and the phase difference  $\phi = \pi$ . The dashed lines belong to an order-parameter field which is real everywhere while the solid lines correspond to the field with a non-vanishing current through the aperture. The radii are  $a = \xi_0$  (top curves) and  $a = 2 \xi_0$ . On the right: Free energy versus phase difference for  $T = 0.3 T_c$ . The radii are  $a = \xi_0$  and  $a = 2 \xi_0$  for the solid and dashed lines, respectively.

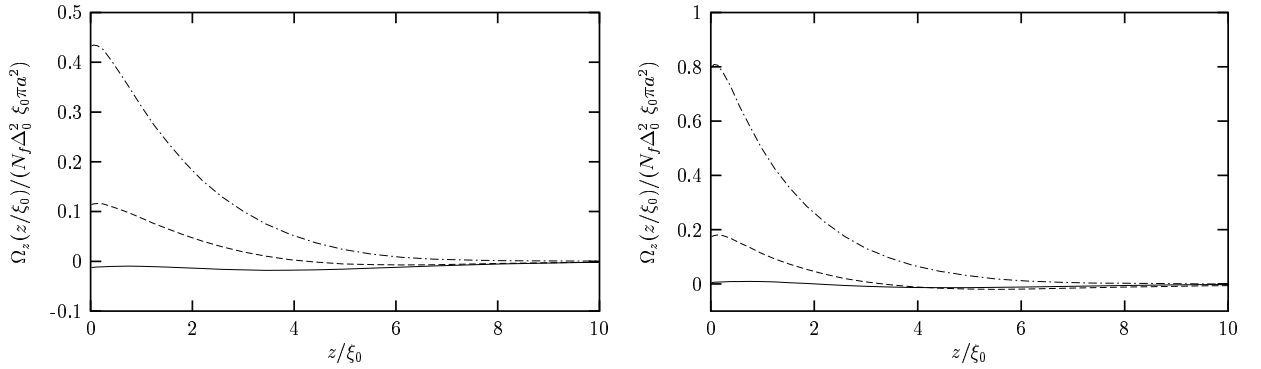


Figure 4.10: Free-energy density integrated over the radial variable,  $\rho$ , for the temperature  $T = 0.3 T_c$ . The solid lines, which correspond to a constant phase, result in a negative free energy as the hole reduces the pair-breaking effect of the wall. On the left: Orifice with radius  $a = 2 \xi_0$  and phase differences  $\phi/\pi = 0, 0.53$ , and 1. On the right:  $a = \xi_0$ ,  $\phi/\pi = 0, 0.5$ , and 1.

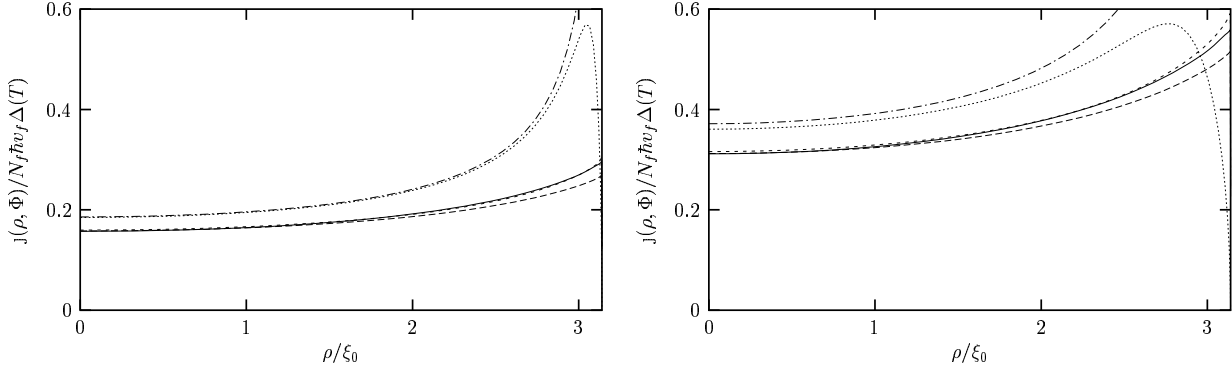


Figure 4.11: Particle current density for a hole between two  $^3\text{He-B}$  reservoirs. Various steps of simplification are compared with the fully self-consistent calculations which are shown in solid lines. The temperature is  $0.3 T_c$  and the hole radius is  $\pi \xi_0$ . The phase difference is  $\pi/2$  in the graph on the left. Three lines assume a constant magnitude of the order parameter with a phase variation given by eq. (4.24). The dashed-dotted line then corresponds to the hydrodynamic limit with a current density proportional to the local phase gradient. The difference to the dotted line displays the nonlinear contribution, and the dashed line shows the current density which results from the correct solution of the transport equation. For the long-dashed curve the self-consistent order parameter for vanishing phase difference was multiplied by the hydrodynamic phase factor. In the right graph the phase difference is changed to  $\pi$ .

parameter, the phase is constant on either side of the weak link. Therefore, the order-parameter field and the current must be a periodic function of the phase difference. This is not valid in the finite size apertures given here which lead to a continuous change of the phase throughout the hole. The phase can wind up until, finally, the critical current is reached inside the hole and superfluidity breaks down locally. For a hole of radius  $a = \xi_0$  at a temperature  $T = 0.3 T_c$  the critical current is first reached at the edges of the hole for a phase difference  $\phi \sim \pi$ . Close to this point convergence becomes increasingly difficult. If the phase difference is chosen slightly above the critical value the iteration does not converge at all. Instead, the order parameter becomes step by step more suppressed, goes to zero, and, finally, the phase starts to unwind. The iteration would eventually lead to a self-consistent solution for a smaller phase difference  $\phi \rightarrow 2\pi - \phi$  and an inverted current. Note that this is only the observation of steps in a numerical iteration and is not meant as a description of time evolution of phase slippage, a concept introduced by Anderson and Dayem and Shapiro [68, 109, 110].

In figs. 4.11 to 4.13 the particle current density is shown for five different models. The model which is poor for all parameters studied is the hydrodynamic limit which assumes



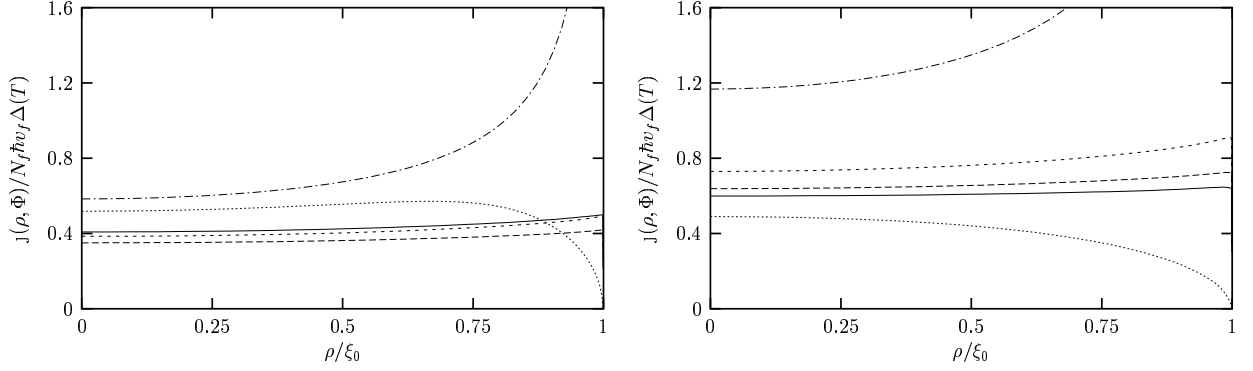


Figure 4.12: Particle current density for an orifice of radius  $a = \xi_0$ . The notation is the same as in fig. 4.11. The phase differences are  $\pi/2$  in the left and  $\pi$  in the right graph.

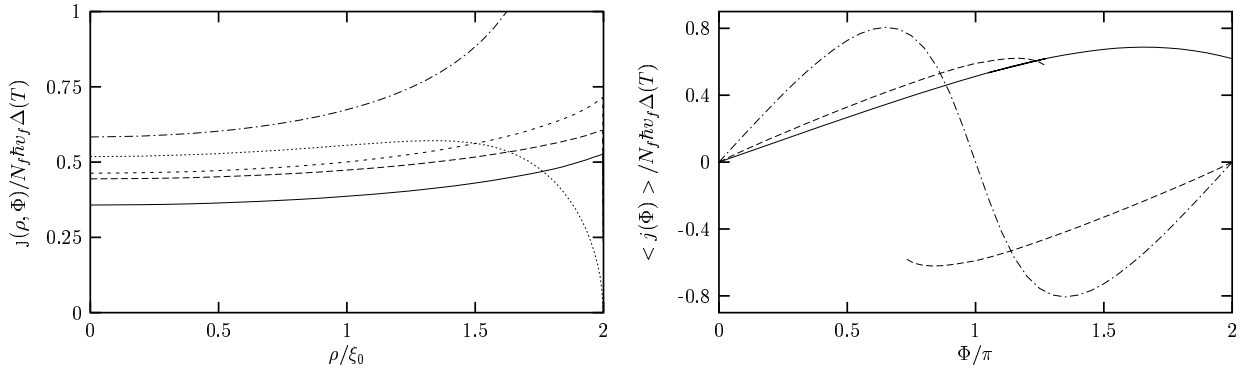


Figure 4.13: Particle current density for an orifice of radius  $2 \xi_0$ . The left graph shows the dependence on the distance from the symmetry axis for the phase difference  $\pi/2$ . The notation is as explained in fig. 4.11. The averaged particle current density as explained in fig. 4.14 is plotted on the right.

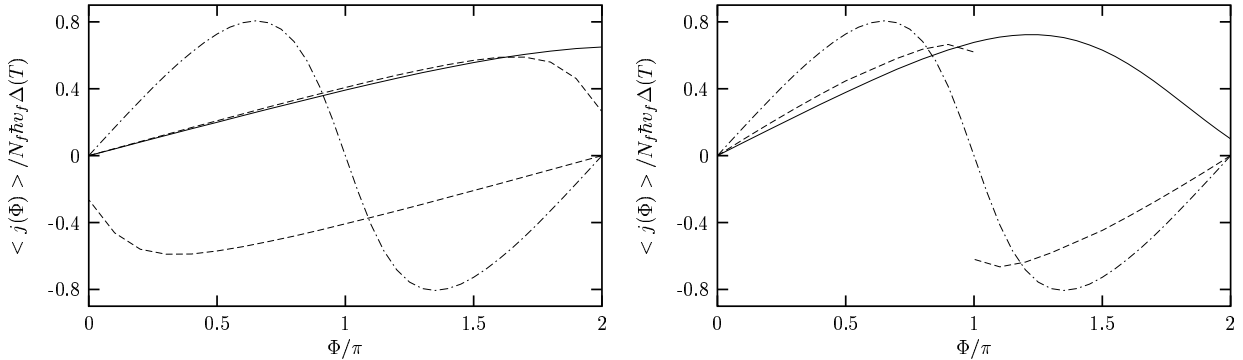


Figure 4.14: Averaged particle current density for a hole between two  $^3\text{He-B}$  reservoirs at  $T = 0.3 T_c$ . The graph compares the pinhole model (dashed-dotted lines), which includes the pair-breaking effect of the walls, with the fully self-consistent solution (dashed lines) and the current density for the self-consistent order parameter for vanishing phase difference multiplied by a phase which solves the Laplace equation (4.23) (solid lines). The radii of the orifices are  $\pi \xi_0$  on the left and  $\xi_0$  for the other graph.

that the current density is linear in the local phase gradient leading to a diverging current density near the edges of the aperture (eq. (4.25)). This divergence is cut off if the linearity is given up and eq. (4.8) is used instead. This approximation results in a vanishing current density for  $\rho = a$ , in contradiction to the self-consistent result. The reason for this failure is the fact that the current is nonlocal but only the information of the local order parameter has been used so far. The simplest way to incorporate nonlocal effects is to solve the quasiclassical transport equation for a constant modulus of the order parameter and a phase given by the solution of the Laplace equation (4.24). This approximation already is qualitatively in good agreement with the exact solution showing the highest current density at the edge of the aperture. For  $a = \pi \xi_0$  this simple model agrees also quantitatively very well with the full numerical treatment for a wide range of phase differences. Replacing the constant modulus of the order parameter by the profile calculated self-consistently for vanishing phase difference does not improve the approximation.

The figs. 4.13 and 4.14 show the phase dependence of the current normalised by the area of the orifice. The maximal averaged current density does not vary much with the hole size and is confined by the pinhole current density and the bulk critical current density which differ only by a factor of two at  $T = 0.3 T_c$ . The position of the maximal current density shifts, of course, with increasing orifice to larger phase differences as does the range of phases with two (or more) coexisting branches of the current-phase relation,  $I(\phi)$ .

# Chapter 5

## Summary

### NS contact

We studied the linear response of a normal metal superconducting metal contact to a small electric field. In a preparatory section the order-parameter profile and the density of states were calculated in equilibrium. We showed that the density of states in the normal metal is unaltered if the impurity self-energies are not taken into account while the coherence in the superconductor is always affected by the presence of the normal metal. Self-consistent calculations result in an impurity-induced proximity effect in the normal metal. This proximity effect causes a spatially constant gap in the density of states of the normal metal if the normal metal is sandwiched between two superconductors.

The dynamics of the NS contact is strongly dominated by the conservation law for charge and local charge neutrality which together fully determine the current in one-dimensional systems. For answering the question how this constant current is established in the non-homogeneous NS contact, the quasiclassical equations were solved including the self-consistencies for the order parameter, the impurity self-energies, and the electrochemical potential. The latter was used to deduce an internal electric field as response to the external perturbation. The internal field is of same order as the perturbation and is caused by charges which are either bound to the interface or spread over several coherence lengths. The surface charges are not due to the step in the order parameter at the interface but solely to abrupt changes of the impurity scattering. The order parameter itself can only produce continuous charge densities. The charges are indirectly calculated using Maxwell's equations. They are of higher order in the expansion parameters of Fermi-liquid theory

and are hence beyond this theory. Nevertheless, their effect has to be considered to be consistent in leading order.

## Weak links in $^3\text{He}$

We investigated several methods of calculating the current-phase relation of weak links in  $^3\text{He}$ . In the limit of small holes the hole itself and the current through it does not affect the order parameter in the superfluid and the current can hence be calculated using the pinhole model. This leads to a periodic current-phase relation. It was shown that the pair-breaking effect of the separating wall has no significant influence on the functional dependence of the current on the phase difference. The wall mainly reduces the amplitude of the current.

For orifices with radii comparable with the coherence length, self-consistent order-parameter fields were calculated. The two fixed phases of the pinhole model are then replaced by a field which allows the phase to wind up continuously. This not only breaks the periodicity, but also leads to multivalued current-phase relations.

Over a wide range the current through the orifice is linear in the phase difference between the reservoirs. Although this is expected in the hydrodynamic limit, the hydrodynamic equations are not applicable as they always fail at the edges of the circular apertures. However, calculating the current quasiclassically with the phase determined via the Laplace equation gives a fairly good approximation to the fully self-consistent solution. This approximation becomes weak for larger phase differences when pair-breaking due to the current itself has to be taken into account.

Remarkably, the maximal current through the aperture is sandwiched between the pinhole current and the depairing current for a homogeneous superfluid which differ only by a factor of about two at low temperature in spite of the drastic difference of the models.

A quasiclassical free-energy functional was introduced and it was stressed that this choice is not unique and that a whole zoo of different functionals exists. The functional was used to investigate the change in free energy due to the wall, the orifice, and the phase difference.

# Appendix A

## Notation

For two functions  $A(\epsilon, t)$  and  $B(\epsilon, t)$  the folding product  $\otimes$  is defined as follows:

$$A \otimes B = e^{\frac{i\hbar}{2}(\partial_\epsilon^A \partial_t^B - \partial_t^A \partial_\epsilon^B)} AB. \quad (\text{A.1})$$

Hence, this product involves infinitely many differentiations with respect to time and energy. However, in equilibrium this product reduces to a multiplication in Keldysh, Nambu, or spin space.

When time dependencies are treated in linear response, for typical products either A or B are equilibrium quantities, i.e. independent of time. For Fourier transformed functions the product then results in a shift of the energy variable in the equilibrium quantity:

$$A(\epsilon) \otimes B(\epsilon, \omega) = A(\epsilon + \frac{\hbar\omega}{2})B(\epsilon, \omega) \quad , \quad A(\epsilon, t) \otimes B(\epsilon) = A(\epsilon)B(\epsilon - \frac{\hbar\omega}{2}). \quad (\text{A.2})$$

Finally, in a high-energy expansion of the Green's functions up to the four lowest orders in  $1/\epsilon$  only the first order derivatives contribute (see appendix B):

$$A \otimes B = \left[ 1 + \frac{i\hbar}{2} (\partial_\epsilon^A \partial_t^B - \partial_t^A \partial_\epsilon^B) + \dots \right] AB. \quad (\text{A.3})$$

The Fermi-surface average  $\langle \dots \rangle_{\mathbf{p}_f}$  is defined by

$$\langle \dots \rangle_{\mathbf{p}_f} = \frac{1}{\int_{FS} \frac{d^2 \mathbf{p}_f}{|\mathbf{v}_f|}} \int_{FS} \frac{d^2 \mathbf{p}_f}{|\mathbf{v}_f|} \dots \quad (\text{A.4})$$

## APPENDIX A. NOTATION

---

In the normal state the density of states per spin is at the Fermi surface given by

$$N_f = \int_{FS} \frac{d^2 \mathbf{p}_f}{(2\pi\hbar)^3 |\mathbf{v}_f|} , \quad (\text{A.5})$$

with a Fermi velocity  $\mathbf{v}_f$  which is determined by the normal state quasiparticle dispersion relation,  $\varepsilon(\mathbf{p})$ ,

$$\mathbf{v}_f(\mathbf{p}_f) = \frac{\partial \varepsilon(\mathbf{p}')}{\partial \mathbf{p}'} \Big|_{\mathbf{p}'=\mathbf{p}_f} . \quad (\text{A.6})$$

# Appendix B

## High-energy expansion

Physical quantities involve integrals over the energy variable. In numerical calculations these integrals are truncated at a cutoff energy. To increase the accuracy or improve convergence, the high-energy contributions may be necessary. To calculate these, the asymptotic behaviour of the Green's functions is needed. To achieve this, retarded and advanced Green's functions are expanded in powers of the inverse energy,  $1/\epsilon$ :

$$\hat{g} = \hat{g}_0 + \frac{1}{\epsilon} \hat{g}_1 + \frac{1}{\epsilon^2} \hat{g}_2 + \frac{1}{\epsilon^3} \hat{g}_3 + \dots \quad (\text{B.1})$$

The functions  $\hat{g}_i$  may still depend on  $\mathbf{p}_f$ ,  $\mathbf{R}$ , and  $t$  but not on the energy  $\epsilon$ . Below, isotropic impurity scattering with lifetime  $\tau$  is assumed. In the Born limit this gives for the impurity self-energies the expression

$$\hat{\sigma}_{imp} = \frac{\hbar}{2\pi\tau} \langle \hat{g} \rangle_{\mathbf{p}'_f} . \quad (\text{B.2})$$

The restriction to the Born limit is for simplicity, only, as it does not affect the Green's functions up to the order  $\left(\frac{1}{\epsilon}\right)^3$ . When the expansion (B.1) is set into the transport equation

$$\left[ \left( \epsilon + \frac{e}{c} \mathbf{v}_f \cdot \mathbf{A} \right) \hat{\tau}_3 - \hat{\Delta} - \hat{\sigma}_{imp} - e\hat{\Phi}, \hat{g} \right]_{\otimes} + i\hbar \mathbf{v}_f \cdot \nabla \hat{g} = \hat{0} , \quad (\text{B.3})$$

the four lowest orders then read:

$$\epsilon^1: \quad [\hat{\tau}_3, \hat{g}_0] = \hat{0} , \quad (\text{B.4})$$

$$\epsilon^0: \quad [\hat{\tau}_3, \hat{g}_1] + \left[ \frac{e}{c} \mathbf{v}_f \cdot \mathbf{A} \hat{\tau}_3 - \hat{\Delta} - e\hat{\Phi} - \frac{\hbar}{2\pi\tau} \langle \hat{g}_0 \rangle_{\mathbf{p}'_f}, \hat{g}_0 \right] + i\hbar \mathbf{v}_f \cdot \nabla \hat{g}_0 = \hat{0} , \quad (\text{B.5})$$

## APPENDIX B. HIGH-ENERGY EXPANSION

---

$$\begin{aligned} \epsilon^{-1}: \quad & [\hat{\tau}_3, \hat{g}_2] + \frac{i\hbar}{2} \{\hat{\tau}_3, \partial_t \hat{g}_1\} + \left[ \frac{e}{c} \mathbf{v}_f \cdot \mathbf{A} \hat{\tau}_3 - \hat{\Delta} - e\hat{\Phi} - \frac{\hbar}{2\pi\tau} \langle \hat{g}_0 \rangle_{\mathbf{p}'_f}, \hat{g}_1 \right] \\ & - \left[ \frac{\hbar}{2\pi\tau} \langle \hat{g}_1 \rangle_{\mathbf{p}'_f}, \hat{g}_0 \right] + i\hbar \mathbf{v}_f \cdot \nabla \hat{g}_1 = \hat{0} , \end{aligned} \quad (\text{B.6})$$

$$\begin{aligned} \epsilon^{-2}: \quad & [\hat{\tau}_3, \hat{g}_3] + \frac{i\hbar}{2} \{\hat{\tau}_3, \partial_t \hat{g}_2\} + \left[ \frac{e}{c} \mathbf{v}_f \cdot \mathbf{A} \hat{\tau}_3 - \hat{\Delta} - e\hat{\Phi} - \frac{\hbar}{2\pi\tau} \langle \hat{g}_0 \rangle_{\mathbf{p}'_f}, \hat{g}_2 \right] \\ & - \left[ \frac{\hbar}{2\pi\tau} \langle \hat{g}_2 \rangle_{\mathbf{p}'_f}, \hat{g}_0 \right] - \left[ \frac{\hbar}{2\pi\tau} \langle \hat{g}_1 \rangle_{\mathbf{p}'_f}, \hat{g}_1 \right] \\ & + \frac{i\hbar}{2} \left\{ \partial_t \left( \frac{e}{c} \mathbf{v}_f \cdot \mathbf{A} \hat{\tau}_3 - \hat{\Delta} - e\hat{\Phi} \right), \hat{g}_1 \right\} + i\hbar \mathbf{v}_f \cdot \nabla \hat{g}_2 = \hat{0} . \end{aligned} \quad (\text{B.7})$$

The normalization condition  $\hat{g} \otimes \hat{g} = -\pi^2 \hat{1}$  leads to

$$\begin{aligned} -\pi^2 \hat{1} &= \hat{g}_0^2 + \frac{1}{\epsilon} \{\hat{g}_0, \hat{g}_1\} + \frac{1}{\epsilon^2} [\{\hat{g}_0, \hat{g}_2\} + \hat{g}_1^2] \\ &+ \frac{1}{\epsilon^3} [\{\hat{g}_0, \hat{g}_3\} + \{\hat{g}_1, \hat{g}_2\} + \frac{i\hbar}{2} [\partial_t \hat{g}_1, \hat{g}_1]] + \dots \end{aligned} \quad (\text{B.8})$$

In eqs. (B.3) to (B.8) it was already used that  $\hat{g}_0$  does not depend on time. As a consequence, time derivatives appear only up to first order. Introducing the differential operators  $D^{R,A}$  via

$$D^{R,A} \hat{X} = \left\{ \hat{\tau}_3 i\hbar \mathbf{v}_f \cdot \nabla + \hat{1} \frac{2e}{c} \mathbf{v}_f \cdot \mathbf{A} \right\} \hat{X} \pm \frac{i\hbar}{\tau} \left\{ \hat{X} - \langle \hat{X} \rangle_{\mathbf{p}'_f} \right\} , \quad (\text{B.9})$$

the solution of eqs. (B.3) to (B.8) can be written in the form:

$$\begin{aligned} \hat{g}_0^{R,A} &= \pm i\pi \hat{\tau}_3 , \\ \hat{g}_1^{R,A} &= \pm i\pi (-\hat{\Delta}) , \\ \hat{g}_2^{R,A} &= \pm i\pi \frac{1}{2} [\hat{\Delta} \hat{\tau}_3 + D^{R,A}] \hat{\Delta} , \\ \hat{g}_3^{R,A} &= \pm i\pi \frac{1}{4} \left( -D^{R,A} D^{R,A} \hat{\Delta} + \hat{\tau}_3 \{ \hat{\Delta}, D^{R,A} \hat{\Delta} \} \right. \\ &\quad \left. + 2\hat{\Delta}^3 + i\hbar \hat{\tau}_3 [\hat{\Delta}, \partial_t (\hat{\Delta} - e\hat{\Phi})] \right) . \end{aligned} \quad (\text{B.10})$$

The Keldysh Green's function for large energies is related to retarded and advanced functions via

$$\hat{g}^K = \text{sign}(\epsilon) (\hat{g}^R - \hat{g}^A) . \quad (\text{B.11})$$



# Appendix C

## Charge conservation

We discuss charge conservation in the quasiclassical theory, starting from the transport equation in “Nambu-Keldysh” matrix form (2.2),

$$i\hbar \mathbf{v}_f \cdot \nabla \check{g} = -[\epsilon \hat{\tau}_3 \check{1} - \hat{\Delta}_{mf} - \check{\sigma}_{imp} - \check{v}_{ext}, \check{g}]_{\otimes} . \quad (\text{C.1})$$

The gap equation (2.10) for a singlet pairing superconductor is here used in a slightly different but equivalent form:

$$\hat{\Delta}_{mf}(\mathbf{R}, \mathbf{p}_f, t) = N_f \int_{-\epsilon_c}^{+\epsilon_c} \frac{d\epsilon}{4\pi i} \left\langle V(\mathbf{p}_f, \mathbf{p}'_f) \hat{f}^K(\mathbf{R}, \mathbf{p}'_f, \epsilon, t) \right\rangle_{\mathbf{p}'_f} , \quad (\text{C.2})$$

where the matrix  $\hat{f}^K$  is the off-diagonal part of  $\hat{g}^K$ .

The conservation of charge can be derived from the transport equation for the Keldysh propagator,

$$i\hbar \mathbf{v}_f \cdot \nabla \hat{g}^K = - \left[ \epsilon \hat{\tau}_3 - \hat{\Delta}_{mf} - \hat{v}_{ext}, \hat{g}^K \right]_{\otimes} + \hat{\sigma}_{imp}^K \otimes \hat{g}^A - \hat{g}^R \otimes \hat{\sigma}_{imp}^K + \hat{\sigma}_{imp}^R \otimes \hat{g}^K - \hat{g}^K \otimes \hat{\sigma}_{imp}^A , \quad (\text{C.3})$$

by multiplying by  $\hat{\tau}_3$ , taking the trace, and integration over Fermi surface and energy. In the following each term in eq. (C.3) is treated separately. The integration of the gradient term directly leads to the divergence of the current density.

$$\int_{-\epsilon_c}^{+\epsilon_c} \frac{d\epsilon}{4\pi i} \text{Tr}_4 \left\langle \hat{\tau}_3 i\hbar \mathbf{v}_f \cdot \nabla \hat{g}^K \right\rangle_{\mathbf{p}_f} = \frac{2i}{eN_f} \nabla \cdot \mathbf{j} . \quad (\text{C.4})$$

## APPENDIX C. CHARGE CONSERVATION

---

The commutator of the energy variable with the Keldysh propagator is related to the low-energy contribution of the time derivative of the charge density:

$$\begin{aligned}
 \int_{-\epsilon_c}^{+\epsilon_c} \frac{d\epsilon}{4\pi i} Tr_4 \left\langle \hat{\tau}_3 \left[ -\epsilon \hat{\tau}_3, \hat{g}^K \right]_{\otimes} \right\rangle_{\mathbf{p}_f} &= - \int_{-\epsilon_c}^{+\epsilon_c} \frac{d\epsilon}{4\pi i} Tr_4 \left\langle \left[ \epsilon, \hat{g}^K \right]_{\otimes} \right\rangle_{\mathbf{p}_f} \\
 &= -i \partial_t \int_{-\epsilon_c}^{+\epsilon_c} \frac{d\epsilon}{4\pi i} Tr_4 \left\langle \hat{g}^K \right\rangle_{\mathbf{p}_f} .
 \end{aligned} \tag{C.5}$$

The corresponding high-energy contribution results from the commutator which includes the external perturbation:

$$\begin{aligned}
 \int_{-\epsilon_c}^{+\epsilon_c} \frac{d\epsilon}{4\pi i} Tr_4 \left\langle \hat{\tau}_3 \left[ \hat{v}_{ext}, \hat{g}^K \right]_{\otimes} \right\rangle_{\mathbf{p}_f} &= \int_{-\epsilon_c}^{+\epsilon_c} \frac{d\epsilon}{4\pi i} Tr_4 \left\langle \left[ -\frac{e}{c} \mathbf{v}_f \cdot \mathbf{A} \hat{1} + e\Phi \hat{\tau}_3, \hat{g}^K \right]_{\otimes} \right\rangle_{\mathbf{p}_f} \\
 &= \frac{1}{4\pi i} 2 \sum_{n=0}^{\infty} \left( \frac{-i}{2} \right)^{2n+1} \frac{1}{(2n+1)!} Tr_4 \left\langle \partial_t^{2n+1} \left( -\frac{e}{c} \mathbf{v}_f \cdot \mathbf{A} \hat{1} + e\Phi \hat{\tau}_3 \right) \left[ \partial_{\epsilon}^{2n} \hat{g}^K \right]_{-\epsilon_c}^{+\epsilon_c} \right\rangle_{\mathbf{p}_f} \\
 &= \frac{1}{4\pi i} 2 \frac{-i}{2} \partial_t Tr_4 \left\langle \left( -\frac{e}{c} \mathbf{v}_f \cdot \mathbf{A} \hat{1} + e\Phi \hat{\tau}_3 \right) \left[ -2i\pi \text{sign}(\epsilon) \hat{\tau}_3 \right]_{-\epsilon_c}^{+\epsilon_c} \right\rangle_{\mathbf{p}_f} \\
 &= 4i \partial_t e\Phi .
 \end{aligned} \tag{C.6}$$

In the last equation the asymptotic, high-energy expression for the Keldysh propagator was used, namely

$$\hat{g}^K \rightarrow -2\pi i \text{sign}(\epsilon) \left[ \hat{\tau}_3 + \frac{\hat{\Delta}_{mf}}{\epsilon} \right]. \tag{C.7}$$

The commutator involving the order parameter does not contribute if the gap equation holds:

$$\begin{aligned}
 \int_{-\epsilon_c}^{+\epsilon_c} \frac{d\epsilon}{4\pi i} Tr_4 \left\langle \hat{\tau}_3 \left[ \hat{\Delta}_{mf}, \hat{g}^K \right]_{\otimes} \right\rangle_{\mathbf{p}_f} &= \int_{-\epsilon_c}^{+\epsilon_c} \frac{d\epsilon}{4\pi i} Tr_4 \left\langle \hat{\tau}_3 \left[ \hat{\Delta}_{mf}, \hat{f}^K \right]_{\otimes} \right\rangle_{\mathbf{p}_f} \\
 &= N_f \int_{-\epsilon_c}^{+\epsilon_c} \frac{d\epsilon}{4\pi i} \int_{-\epsilon_c}^{+\epsilon_c} \frac{d\epsilon'}{4\pi i} Tr_4 \left\langle \left\langle \hat{\tau}_3 V(\mathbf{p}_f, \mathbf{p}'_f) \left[ \hat{f}^K(\mathbf{p}'_f, \epsilon'), \hat{f}^K(\mathbf{p}_f, \epsilon) \right] \right\rangle_{\mathbf{p}'_f} \right\rangle_{\mathbf{p}_f} \\
 &\quad + \int_{-\epsilon_c}^{+\epsilon_c} \frac{d\epsilon}{4\pi i} \sum_{n=1}^{\infty} \left( \frac{i}{2} \right)^n \frac{1}{n!} Tr_4 \left\langle \hat{\tau}_3 \left[ (-1)^n \partial_t^n \hat{\Delta}_{mf} \partial_{\epsilon}^n \hat{f}^K - \partial_{\epsilon}^n \hat{f}^K \partial_t^n \hat{\Delta}_{mf} \right] \right\rangle_{\mathbf{p}_f}
 \end{aligned}$$

---


$$\begin{aligned}
&= 0 + \int_{-\epsilon_c}^{+\epsilon_c} \frac{d\epsilon}{4\pi i} \sum_{n=1}^{\infty} \left(\frac{i}{2}\right)^{2n} \frac{1}{(2n)!} 2 \operatorname{Tr}_4 \left\langle \hat{\tau}_3 \partial_t^{2n} \hat{\Delta}_{mf} \partial_\epsilon^{2n} \hat{f}^K \right\rangle_{\mathbf{p}_f} \\
&= \frac{1}{4\pi i} \sum_{n=1}^{\infty} \left(\frac{-1}{4}\right)^n \frac{1}{(2n)!} 2 \operatorname{Tr}_4 \left\langle \hat{\tau}_3 \partial_t^{2n} \hat{\Delta}_{mf} \left[ \partial_\epsilon^{2n-1} \hat{f}^K \right]_{-\epsilon_c}^{+\epsilon_c} \right\rangle_{\mathbf{p}_f} \\
&= \sum_{n=1}^{\infty} \left(\frac{-1}{4}\right)^n \frac{1}{n} \frac{2}{\epsilon_c^{2n}} \operatorname{Tr}_4 \left\langle \hat{\tau}_3 \left( \partial_t^{2n} \hat{\Delta}_{mf} \right) \hat{\Delta}_{mf} \right\rangle_{\mathbf{p}_f} \\
&\sim \left(\frac{\omega}{\epsilon_c}\right)^2 \longrightarrow 0 .
\end{aligned} \tag{C.8}$$

In the equation above, the vanishing of the term without derivatives follows from a redeclaration of variables, i.e.  $(\mathbf{p}'_f, \epsilon') \leftrightarrow (\mathbf{p}_f, \epsilon)$ , and  $V(\mathbf{p}_f, \mathbf{p}'_f) = V(\mathbf{p}'_f, \mathbf{p}_f)$ . To evaluate the second term, the asymptotic high-energy expression for the Keldysh propagator (C.7) was used. Assuming a harmonic time dependence, the time derivative contributes the factor  $\omega$  which is small compared to the energy cutoff.

The remaining term involves the impurity self-energies which vanishes if integrated over the Fermi surface. To show this, we use an operator  $\check{L}$  which is defined as follows:

$$\check{L}(\mathbf{p}_f, \mathbf{p}'_f) = \left[ -N_f \check{u}(\mathbf{p}_f, \mathbf{p}'_f) \check{g}(\mathbf{p}'_f) + \delta(\mathbf{p}_f - \mathbf{p}'_f) \check{1} \right]^{-1}.$$

Here, the inverse means

$$\left\langle \check{A}(\mathbf{p}_f, \mathbf{p}''_f) \otimes \check{A}^{-1}(\mathbf{p}''_f, \mathbf{p}'_f) \right\rangle_{\mathbf{p}''_f} = \delta(\mathbf{p}_f - \mathbf{p}'_f) \check{1}.$$

The t-matrix for impurities with concentration  $c_{imp}$  and potential  $\check{u} = \hat{u} \check{1}$  can now be written as

$$\check{t}(\mathbf{p}_f, \mathbf{p}'_f) = \left\langle \check{L}(\mathbf{p}_f, \mathbf{p}''_f) \check{u}(\mathbf{p}''_f, \mathbf{p}'_f) \right\rangle_{\mathbf{p}''_f}.$$

The remaining term can then easily be calculated.

$$\begin{aligned}
\left\langle [\check{\sigma}_{imp}(\mathbf{p}_f), \check{g}(\mathbf{p}_f)]_{\otimes} \right\rangle_{\mathbf{p}_f} &= \left\langle \left\langle c_{imp} \left[ \check{L}(\mathbf{p}_f, \mathbf{p}'_f) \check{u}(\mathbf{p}'_f, \mathbf{p}_f), \check{g}(\mathbf{p}_f) \right]_{\otimes} \right\rangle_{\mathbf{p}'_f} \right\rangle_{\mathbf{p}_f} \\
&= \left\langle \left\langle c_{imp} \left[ \check{L}(\mathbf{p}_f, \mathbf{p}'_f), \check{u}(\mathbf{p}'_f, \mathbf{p}_f) \check{g}(\mathbf{p}_f) - \delta(\mathbf{p}_f - \mathbf{p}'_f) \check{1} + \delta(\mathbf{p}_f - \mathbf{p}'_f) \check{1} \right]_{\otimes} \right\rangle_{\mathbf{p}'_f} \right\rangle_{\mathbf{p}_f}
\end{aligned}$$

## APPENDIX C. CHARGE CONSERVATION

---

$$\begin{aligned}
&= \left\langle \left\langle c_{imp} \left[ \check{L}(\mathbf{p}_f, \mathbf{p}'_f), -\check{L}^{-1}(\mathbf{p}'_f, \mathbf{p}_f) + \delta(\mathbf{p}_f - \mathbf{p}'_f) \check{1} \right]_{\otimes} \right\rangle_{\mathbf{p}'_f} \right\rangle_{\mathbf{p}_f} \\
&= \check{0}
\end{aligned} \tag{C.9}$$

From eqs. (2.13), (2.14), and (C.4) to (C.9) the continuum equation for charge follows:

$$\nabla \cdot \mathbf{j} = -\partial_t \rho . \tag{C.10}$$

# Bibliography

- [1] H. Kamerlingh Onnes, Leiden Comm. **120b**, **122b**, **124c** (1911).
- [2] F. London and H. London, Proc. Roy. Soc. **A149**, 71 (1935).
- [3] W. Meissner and R. Ochsenfeld, Naturwissenschaften **21**, 787 (1933).
- [4] V. L. Ginzburg and L. D. Landau, Zh. Eksp. Teor. Fiz. **20**, 1064 (1950), [Phys. Abh. Sow., Tieftemperaturphysik, S. 1, Leipzig, Geest und Portig (1958)].
- [5] A. A. Abrikosov, Zh. Eksp. Teor. Fiz. **32**, 1442 (1957), [Sov. Phys. JETP **5**, 1174 (1957)].
- [6] L. P. Gor'kov, Zh. Eksp. Teor. Fiz. **36**, 1918 (1959), [Sov. Phys. JETP **9**, 1364 (1959)].
- [7] J. Bardeen, L. N. Cooper, and J. R. Schrieffer, Phys. Rev. **108**, 1175 (1957).
- [8] L. P. Gor'kov, Zh. Eksp. Teor. Fiz. **34**, 735 (1958), [Sov. Phys. JETP **7**, 505 (1958)].
- [9] G. Eilenberger, Z. Phys. **214**, 195 (1968).
- [10] A. I. Larkin and Y. N. Ovchinnikov, Zh. Eksp. Teor. Fiz. **55**, 2262 (1968), [Sov. Phys. JETP **28**, 1200 (1969)].
- [11] A. I. Larkin and Y. N. Ovchinnikov, Zh. Eksp. Teor. Fiz. **68**, 1915 (1975), [Sov. Phys. JETP **41**, 960 (1976)].
- [12] G. M. Éliashberg, Zh. Eksp. Teor. Fiz. **61**, 1254 (1971), [Sov. Phys. JETP **34**, 668 (1972)].
- [13] A. I. Larkin and Y. N. Ovchinnikov, Zh. Eksp. Teor. Fiz. **73**, 299 (1977), [Sov. Phys. JETP **46**, 155 (1977)].

## BIBLIOGRAPHY

---

- [14] A. F. Andreev, Zh. Eksp. Teor. Fiz. **46**, 1823 (1964), [Sov. Phys. JETP **19**, 1228 (1964)].
- [15] P. G. de Gennes, “*Superconductivity of Metals and Alloys*” (Benjamin, New York, 1966).
- [16] K. D. Usadel, Phys. Rev. Lett. **25**, 507 (1970).
- [17] D. D. Osheroff, R. C. Richardson, and D. M. Lee, Phys. Rev. Lett. **28**, 885 (1972).
- [18] P. W. Anderson and W. F. Brinkman, *The Physics of Liquid and Solid Helium, Part II* (Wiley, New York, 1978), p. 177.
- [19] U. Eckern, Ann. Phys. **133**, 390 (1981).
- [20] J. W. Serene and D. Rainer, Phys. Rep. **101**, 221 (1983).
- [21] L. D. Landau, Zh. Eksp. Teor. Fiz. **32**, 59 (1957), [Sov. Phys. JETP **5**, 101 (1957)].
- [22] L. D. Landau, Zh. Eksp. Teor. Fiz. **30**, 1058 (1956), [Sov. Phys. JETP **3**, 920 (1957)].
- [23] L. D. Landau, Zh. Eksp. Teor. Fiz. **35**, 97 (1958), [Sov. Phys. JETP **8**, 70 (1959)].
- [24] L. V. Keldysh, Zh. Eksp. Teor. Fiz. **47**, 1515 (1964), [Sov. Phys. JETP **20**, 1018 (1965)].
- [25] M. Eschrig, Phys. Rev. B **61**, 9061 (2000).
- [26] M. Eschrig, Doktorarbeit, Universität Bayreuth (1997).
- [27] E. V. Thuneberg, J. Kurkijärvi, and D. Rainer, Phys. Rev. B **29**, 3913 (1984).
- [28] Y. Nagato, K. Nagai, and J. Hara, J. Low Temp. Phys. **93**, 33 (1993).
- [29] S. Higashitani and K. Nagai, J. Phys. Soc. Jpn. **64**, 549 (1995).
- [30] L. J. Buchholtz, H. Burkhardt, and M. Eschrig, Internal Report, Universität Bayreuth (1995).
- [31] Y. Nagato, S. Higashitani, K. Yamada, and K. Nagai, J. Low Temp. Phys. **103**, 1 (1996).
- [32] N. Schopohl and K. Maki, Phys. Rev. B **52**, 490 (1995).

- [33] A. B. Pippard, F. R. S., J. G. Shepherd, and D. A. Tindall, Proc. Roy. Soc. Lond. A **324**, 17 (1971).
- [34] M. L. Yu and J. E. Mercereau, Phys. Rev. Lett. **28**, 1117 (1972).
- [35] I. L. Landau, Zh. Eksp. Teor. Fiz. Pis. Red. **11**, 437 (1970), [Sov. Phys. JETP Lett. **9**, 295 (1970)].
- [36] J. Clarke, Phys. Rev. Lett. **28**, 1363 (1972).
- [37] T. J. Rieger, D. J. Scalapino, and J. E. Mercereau, Phys. Rev. Lett. **27**, 1787 (1971).
- [38] M. Tinkham and J. Clarke, Phys. Rev. Lett. **28**, 1366 (1972).
- [39] M. Tinkham, Phys. Rev. B **6**, 1747 (1972).
- [40] A. Schmid and G. Schön, J. Low Temp. Phys. **20**, 207 (1975).
- [41] Y. N. Ovchinnikov, J. Low Temp. Phys. **28**, 43 (1977).
- [42] Y. N. Ovchinnikov, J. Low Temp. Phys. **31**, 785 (1978).
- [43] S. N. Artemenko, A. F. Volkov, and A. V. Zaitsev, J. Low Temp. Phys. **30**, 487 (1978).
- [44] S. N. Artemenko and A. F. Volkov, Zh. Eksp. Teor. Fiz. **72**, 1018 (1977), [Sov. Phys. JETP **45**, 533 (1977)].
- [45] Y. Krähenbühl and R. J. Watts-Tobin, J. Low Temp. Phys. **35**, 569 (1979).
- [46] J. Clarke, U. Eckern, A. Schmid, G. Schön, and M. Tinkham, Phys. Rev. B **20**, 3933 (1979).
- [47] G. E. Blonder, M. Tinkham, and T. M. Klapwijk, Phys. Rev. B **25**, 4515 (1982).
- [48] F. Marquardt, Diplomarbeit, Universität Bayreuth (1998).
- [49] A. V. Zaitsev, Zh. Eksp. Teor. Fiz. **86**, 1742 (1984), [Sov. Phys. JETP **59**, 1015 (1984)].
- [50] S. Guéron, H. Pothier, N. O. Birge, D. Esteve, and M. H. Devoret, Phys. Rev. Lett. **77**, 3025 (1996).
- [51] W. Belzig, C. Bruder, and G. Schön, Phys. Rev. B **54**, 9443 (1996).

## BIBLIOGRAPHY

---

- [52] W. Belzig, F. K. Wilhelm, C. Bruder, G. Schön, and A. D. Zaikin, Superlattices and Microstructures **25**, 1251 (1999).
- [53] A. F. Volkov, Physica B **203**, 267 (1994).
- [54] A. F. Volkov, P. H. C. Magnée, B. J. van Wees, and T. M. Klapwijk, Physica C **242**, 261 (1995).
- [55] A. A. Golubov, E. P. Houwman, J. G. Gijsbertsen, V. M. Krasnov, J. Flokstra, H. Rogalla, and M. Y. Kupriyanov, Phys. Rev. B **51**, 1073 (1995).
- [56] A. A. Golubov and M. Y. Kupriyanov, J. Low Temp. Phys. **70**, 83 (1988).
- [57] W. L. McMillan, Phys. Rev. **175**, 537 (1968).
- [58] D. Saint-James, Journal de Physique **25**, 899 (1964).
- [59] B. D. Josephson, Phys. Lett. **1**, 251 (1962).
- [60] K. K. Likharev, Rev. Mod. Phys. **51**, 101 (1979).
- [61] C. C. Tsuei, J. R. Kirtley, C. C. Chi, L. S. Yu-Jahnes, A. Gupta, T. Shaw, J. Z. Sun, and M. B. Ketchen, Phys. Rev. Lett. **73**, 593 (1994).
- [62] J. R. Kirtley, C. C. Tsuei, J. Z. Sun, C. C. Chi, L. S. Yu-Jahnes, A. Gupta, M. Rupp, and M. B. Ketchen, Nature **373**, 225 (1995).
- [63] D. S. Greywall, Phys. Rev. B **33**, 7520 (1986).
- [64] O. Avenel and E. Varoquaux, Phys. Rev. Lett. **60**, 416 (1988).
- [65] K. Sukhatme, Y. Mukharsky, T. Chui, and D. Pearson, Nature **411**, 280 (2001).
- [66] O. Avenel and E. Varoquaux, Jpn. J. Appl. Phys. **26**, 1798 (1987).
- [67] S. V. Pereverzev, A. Loshak, S. Backhaus, J. C. Davis, and R. E. Packard, Nature **388**, 449 (1997).
- [68] P. W. Anderson, Rev. Mod. Phys. **38**, 298 (1966).
- [69] R. W. Simmonds, A. Marchenkov, J. C. Davis, and R. E. Packard, Phys. Rev. Lett. **87**, 0353011 (2001).



- [70] R. W. Simmonds, A. Marchenkov, E. Hoskinson, J. C. Davis, and R. E. Packard, *Nature* **412**, 55 (2001).
- [71] D. Rainer and J. A. Sauls, *Jpn. J. Appl. Phys.* **26**, 1804 (1987).
- [72] S. Backhaus, S. V. Pereverzev, R. W. Simmonds, A. Loshak, J. C. Davis, and R. E. Packard, *Nature* **392**, 687 (1998).
- [73] A. Marchenkov, R. W. Simmonds, S. Backhaus, A. Loshak, J. C. Davis, and R. E. Packard, *Phys. Rev. Lett.* **83**, 3860 (1999).
- [74] J. K. Viljas and E. V. Thuneberg, *Phys. Rev. B* **65**, 064530 (2002).
- [75] J. K. Viljas and E. V. Thuneberg, *J. Low Temp. Phys.* **129**, 423 (2002).
- [76] S.-K. Yip, *Phys. Rev. Lett.* **83**, 3864 (1999).
- [77] J. K. Viljas and E. V. Thuneberg, *Phys. Rev. Lett.* **83**, 3868 (1999).
- [78] H. Burkhardt, *Doktorarbeit, Universität Bayreuth* (1997).
- [79] A. J. Leggett, *Phys. Rev. Lett.* **31**, 352 (1973).
- [80] A. J. Leggett, *Rev. Mod. Phys.* **47**, 331 (1975).
- [81] S. Engelsberg, W. F. Brinkman, and P. W. Anderson, *Phys. Rev.* **A9**, 2592 (1974).
- [82] D. Vollhardt, K. Maki, and N. Schopohl, *J. Low Temp. Phys.* **39**, 79 (1980).
- [83] H. Kleinert, *J. Low Temp. Phys.* **39**, 451 (1980).
- [84] A. L. Fetter, *Quantum Statistics and the Many-Body Problem* (Plenum Press, New York, 1975), p. 127.
- [85] M. Y. Kupriyanov and V. F. Lukichev, *Fiz. Nizk. Temp.* **6**, 445 (1980), [*Sov. J. Low Temp. Phys.* **6**, 210 (1980)].
- [86] R. H. Permenter, *RCA Rev.* **23**, 323 (1962).
- [87] G. D. Mahan, *Many-Particle Physics* (Plenum Press, New York, 1990), p. 168.
- [88] J. Kurkijärvi, *Phys. Rev. B* **38**, 11184 (1988).

## BIBLIOGRAPHY

---

- [89] I. O. Kulik and A. N. Omel'yanchuk, Fiz. Nizk. Temp. **3**, 945 (1977), [Sov. J. Low Temp. Phys. **3**, 459 (1977)].
- [90] L. J. Buchholtz and G. Zwicknagl, Phys. Rev. B **23**, 5788 (1981).
- [91] L. J. Buchholtz, Phys. Rev. B **33**, 1579 (1986).
- [92] L. J. Buchholtz and D. Rainer, Z. Phys. B – Condensed Matter **35**, 151 (1979).
- [93] E. V. Thuneberg, M. Fogelström, and J. Kurkijärvi, Physica B **178**, 176 (1992).
- [94] W. Zhang, J. Kurkijärvi, and E. V. Thuneberg, Phys. Rev. B **36**, 1987 (1987).
- [95] W. Zhang, J. Kurkijärvi, and E. V. Thuneberg, Phys. Lett. **109A**, 238 (1985).
- [96] F. J. Culetto, G. Kieselmann, and D. Rainer, in *Proceedings of the 17th International Conference on Low Temperature Physics - LT-17*, edited by U. Eckern, A. Schmid, W. Weber, and H. Wuehl (North-Holland, Amsterdam, 1984), p. 1027.
- [97] N. B. Kopnin, P. I. Soininen, and M. M. Salomaa, J. Low Temp. Phys. **85**, 267 (1991).
- [98] Y. N. Ovchinnikov, Zh. Eksp. Teor. Fiz. **56**, 1590 (1969), [Sov. Phys. JETP **29**, 853 (1969)].
- [99] E. V. Thuneberg, J. Kurkijärvi, and J. A. Sauls, Physica B **165&166**, 755 (1990).
- [100] E. C. Titchmarsh, *Introduction to the theory of Fourier integrals* (Clarendon Press, 1967), p. 334.
- [101] J. M. Luttinger and J. C. Ward, Phys. Rev. **118**, 1417 (1960).
- [102] A. L. Shelankov, J. Low Temp. Phys. **60**, 29 (1985).
- [103] A. B. Vorontsov and J. A. Sauls, Phys. Rev. B **68**, 064508 (2003).
- [104] A. L. Fetter and J. D. Walecka, *Quantum Theory of Many-Particle Systems* (McGraw-Hill, 1971).
- [105] R. D. Parks, ed., *Superconductivity* (Marcel Dekker, INC., New York, 1969), vol. I, chap. 5.
- [106] A. A. Abrikosov, L. P. Gor'kov, and I. E. Dzyaloshinski, *Methods of Quantum Field Theory in Statistical Physics* (Prentice-Hall, Englewood Cliffs, NJ, 1963).

- [107] S. Shulga and D. Rainer, Internal Report, Universität Bayreuth (1998).
- [108] N. Schopohl and L. Tewordt, J. Low Temp. Phys. **41**, 305 (1980).
- [109] P. W. Anderson and A. H. Dayem, Phys. Rev. Lett. **13**, 195 (1964).
- [110] S. Shapiro, Phys. Rev. Lett. **11**, 80 (1963).



# Danksagung

Mein erster Dank geht an Dierk für eine sehr angenehme Arbeitsatmosphäre und einen Einblick in Deine Art Physik zu betreiben. Lehrstunden zur Buchhaltung für Fortgeschrittene beeindruckten dauerhaft.

Herrn Prof. Werner Pesch möchte ich dafür danken, dass er auch im Ruhestand nicht ruhte und als Gutachter zur Verfügung stand.

Ich weiß die Unterstützung jener zu schätzen, die für die ausgezeichnete Infrastruktur sorgten.

Den frühen und späten Teilnehmern der Tafelrunde sei Dank für die angenehme Ablenkung vor, während und lang nach der Mittagspause. Habe ich alle Ohren zurückgegeben, welche mir geliehen wurden? Ach ja, meinen Rechner kann ich jetzt auch schon selbst anschalten.

Ausgesprochenes Glück hatte ich in Bayreuth mit meinen Mitbewohnerinnen und dem Philosophen nebenan. Glücklicherweise fanden sich nach Kalorienattentaten der leckeren Art auch leicht Freiwillige für ausgleichende Ausritte.

Ich möchte schließen mit dem Dank an alle, die in den entscheidenden Phasen der vergangenen drei Jahrzehnte den rechten Schubser gaben.



# Lebenslauf

10. September 1971	Geboren in Hermeskeil, Rheinland-Pfalz
August 1978 bis Juni 1982	Grundschule Schmelz-Limbach
August 1982 bis Mai 1991	Johannes-Kepler-Gymnasium Lebach
Mai 1991	Allgemeine Hochschulreife
Juli 1991 bis Juni 1992	Grundwehrdienst
Oktober 1992 bis September 1994	Grundstudium Mathematik und Physik an der Universität des Saarlandes in Saarbrücken
September 1994	Vordiplom in Mathematik
Oktober 1994	Vordiplom in Physik
Oktober 1994 bis Juli 1998	Hauptstudium Diplom-Physik an der Eberhardt-Karls-Universität in Tübingen
September 1996 bis Februar 1998	Auslandsstudium an der University of Birmingham, GB, Diplomarbeit
Juli 1998	Diplom in Physik
Seit Januar 1999	Promotionsstudium an der Universität Bayreuth





# Erklärung

Ich habe die vorliegende Arbeit selbständig verfasst und keine anderen als die angegebenen Quellen und Hilfsmittel benutzt. Ferner habe ich noch keinen früheren Promotionsversuch unternommen.

Bayreuth, den 23. April 2004

Martin Endres